A study of direct data-driven control and its application to automobile systems

Doctoral dissertation

Shuichi Yahagi

Division of Human Mechanical Systems and Design

Graduate School of Engineering Hokkaido University

November 2021

Acknowledgements

First and foremost, I would like to thank my supervisor, Professor Itsuro Kajiwara, for his valuable suggestions, guidance, support, patience, and encouragement during my studies at Hokkaido University. His support helped me in all aspects of my research and my writing of this thesis.

I wish to express my special thanks to Professor Toshiro Ohashi, Professor Yuki Shimizu, and Professor Yuh Yamashita of Hokkaido University for their efforts in the oral examination and for providing helpful advice for improving this thesis.

I also thank Associate Professor Hiroyuki Harada in the laboratory of Smart Structures and Systems, and the lab members—Dr. Heisei Yonezawa, Toshiki Hiruta, Ansei Yonezawa and Tatsunari Sakai—for their support. I wish you all great success in your future endeavors.

I would like to thank the staff of the ISUZU Advanced Engineering Center for providing me the opportunity to pursue this thesis. I also thank all the members of the 6th research department. This thesis would not have been possible without their support and patience.

Finally, I am grateful to the numerous people who have supported me during my work on this thesis. Special thanks are extended to my family, who consistently supported me and encouraged me with their best wishes.

November 2021

Shuichi Yahagi

Contents

Chapter 1
Introduction

1.1 Background and objective

Feedback control systems have been known for over 2000 years; the oldest case is speculated to be the water clock devised by Ktesibios (ca. 270 BC) in Alexandria, ancient Greece [1]. The first full-scale use of feedback control in industry was the centrifugal governor used in J. Watt's steam engine in 1778 [2]. In the nineteenth century, J. C. Maxwell, E. J. Routh, A. Hurwitz, A. M. Lyapunov, and others conducted research on stability. The Routh–Hurwitz stability criterion, which is based on characteristic equations for linear systems, and Lyapunov's stability theorem, which can discriminate stability for a wide range of systems, including nonlinear systems, are well known today. In 1922, N. Minorsky conceived the prototype proportional–integral–derivative (PID) controller. H. Nyquist and H. W. Bode subsequently established the frequency-domain response method. The Nyquist stability criterion was devised in 1932, and the concepts of gain margin and phase margin were devised in 1940. In 1948, W. R. Evans proposed root locus analysis, which is a technique used as a stability criterion that differs completely from the method based on characteristic equations. Thus, by the 1950s, classical control theory, which is based on analysis and design in the frequency domain using the concept of a transfer function, was established [3] [4].

A paper authored by R. E. Kalman in 1960 [5] led to the systematization of modern control theory by the 1970s. Modern control theory is a control system design method that operates in the time domain using state variables. With advances in the practical use of computers, optimizing control and using Kalman filters became compatible with numerical computation and were rapidly developed. Research on adaptive control began in 1965; in the 1980s, robust control and model predictive control became active research topics. In addition to modern control theory, advanced methods such as robust control, adaptive control, and model predictive control are model-based control methods that enable a control system to be designed on the basis of the state-space model of the

controlled object. Whereas classical control involves extensive human intervention, such as in the design of PID controllers, model-based control is a systematic design method in which mathematical models are used to design an optimal control system by minimizing a cost function that quantifies the control performance.

In control system design, knowledge of the controlled object model, such as its transfer function and state space, is important. In classical control, the control system is designed in the frequency domain; however, in reality, there are numerous aspects in which humans intervene and in which the experience and intuition of the designer are important factors [2]. In particular, the structure of the controller is commonly determined in advance and the controller parameters are tuned by trial and error so that indicators such as the steady-state deviation, damping coefficient, gain margin, and the phase margin can be satisfied to some extent [6]. On the other hand, model-based control, which includes modern control, is a design method that requires less human intervention; however, it requires a state space model of the controlled object. Thus, an accurate understanding of the model of the controlled object is important. Although model-based control has produced extensive research results, an accurate mathematical model cannot be obtained for a complex controlled object with strong nonlinearity, such as an industrial system, which has led to the effects of model-based control not being fully demonstrated. In addition, the application of model-based control to industrial products is limited by the facts that (i) the order of the controller cannot be increased because of factors that limit the controller performance, such as its CPU and ROM/RAM area, and (ii) the model-based control system design requires specialized knowledge. Therefore, more than 90% of the closed-loop systems used in industry are PID controllers treated in classical control theory [7]. That is, PID controllers are highly compatible with industrial products because of their controller structure, which is suitable for implementation in mass production and is easy to understand intuitively. However, the trial-and-error tuning of controller parameters is required for high control performance. Although the well-known classical PID gain tuning methods are the frequency-domain method and the step-response method proposed by Ziegler and Nichols in 1942 and 1943 [8] [9], respectively, and the Chien–Hrones–Reswick (CHR) method proposed by K. L. Chien, J. A. Hrones, and J. B. Reswick in 1952 [10], these are not methods to obtain the parameters that minimize the cost function. Indeed, they do not always yield the optimal PID gain. Moreover, they are

limited to PID controllers, single-input single-output (SISO) systems, and linear controllers.

In recent years, data-driven control without using a controlled object model has been widely studied. Figure 1.1 shows the design procedures for model-based control and data-driven control. Because model-based control is based on a mathematical model, a nominal model that represents the main dynamics of the actual system is needed. However, a nominal model does not match the actual system, causing uncertainty. In addition, models for complex systems are not easily obtained. By contrast, data-driven control does not require a mathematical model of the controlled object; it is therefore expected to be applied to controlled objects for which system identification is difficult and to reduce the man-hours devoted to control system design. The proper use of model-based control and data-driven control is summarized in Figure 1.2 [11].

Well-known methods of data-driven control include simultaneous perturbation stochastic approximation (SPSA) [12] [13], model-free adaptive control (MFAC) [14], unfalsified control (UC) [15], iterative feedback tuning (IFT) [16] [17], correlation-based tuning (CbT) [18] [19], virtual reference feedback tuning (VRFT) [20] [21], fictitious reference iterative tuning (FRIT) [22] [23], iterative learning control (ILC) [24], lazy learning (LL) [25], and Bayesian optimization (BO) [26]. These data-driven control methods, which do not use a model of the controlled object, are currently applied to industrial systems such as process systems, automobile systems, and vibration control problems [27] [28] [29] [30] [31] [32]. Among the aforementioned methods, this thesis focuses on VRFT and FRIT, which are data-driven control methods. VRFT and FRIT enable the optimal parameters of a controller with a fixed structure to be obtained using only the input/output data acquired from a single experiment. In particular, because the parameters of a fixed controller whose structure is specified in advance are optimized, VRFT/FRIT is suitable for designing low-order controllers such as PID controllers and is highly compatible with industrial system control. Other methods require repeated experiments and cannot be applied to PID controllers. Although numerous prior studies on data-driven control related to VRFT/FRIT have been reported, most of them have been limited in that a linear system was assumed and stability was not guaranteed. In addition,

although numerous applications to process systems have been examined, few examples of their application to automobile systems have been reported.

In this thesis, direct data-driven methods for feedback controllers, which are required in industry, especially in the automobile industry, are developed and their applicability is investigated. Mass-produced controllers for industrial systems should exhibit the following features:

- A controller with low computational cost that can be implemented;
- Countermeasures against aging and degradation over time;
- A stable control system;
- Nonlinear control that can be understood intuitively.

To satisfy these requirements, our aim is to develop a new direct data-driven method for a feedback controller and an automobile control system to address some actual problems. The details are described in the next section.

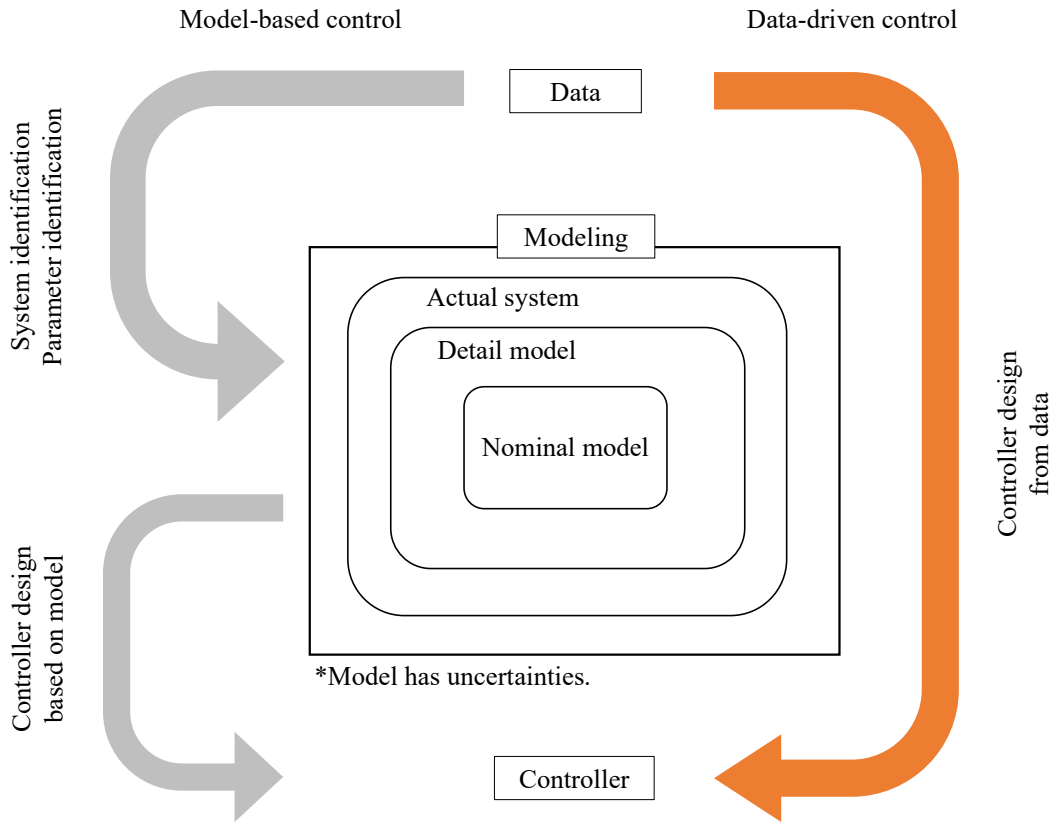

Figure 1.1. Design procedures of the model-based control and data-driven control methods.

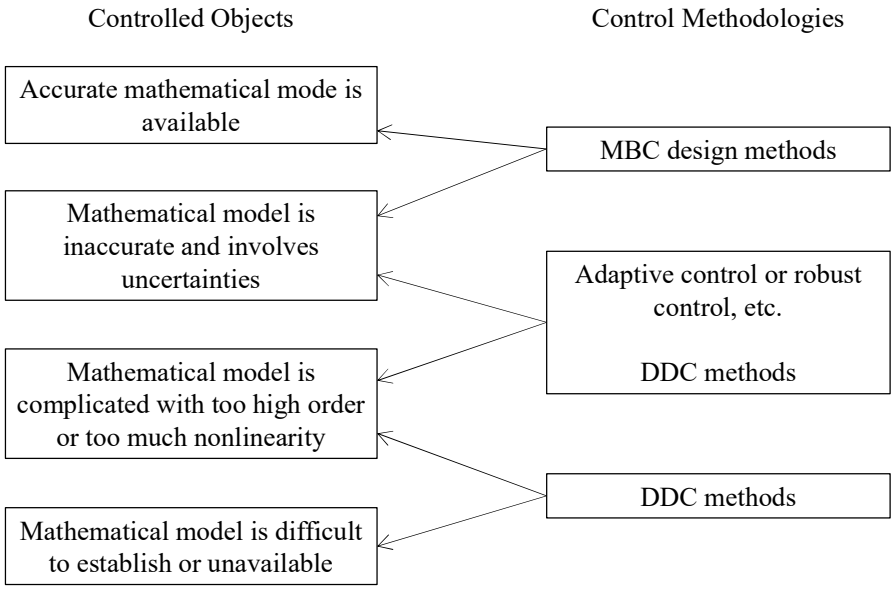

Figure 1.2. Controlled objects of data-driven control [11].

1.2 **Data-driven control required for automobile systems**

The theoretical extensions of data-driven control required for application to automobile systems and the practical application of data-driven control to solve actual problems in automobile systems are described. The data-driven control used in this thesis is based on VRFT/FRIT, in which controller parameters can be obtained from the input/output data acquired from a single experiment.

1.2.1 **Theoretical extensions of data-driven control**

The requirements for automobile systems considered in this work include coping with aging and product dispersion, ensuring the stability of closed-loop systems, coping with nonlinear systems, and considering sparsity.

(a) Aging and product dispersion

Mass-produced products such as automobile systems are subject to aging and product variation. Online tuning methods of controller parameters according to characteristic fluctuations are required. Previous studies have proposed online tuning methods based on data-driven control [33] [34] [35] [36]. However, no examples of their application to automated transmissions, which are components of automobile systems, have been reported. We aim to verify the effectiveness of our proposed tuning method for slip control of automated transmissions, which will be described later.

(b) Closed-loop stability

When the controller with optimized parameters by the conventional FRIT and VRFT is implemented, a problem arises in that the closed-loop system is not always stable [37] [38] [39]. Moreover, if the designer demands a fast response that cannot be achieved by the system, model matching becomes impossible. Therefore, the complementary sensitivity function must be tuned by trial and error. One of our objectives is to guarantee bounded-input bounded-output (BIBO) stability for linear systems and to construct an automatic tuning method of reference model parameters for model matching.

(c) Nonlinear control

Many industrial systems have nonlinear characteristics. Gain-scheduled control is one of the most effective methods for nonlinear systems [40] [41]. In particular, gain-scheduled PID control is easy to understand intuitively and its calculation cost can be kept low. Gain-scheduled PID control is therefore favored in industry and can be sufficiently implemented in a mass-production controller. Another of our objectives is to construct a direct design method for the gain-scheduled PID control law.

(d) Sparsity

Data-driven control calculates the optimum parameters from a set of input/output data. If the number of data points is small, overfitting can occur and the closed system might not be stable. This problem is the same as that faced by machine learning. In particular, it is considered to occur in the design of nonlinear controllers for nonlinear systems. In addition, mass-produced controllers should ideally have as small a ROM capacity as possible. In recent years, attention has been devoted to a property called *sparsity*, in which elements with small contributions become zeros [42]. We aim to develop a direct design method for a high-sparsity controller.

1.2.2 **Practical application to automobile systems**

For applications to automobile systems, with a focus on shift control of an automated transmission and position control for a pneumatic actuator, we aim to solve actual problems of automobile system control by applying data-driven control.

(a) Application to slip control of automated transmission

Automated transmissions, which are components of automobiles, are required to have a good shift feeling perceived by the driver and to improve fuel efficiency. To obtain a good shift feeling, tracking the difference between the engine speed and the input shaft speed to reach the target value is important. Failure of the actual value to reach the target value results in the driver feeling a delay or shock. In industry, the required specifications are achieved by tuning the control parameters via trial and error, which results in a low development efficiency. Therefore, it is necessary to design a control law and

automatically tune parameters that can achieve the desired response. Updating the parameters online is also important because the engine and clutch wear will change over time. That is, aging occurs. For the control law, a control system that realizes coordinated control of the engine and transmission is constructed. For the tuning process, online data-driven control is used to self-tune the PID gain. We aim to realize the desired slip speed control of the automated transmission by applying the proposed control system and online data-driven control.

(b) Application to position control of pneumatic clutch actuator

Consumers are demanding greater driving comfort, and automated transmissions are required not only for passenger cars but also for heavy-duty trucks. An automated manual transmission (AMT), which automates a manual transmission (MT), has advantages such as low cost, high efficiency, reduced clutch wear, and reduced fuel consumption. Automatic control of the clutch connection plays an important role in AMT vehicles [43]. Pneumatic clutch actuators are used in heavy-duty trucks because compressed air is installed in the vehicles. In addition, an ON/OFF valve is used because such valves are inexpensive, small, and robust. In such a pneumatic clutch system, controlling the desired position is difficult because of the compressibility of the air, the nonlinearity of the clutch spring force, and the operation of an ON/OFF valve. To address these nonlinearities, we aim to construct a practical controller design that consists of a gain-scheduled control and a direct tuning method of gain scheduler parameters.

1.3 **Dissertation outline**

This thesis comprises seven chapters. Chapter 1 introduces this research. Chapter 2 explains the previously proposed data-driven control. In Chapters 3 and 4, the theoretical extension of data-driven control is explored. In Chapters 5 and 6, the application of data-driven control to an automobile system is examined. The outline of each chapter is as follows.

In Chapter 2, VRFT and FRIT are introduced. These methods are model-referenced data-driven control methods that directly tune the parameters of a pre-specified controller

on the basis of input and output data obtained from a single experiment. The problem setup and the VRFT/FRIT algorithm is described. FRIT is used in Chapters 3 and 5, and VRFT is used in Chapters 4 and 6.

In Chapter 3, a direct controller design method using a fictitious reference signal to ensure stability is proposed because poor stability is a problem in conventional data-driven control. A direct design method that guarantees BIBO stability for linear time-invariant (LTI) systems is theoretically constructed. In addition, an automatic tuning method for the reference model parameters, which have previously required tuning by the user, is proposed. The effectiveness of the proposed method is confirmed using simulations and a simple experimental setup.

In Chapter 4, a direct design method for a gain-scheduled PID controller with sparsity is proposed. The proposed direct design method is based on VRFT, and the parameters of the gain scheduler are obtained from a set of input and output data. In addition, sparsity is introduced to suppress overtraining and reduce the ROM size. The effectiveness of the proposed method is verified by performing simulations on two systems: a linear parameter-varying (LPV) system and the Hammerstein model.

In Chapter 5, a control law with an online PID gain tuning method is proposed for slip control of an automated transmission, which is a device in an automobile. The control law consists of a PID controller and a disturbance observer to achieve cooperative control between engine and clutch systems. Under this cooperative control, the system can be treated as a linear system. In addition, the PID gain can be tuned using online-FRIT to address aging. The effectiveness of the proposed method is verified via gear-shifting tests on an actual vehicle.

In Chapter 6, a direct design method for the position control of a pneumatic clutch actuator, which is installed in heavy-duty trucks, is presented. It is shown that the pneumatic clutch actuator is a nonlinear, integral system. A gain-scheduled PD control law and its direct tuning are proposed. The effectiveness of the proposed method is verified through position control in an actual vehicle test.

In Chapter 7, the results obtained in this study is summarized and various prospects for further applications of the proposed methods is discussed.

Chapter 2
Direct data-driven tuning method

This chapter describes the direct tuning methods known as VRFT and FRIT, which are data-driven controls used in this thesis. These methods enable the parameters of a controller with a pre-specified structure to be tuned using input/output data obtained by a single experiment. The problem setting for each method is first described, followed by a description of the algorithm for each method.

2.1 Problem formulation for model-referenced data-driven control

We consider a general feedback control system with a reference model (Figure 2.1). Parameters r, u, y, and y_r represent the target value (reference input, setpoint), control input (manipulated variable), controlled-object output (controlled variable), and the reference model output, respectively. P is the controlled object, which is an unknown linear time-invariant (LTI) and single-input single-output (SISO) system. $C(\rho, z)$ is a linear fixed-order controller parameterized using the tunable parameter vector ρ. For instance, $C(\rho, z)$ in the *z*-domain is described as

$$C(\rho, z) = \frac{\rho_{m+n+1} z^m + \cdots + \rho_{n+2} z + \rho_{n+1}}{\rho_n z^n + \cdots + \rho_1 z + 1}, \tag{2.1}$$

where $\rho = [\rho_1 \quad \rho_2 \quad \cdots \quad \rho_{m+n+1}]^T$. M_d is the reference model, which is a user-defined target response transfer function (i.e., target complementary sensitivity function) from the target value r to the controlled variable y, and z represents the shift operator. We aim for model matching by obtaining the controller parameters that minimize the cost function:

$$J_0(\rho) = \frac{1}{N} \sum_{k=1}^{N} (e_0(\rho, k))^2, \tag{2.2}$$

where

$$e_0(\rho, k) = \ y(\rho, k) - M_d(z)r(k). \tag{2.3}$$

Alternatively, the cost function can be expressed as

$$J_0(\rho) = \left\| \left(M_d(z) - \frac{P(z)C(\rho, z)}{1 + P(z)C(\rho, z)} \right) W(z) \right\|_2^2, \tag{2.4}$$

where $W(z)$ is a weighting function chosen by the user.

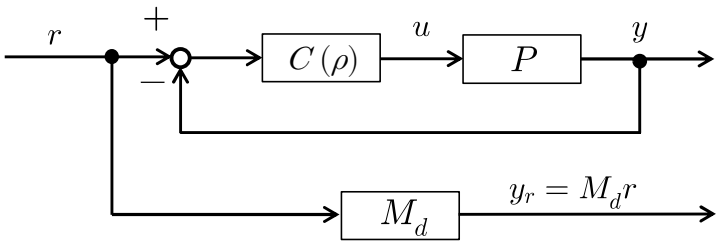

Figure 2.1. Feedback control system with a reference model.

2.2 **Virtual reference feedback tuning**

VRFT [20] [21] is a method for directly tuning the control parameters from input/output data without the system model. The optimal control parameters are tuned so that the reference model and closed-loop system have the same characteristics. Figure 2.2 shows the structure of the VRFT method. Here, $C(\rho, z)$, M_d, and P represent the fixed-order controller, which is parameterized through ρ, the reference model, and the controlled object (plant), which is the stable LTI system, respectively; $u(t)$ and $y(t)$ denote the input and output, respectively; ρ denotes the controller parameters; and $\bar{r}(t)$ and $\bar{e}(t)$ are the proposed virtual reference input and virtual error in the VRFT, respectively. The VRFT procedure is described as follows:

[Step 1] The input and output data of the controlled object, $u(t)$, $y(t)$, $t = 1, \ldots, N$, are acquired via a test.

[Step 2] The reference model M_d, which is the desired closed-loop, is set.

[Step 3] Considering $y(t)$ as the output of the reference model, the virtual reference input, which generates $y(t)$, is expressed as

$$\bar{r}(t) = M_d^{-1} y(t). \tag{2.5}$$

[Step 4] Considering $\bar{r}(t)$ as the reference input of the closed-loop in Figure 2.2, the virtual control input is described as

$$\bar{u}(t) = C(\rho, z)\big(\bar{r}(t) - y(t)\big). \tag{2.6}$$

[Step 5] When the virtual control input and the acquired control input data from Step 1 are similar, the closed loop can be regarded as being close to the reference model. Therefore, the cost function can be minimized as

$$J_{VR} = \frac{1}{N}\sum_{k=1}^{N}(u(t) - \bar{u}(t))^2. \tag{2.7}$$

The combination of Equations (2.6) and (2.7) gives

$$J_{VR}(\rho) = \frac{1}{N}\sum_{k=1}^{N}(u(t) - C(\rho, z)\bar{e}(t))^2, \tag{2.8}$$

where

$$\begin{aligned} \bar{e}(t) &= \bar{r}(t) - y(t) \\ &= M_d^{-1} y(t) - y(t) \\ &= (M_d^{-1} - 1) y(t). \end{aligned} \tag{2.9}$$

[Step 6] Prefilter L is introduced. Equation (2.8) includes a term that represents the inverse matrix of the reference model, which means that the equation has a nonproper characteristic. A prefilter avoids nonproper characteristics. Equation (2.10) is obtained by adding the prefilter to Equation (2.8):

$$J_{VR}(\rho) = \frac{1}{N}\sum_{k=1}^{N}(u_L(t) - C(\rho, z)\bar{e}_L(t))^2, \tag{2.10}$$

where

$$u_L(t) = Lu(t), \bar{e}_L(t) = L\bar{e}(t). \tag{2.11}$$

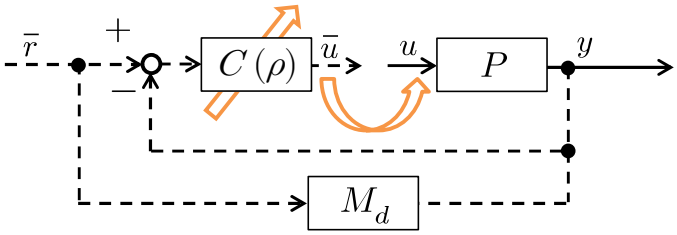

Figure 2.2. The VRFT concept.

Remark 2.1. On the basis of the literature [27], using Parseval's theorem, the interpretation of the cost function is explained. As N approaches infinity, we obtain the following equation:

$$J_{VR}(\rho) = \frac{1}{2\pi}\int_{-\pi}^{\pi}\left|\left(1 - \frac{C(\rho, e^{j\omega})}{C_d(\rho, e^{j\omega})}\right)\right|^2 \Phi_u d\omega, \tag{2.12}$$

where C_d is the controller that achieves the reference model, Φ_u is the power spectral density of u, and ω is the angular frequency. Here, the expressions $M_d = (1 + PC_d)^{-1}PC_d$ and $y(t) = Pu(t)$ was used. The relative error between the reference model C_d and $C(\rho)$ is evaluated under a weighted controlled variable. Also, we can rewrite Equation (2.10) as

$$J_{VR}(\rho) = \frac{1}{N}\sum_{k=1}^{N}(Lu(t) - C(\rho, z)(PC_d)^{-1}LPu(t))^2. \tag{2.13}$$

Rearranging this equation, we obtain the equation

$$J_{VR}(\rho) = \frac{1}{N}\sum_{k=1}^{N}\left((C_d - C(\rho, z))C_d^{-1}Lu(t)\right)^2. \tag{2.14}$$

From this equation, if $C_d^{-1}Lu$ has a value, then $C(\rho)$ approaches C_d when $J_{VR}(\rho)$ becomes small. That is, even if model matching cannot be achieved, the closed-loop system has characteristics similar to those of the reference model.

Remark 2.2. The design of the prefilter is introduced. For simplicity, let $W(z) = 1$ in Equation (2.4). Adopting a previously reported approach [21], the following prefilter is introduced:

$$L = M_d(1 - M_d). \tag{2.15}$$

In the literature [28], the following prefilter is introduced:

$$L = M_d. \tag{2.16}$$

In the both cases, $\Phi_u^{1/2}$ can be used as a frequency-weighting function. The prefilters in Equations (2.15) and (2.16) differ; however, this difference is attributable to different derivation processes. The two prefilters are essentially equivalent. In the process of deriving both filters, the desired sensitivity function $1 - M_d$ is assumed to be close to the actual sensitivity function $\left(1 + PC(\hat{\rho})\right)^{-1}$ at the minimum value $\hat{\rho}$. In Equation (2.15), the prefilter is derived from the assumption after Parseval's equation is applied. By contrast, in Equation (2.16), the assumption is invoked before Parseval's equation is applied. The derivation process of the two prefilters is described as follows.

First, the derivation of the prefilter shown in Equation (2.15) is described. From the definition of 2-norm, Equation (2.4) can be written as

$$J_0(\rho) = \frac{1}{2\pi}\int_{-\pi}^{\pi} \frac{|P(e^{j\omega})|^2}{|1 + PC(\rho, e^{j\omega})|^2} \frac{|C_d(e^{j\omega}) - C(\rho, e^{j\omega})|^2}{|1 + P(e^{j\omega})C_d(e^{j\omega})|^2} d\omega,$$

or, more compactly, by dropping the argument $e^{j\omega}$:

$$J_0(\rho) = \frac{1}{2\pi}\int_{-\pi}^{\pi} \frac{|P|^2}{|1+PC(\rho)|^2}\frac{|C_d - C(\rho)|^2}{|1+PC_d|^2}d\omega, \tag{2.17}$$

where ω is the angular frequency. When Parseval's theorem is applied to Equation (2.10), as *N* approaches infinity, we obtain the equation

$$J_{VR}(\rho) = \frac{1}{2\pi}\int_{-\pi}^{\pi} |P|^2|(C_d - C(\rho)|^2|(1-M_d)|^2\frac{|L|^2}{|M_d|^2}\Phi_u\, d\omega, \tag{2.18}$$

where Φ_u is the power spectral density of u. By comparing Equations (2.17) and (2.18), we can describe the prefilter as

$$|L|^2 = \frac{|M|^2}{|1+PC(\rho)|^2}\frac{1}{\Phi_u}. \tag{2.19}$$

This equation is ρ-dependent. Here, using the assumption $\left(1+PC(\hat{\rho})\right)^{-1} \cong 1 - M_d$, we express the prefilter as

$$|L|^2 = |1-M|^2|M|^2\frac{1}{\Phi_u}. \tag{2.20}$$

Next, the derivation of the prefilter shown in Equation (2.16) is described. We consider following equation instead of Equation (2.11):

$$u_L(t) = L_u u(t), \bar{e}_L(t) = L_e\bar{e}(t) = L_e(M^{-1}-1)PL_y u, \tag{2.21}$$

where L_u, L_e, and L_y are suitable prefilters. Here, by applying the assumption $\left(1+PC(\hat{\rho})\right)^{-1} \cong 1 - M_d$ to Equation (2.4), we obtain the equation

$$J_0(\rho) = \|M_d - (1-M)PC(\rho))\|_2^2. \tag{2.22}$$

By applying Parseval's theorem to this equation, as *N* approaches infinity, we obtain the equation

$$J_0(\rho) = \frac{1}{2\pi}\int_{-\pi}^{\pi} |M_d|^2|1 - M_d|^2|P|^2|C(\rho)|^2\, d\omega. \tag{2.23}$$

In the same manner, by applying Parseval's theorem to Equation (2.10), as *N* approaches infinity, we obtain the equation

$$J_{VR}(\rho) = \frac{1}{2\pi}\int_{-\pi}^{\pi} |L_u|^2|C(\rho)|^2|L_e|^2|1 - M_d|^2|P|^2\big|L_y\big|^2\Phi_u\, d\omega. \tag{2.24}$$

Here, if the prefilters in Equation (2.21) are selected as

$$L_u = M_d\Phi_u^{1/2},\ \ L_e = C^{-1}(\rho)M_d,\ \ L_y = C(\rho)\Phi_u^{1/2}, \tag{2.25}$$

then Equations (2.23) and (2.24) match; however, the expressions in Equation (2.25) are ρ-dependent. Thus, we obtain Equation (2.26) by taking $L_u = L_e = L = M_d$ and $L_y = 1$ as feasible solutions:

$$J_{VR}(\rho) = \frac{1}{2\pi}\int_{-\pi}^{\pi} |M_d|^2|C(\rho)|^2|P|^2|1 - M_d|^2\Phi_u\, d\omega. \tag{2.26}$$

This equation can be read as the frequency-wise convex approximation of

$$J_0(\rho) = \left\|(M_d - (1 + C(\rho)P)^{-1}C(\rho)P))\Phi_u^{1/2}\right\|_2^2. \tag{2.27}$$

2.3 **Fictitious reference iterative tuning**

FRIT [22] [23] is a technique for automatically tuning the controller parameters of a closed-loop system from the controlled-object input/output data. Figure 2.3 shows the structure of the FRIT technique. $C(\rho, z)$, M_d, and P represent the fixed-order controller, which is parameterized through ρ, the reference model, and the controlled object, which is the LTI system, respectively. The FRIT procedure is described as follows:

[Step 1] The time-series input/output data $\{u(k)$ and $y(k)$; $k = 1,2,\ldots,N\}$ are obtained by conducting a closed-loop experiment using controller parameters that stabilize the system.

[Step 2] The reference model M_d, which is the desired closed-loop, is set.

[Step 3] Using the acquired initial input/output time-series data and the inverse of the controller, the fictitious reference signal [15] [44] can be calculated as

$$\tilde{r}(\rho, k) = C^{-1}(\rho)u(k) + y(k), \tag{2.28}$$

where $\tilde{r}$ is a fictitious reference signal and (u, y) constitutes the set of input/output time-series data measured in advance via an experiment.

[Step 4] On the basis of this fictitious reference signal, the cost function of FRIT can be expressed as

$$J_{FRIT}(\rho) = \frac{1}{N}\sum_{k=1}^{N}(\varepsilon(\rho, k))^2, \tag{2.29}$$

where

$$\varepsilon(\rho, k) = y_0(k) - M_d(z)\tilde{r}(\rho, k) \tag{2.30}$$

is minimized to obtain the optimal controller parameters.

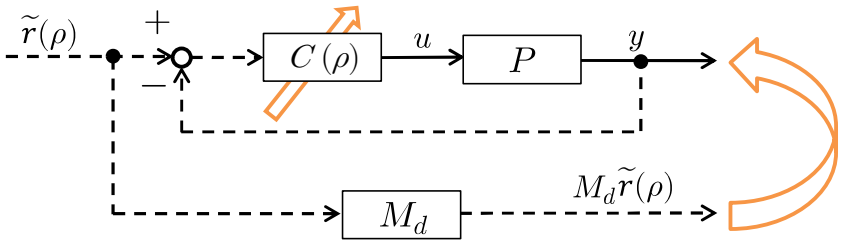

Figure 2.3. The FRIT concept.

Remark 2.3. Using Parseval's theorem, the interpretation of the cost function is explained. As *N* approaches infinity, we obtain the equation

$$J_{FRIT}(\rho) = \frac{1}{2\pi}\int_{-\pi}^{\pi}\left|\left(1-\frac{M_d(e^{j\omega})}{T(\rho,e^{j\omega})}\right)\right|^2 \Phi_y d\omega, \tag{2.31}$$

where

$$T = \frac{PC}{1+PC} \tag{2.32}$$

is the complementary sensitive function, Φ_y is the power spectral density of y, and ω is the angular frequency. The relative error between the reference model M_d and $T(\rho)$ is evaluated under a weighted controlled variable.

Remark 2.4. Unlike the VRFT, the FRIT does not involve a prefilter except in special cases. In other words, the relationship between the FRIT cost function and the model reference cost function is not clear.

2.4 **Conclusions**

In this chapter, the problem formulation and algorithm of VRFT/FRIT were explained, along with meaning of the cost function and the prefilter design methods of VRFT/FRIT. The key feature of VRFT/FRIT is that the controller parameters can be tuned using data obtained from a single experiment. However, the shortcomings of VRFT/FRIT are that an LTI system is assumed and stability is not guaranteed.

Chapter 3
Direct tuning method considering closed-loop stability

In this chapter, a direct tuning method based on a fictitious reference signal that considers the bounded-input bounded-output (BIBO) and an automatic tuning of a reference model for model matching from single-experiment data are proposed. The stability of the closed-loop system and model matching with few design parameters are important features. The direct tuning method to ensure the BIBO stability is introduced. The pole information is lost in the cost function of the conventional method using a fictitious reference signal. Therefore, a new cost function that can prevent the loss of polar information is derived. This approach provides controller parameters that can stabilize the closed-loop system. The parameters of the reference model are then automatically tuned to achieve model matching. In the tuning process, there are no design parameters apart from the dealing noise. Two simulations and an experiment were performed on a system with dead time to verify the effectiveness of the proposed method. The results show that the proposed method provides BIBO stability as well as model-matched control parameters from data collected via a single experiment (i.e., without trial and error). The contents in this chapter are based on the literature [45].

3.1 **Introduction**

Direct tuning methods such as VRFT [20] [21] and FRIT [22] [23] are attracting attention because they can be used to obtain optimal controller parameters via single-experiment input/output data of a controlled object for linear time-invariant (LTI) systems, as mentioned in Chapter 1. These methods are also currently used in industrial systems [29] [46] [47] [48] [49]. One of the problems associated with the data-driven control design methods is that the closed-loop system is not always stable when the obtained control parameters are used [37] [38] [39]. For example, a closed-loop system can be

destabilized using the control parameters obtained with a data-driven control design method that uses a fictitious reference signal [44]. This is likely to occur when an inappropriate reference model is given. This can be mitigated by applying a prefilter to the input and output data; subsequently, a power spectral density (PSD) function is required for designing the prefilter [21]. It is not difficult to estimate the PSD function of the initial input signals because VRFT uses the input/output data from open-loop experiments with random signals as its input signals; thus, a prefilter can be designed. However, although the PSD function is suitable for analyzing stationary random signals, it is not suitable for analyzing transient time-series signals. Therefore, it is difficult to estimate the PSD function using the input/output data obtained from a closed-loop experiment [50]. In addition, although the aforementioned problem can be avoided by tuning the reference model, this is a trial-and-error process. Thus, the control parameters cannot be obtained automatically in all the tuning processes.

Several methods have been proposed that consider data-driven control stability. Extended FRIT (E-FRIT) has been proposed [46] [47], in which the weight of the control input is included in the cost function. This method can effectively suppress any destabilization because of excessive fluctuations in the control input. However, this is not an essential improvement with respect to the general problem of closed-loop system destabilization. The data-driven control method considering the stability [38] [39] has been proposed based on the model validation knowledge in the time domain. However, (i) it takes time to calculate the singular values of the Toeplitz matrix and (ii) the stability must be confirmed each time optimization is performed. VRFT process that considers robust stability has been proposed for a control structure based on the IMC [29]; however, it cannot be applied to a PID controller. The data-driven control design methods are for model matching. In case of unfalsified control, a previous study [51] showed that the instability of a closed-loop system cannot be detected because unstable poles are canceled when calculating the transfer function, namely the sensitivity function, the input of which is the fictitious reference signal and the output of which is the error between the fictitious reference signal and the controlled-object output. Then, a new cost function was proposed to detect the instability of the closed-loop system [51] [52] [53]. Unlike the two aforementioned methods [29] [38] [39] [46] [47], the method proposed in another study [51] sets an cost function that minimizes the error between the target value and the

controlled-object output and is applied to unfalsified control, which switches online between multiple controllers designed in advance. In other words, it is not applied to a method for obtaining optimal control parameters based on model matching such as FRIT.

This study proposes a direct tuning method for the feedback controller parameters based on the fictitious reference signal considering the bounded-input bounded-output (BIBO) stability and an auto-tuning method of the reference model for model matching from single-experiment data. In the first step, BIBO stability is satisfied. Stability cannot be detected with respect to the cost function of the FRIT, which is a conventional data-driven control method that uses fictitious reference signals because of the loss of pole information. This problem is addressed by deriving a new FRIT cost function that retains the pole information using a transfer function (complementary sensitivity function) identified in the time domain, the input and output of which are the fictitious reference signal, which is a function of the control parameters, and the controlled-object output, respectively. Herein, FRIT that enables the detection of instability in a closed-loop system is referred to as instability-detecting FRIT (ID-FRIT). Therefore, parameters that stabilize the closed-loop system are obtained because the pole information is retained in the cost function of the ID-FRIT. In the second step, we aim to obtain the parameters for model matching. When model matching is realized, the characteristics including gain and phase margins between user-defined reference model and closed-loop system are almost identical. The controller parameters and the dead time that minimize the cost function are obtained by including the dead time as the tuning parameter in the cost functions of the ID-FRIT. Further, the parameters related to responsiveness are optimized by comparing the obtained reference-model dead time and the identified controlled-object dead time from the input/output data measured in advance, thereby ensuring that the reference-model and identified dead times match. In this way, the reference-model parameters that enable model matching can be obtained. Thus, we can obtain parameters for model matching by automatically tuning the reference-model parameters. In the conventional method, a designer is used to tune the reference-model parameters. The optimization of the reference-model parameters requires the usage of ID-FRIT to detect destabilization. The effectiveness of the proposed method is verified via two simulations and an experiment.

This chapter is arranged as follows. In Section 3.2, the problem formulation is described. Section 3.3 describes FRIT that considers stability. Section 3.4 describes the reference model parameter tuning. In Section 3.5, the effectiveness of the proposed control method is verified via simulation for two types of systems. In Section 3.6, experimental verification is conducted. For the controlled objects with dead time, the optimum control parameters of the conventional and proposed methods are obtained. By applying each set of obtained parameters to the closed-loop system, (i) ID-FRIT leads to BIBO stable control parameters, whereas standard FRIT leads to an unstable closed-loop system. (ii) Further, the parameters that realize model matching are obtained in the proposed method. Section 3.7 provides the conclusions of this chapter.

3.2 **Problem formulation**

The bounded-input bounded-output (BIBO) stability, the problem with conventional FRIT [22] [23], and the model reference control problem are described.

3.2.1 **Input/Output stability for an LTI system**

The input/output stability for an LTI system is explained herein. We consider the following LTI system:

$$\dot{x} = A_c x + B_c u, y = C_c x, \tag{3.1}$$

where $x \in R^n$ is the state, $u \in R^n$ is the control input, and $y \in R^r$ is the output. The matrices $A_c \in R^{n\times n}$, $B_c \in R^{n\times m}$, and $C_c \in R^{r\times n}$ are constant matrices. This system is said to be BIBO stable if the output for any bounded input is bounded (i.e., if $|u(t)| \leq M_u,\ t \geq 0$ for a bounded value M_u, then $|y(t)| \leq M_y,\ t \geq 0$ for another bounded value M_y is satisfied) when the initial state of the system is zero [4]. In the single-input single-output (SISO) system, the necessary and sufficient condition for the system to be BIBO stable is that the real part of all the poles of the transfer function

$$G(s) = C_c(sI - A_c)^{-1}B_c \tag{3.2}$$

is negative. More generally, a system is stable if and only if its transfer function is analytic in the right-half plane (RHP) [54]. If the system is controllable and observable, the eigenvalues of A_c and the poles of the transfer function will match because pole-zero cancellation does not occur when the state equation is transformed to a transfer function. That is, the conditions of asymptotic stability and BIBO stability match [6]. Conversely, if the system is not controllable and observable, then asymptotic stability is not satisfied even if BIBO stability is satisfied. Here, the system is said to be asymptotically stable if, for any initial value $x(0)$, the solution of $\dot{x} = A_c x$ is $\lim_{t\to\infty}\|x(t)\| = 0$.

3.2.2 **Problem with conventional FRIT**

The instability of a closed-loop system cannot be detected via conventional FRIT. This assertion is based on a method proposed by a previous study [51], which showed that the sensitivity functions with respect to the errors (the differences between the target values and controlled-object responses) and the fictitious reference signals cannot detect unstable poles because the sensitivity function does not contain pole information. Herein, we focus on the transfer function for the tracking error and the fictitious reference signal that we consider in FRIT.

Based on the z-transform of the tracking error of Equation (2.3), we obtain

$$\begin{aligned} E(z) &= Y(z) - M_d(z)R(z,\rho) \\ &= \left(\frac{P(z)C(z,\rho)}{1+P(z)C(z,\rho)} - M_d(z)\right) R(z,\rho) \end{aligned} \tag{3.3}$$

based on which unstable poles can be detected because Equation (3.3) retains the information about the poles of the closed-loop system.

Next, we consider the tracking error handled by the FRIT of Equation (2.30). The relation between the fictitious reference signal $\tilde{r}$ (the fictitious signal) and controlled variable y (the true signal) in the z-domain is

$$\begin{aligned}\widetilde{R}(z) &= ((P(z)C(z,\rho))^{-1}+1)Y(z)\\ &= \frac{1+P(z)C(z,\rho)}{P(z)C(z,\rho)}Y(z),\end{aligned} \tag{3.4}$$

where $Y(z) = P(z)U(z)$ was considered. From Equations (2.28), (2.30), and (3.4), the relation between the error handled by the FRIT and the fictitious reference signal can be given as follows:

$$\begin{aligned}E(z) &= Y(z) - M_d(z)\widetilde{R}(z,\rho)\\ &= \left(\frac{P(z)C(z,\rho)}{1+P(z)C(z,\rho)} - M_d(z)\right)\widetilde{R}(z,\rho)\\ &= \left(\frac{P(z)C(z,\rho) - M_d(z)\big(1+P(z)C(z,\rho)\big)}{P(z)C(z,\rho)}\right)Y(z).\end{aligned} \tag{3.5}$$

This equation shows that no pole can be obtained because of the pole-zero cancelation. Thus, the closed-loop system may become unstable when the control parameter that minimizes the cost function shown in Equation (2.30) is obtained.

3.2.3 **Model reference control problem**

We consider a general feedback control system with a reference model, as shown in Figure 2.1. Refer to Section 2.1 for details. For the model reference control, we aim to obtain the direct tuning method that ensures closed-loop BIBO stability based on a fictitious reference signal and construct a reference model tuning method.

3.3 **Direct tuning guaranteed BIBO stability**

This section presents (i) the derivation of the FRIT cost functions considering the detection of destabilization to ensure that the closed-loop system exhibits BIBO stability and (ii) a method optimizing the reference-model parameters for model matching. Thus, if model matching is realized, the gain and phase margins of the reference model and the closed-loop stability are almost identical. In other words, the gain and phase margins are indirectly considered through the realization of model matching.

3.3.1 **Derivation of the new cost function**

The cost function is derived by considering destabilization detection to obtain the parameters based on which closed-loop BIBO stability can be achieved. Stability can be evaluated by applying the target value r to the complementary sensitivity function for the controller $C(z,\rho)$ and calculating its output y^*. The relation between the target value and the output of the closed-loop system is

$$Y^*(z) = \frac{P(z)C(z,\rho)}{1+P(z)C(z,\rho)}R(z). \tag{3.6}$$

Because $P(z)$ is unknown, the complementary sensitivity function of the controller $C(z,\rho)$ to be tuned can be written as

$$\tilde{T}(z) = \frac{Y_0(z)}{\widetilde{R}(z)} = \frac{Y_0(z)}{C^{-1}(z,\rho)U_0(z)+Y_0(z)} \tag{3.7}$$

using the controlled-object input/output data u_0, y_0 acquired in advance. When the complementary sensitivity function in the frequency domain is identified as shown in Equation (3.7), we require (i) the application of the parametric identification method using an ARX model or similar models and (ii) information about the order of the controlled object.

Here, the complementary sensitivity function is identified in the time domain to automatically tune the control parameters without using prior information such as the model structure and order. In the time domain, the relation between the fictitious reference signal and the controlled-object output is

$$y_0(k) = \tilde{t}(k) * \tilde{r}(\rho,k), \tag{3.8}$$

where $*$ indicates convolution and $\tilde{t}(k)$ is the impulse response of $\tilde{T}(s)$. Further,

$$\boldsymbol{y}_0 = \widetilde{\boldsymbol{R}} \cdot \tilde{\boldsymbol{t}}, \tag{3.9}$$

where

$$\boldsymbol{y}_0 = [y_0(1) \quad \cdots \quad y_0(N)]^T, \tag{3.10}$$

$$\widetilde{\boldsymbol{R}} = \begin{bmatrix} \tilde{r}(\rho,1) & 0 & 0 & \ddots & 0 \\ \vdots & \tilde{r}(\rho,1) & 0 & \ddots & 0 \\ \tilde{r}(\rho,N-2) & \ddots & \tilde{r}(\rho,1) & 0 & \vdots \\ \tilde{r}(\rho,N-1) & \tilde{r}(\rho,N-2) & \ddots & \ddots & 0 \\ \tilde{r}(\rho,N) & \tilde{r}(\rho,N-1) & \tilde{r}(\rho,N-2) & \cdots & \tilde{r}(\rho,1) \end{bmatrix}, \tag{3.11}$$

$$\tilde{\boldsymbol{t}} = [\tilde{t}(1) \quad \cdots \quad \tilde{t}(N)]^T. \tag{3.12}$$

Here, $\tilde{\boldsymbol{t}}$, which is the impulse response of the complementary sensitivity function, is a deconvolution of the fictitious reference signal $\tilde{r}$ and the output y_0 from Equation (3.8). It can be obtained by transforming Equation (3.9) as

$$\tilde{\boldsymbol{t}} = \widetilde{\boldsymbol{R}}^{-1} \cdot \boldsymbol{y}_0. \tag{3.13}$$

Next, the output when the target value is applied to the complementary sensitivity function is

$$y^*(k) = \tilde{t}(k) * r(k), \tag{3.14}$$

which is calculated by considering

$$\boldsymbol{y}^* = \boldsymbol{R} \cdot \tilde{\boldsymbol{t}}, \tag{3.15}$$

where

$$\boldsymbol{y}^* = [y^*(\rho,1) \quad \cdots \quad y^*(\rho,N)]^T, \tag{3.16}$$

$$\boldsymbol{R} = \begin{bmatrix} r(1) & 0 & 0 & \ddots & 0 \\ \vdots & r(1) & 0 & \ddots & 0 \\ r(N-2) & \ddots & r(1) & 0 & \vdots \\ r(N-1) & r(N-2) & \ddots & \ddots & 0 \\ r(N) & r(N-1) & r(N-2) & \cdots & r(1) \end{bmatrix}. \tag{3.17}$$

As described above, the output y^* contains pole information because y^* is calculated using $\tilde{\boldsymbol{t}}$, as shown in Equation (3.15). The sum of squares of the error ε^* between output y^* and the reference model output is a cost function that contains pole information of the closed-loop system:

$$J^*(\rho) = \frac{1}{N}\sum_{k=1}^{N}\left(\varepsilon^*(\rho,k)\right)^2, \tag{3.18}$$

$$\varepsilon^*(\rho,k) = y^*(\rho,k) - M_d(z)r(k). \tag{3.19}$$

The standard FRIT tunes the fictitious reference signal, which is a function of the controller parameters, to match the measured controlled-object output y_0. The proposed method tunes the controlled-object output, which is a function of the control parameters, to ensure that the controlled-object output y^*, which is the predicted value, matches the reference-model output. The standard FRIT obtains the controller parameters to match the controlled-object output measured in advance via an experiment, whereas the proposed method obtains the control parameters to match the reference model output.

As described above, the parameter tuning algorithm is as follows. The part after Step 1-1 differs from the conventional FRIT and is the part in which stability is considered.

[Step 0] Measure the input/output data of the controlled object.

The input/output data u_0, y_0 of the closed-loop system are measured using the initial values of the controller parameters. How to deal with noise is discussed in Section 3.3.2.

[Step 1-1] Calculate the fictitious reference signal.

The fictitious reference signal is calculated from the acquired input/output data obtained using Equation (2.28).

[Step 1-2] Compute complementary sensitivity functions in the time domain.

The complementary sensitivities are obtained from Equation (3.13) using the calculated fictitious reference signal and the controlled-object outputs acquired in Step 0.

[Step 1-3] Calculate the outputs of complementary sensitivity functions.

The output y^* of the complementary sensitivity function when the target value is applied is obtained from Equation (3.15).

[Step 1-4] Optimal parameters calculated by minimizing the cost function J^*.

The controller parameter ρ that minimizes the cost function (3.18) is obtained using an optimization technique.

Using this algorithm, we can obtain the controller parameters that ensure BIBO stability, whereas the conventional FRIT does not ensure BIBO stability because the pole information is lost.

Remark 3.1. Poles are not directly calculated in this algorithm. Instead, we use the output y^* calculated using Equation (3.15) because the complementary sensitivity function $\tilde{t}$ contains pole information. Therefore, the convergence of the control parameters that cause the closed-loop system to become unstable can be avoided when the cost function involving y^* is minimized.

Remark 3.2. There are many global optimization methods, such as particle swarm optimization (PSO) [55] [56], the covariance matrix adaptation evolution strategy (CMA-ES) [57], and differential evolution (DE) [58]. In this chapter, PSO is used.

Remark 3.3. The interpretation of the cost function using Parseval's theorem is described. As *N* approaches infinity, we obtain the equation

$$J^*(\rho) = \frac{1}{2\pi}\int_{-\pi}^{\pi}\left|\left(1-\frac{M_d(e^{j\omega})}{T(\rho,e^{j\omega})}\right)\right|^2 \Phi_r \mathrm{d}\omega, \tag{3.20}$$

where

$$T = \frac{PC}{1 + PC} \tag{3.21}$$

is the complementary sensitive function and Φ_r is the power spectral density of r. The relative error between the target reference model M_d and T is evaluated. Unlike the conventional FRIT shown in Equation (2.31), the ID-FRIT cost function does not depend on the initial controller parameters.

3.3.2 **Dealing with noise**

In an actual environment, the input/output data contain observation noise. In the open-loop test, the output is

$$y(k) = P(z)u(k) + n(k), \tag{3.22}$$

where n is the white noise. In case of the closed-loop test, the measured input and output are

$$\begin{aligned} y(k) &= \frac{P(z)C(z,\rho)}{1 + P(z)C(z,\rho)} r(k) + \frac{1}{1 + P(z)C(z,\rho)} n(k), \\ u(k) &= \frac{C(z,\rho)}{1 + P(z)C(z,\rho)} \big(r(k) - n(k)\big). \end{aligned} \tag{3.23}$$

The r component of y is the low-pass characteristic of the complementary sensitivity function, which exhibits attenuation in the high-frequency range. Additionally, the n component of y is the high-pass characteristic of the sensitivity function, and it is coordinated in the high-frequency range. Therefore, for y, the signal-to-noise ratio (S/N) in the high-frequency range becomes worse. Further, if r and n are assumed to be a step signal and white noise, respectively, the S/N at high frequencies also deteriorates for u [59].

As shown in Equation (3.24), the total variation denoising is used to eliminate noise from the time-series data of the controlled-object output and control input with added noise. This method is based on the regression problem and noisy data are restored to

denoised data. In image processing, the L_1 norm is commonly used as the regularization term; however, in case of time-series data, the L_2 norm is adopted as the regularization term because the L_1 norm tends to be a staircase signal. The denoising equation is described as

$$\begin{aligned} &\min_{\boldsymbol{y_f}} \|\boldsymbol{y_f} - \boldsymbol{y_0}\|_2^2 + \lambda_r \|\boldsymbol{\psi} \boldsymbol{y_f}\|_2^2, \\ &\min_{\boldsymbol{u_f}} \|\boldsymbol{u_f} - \boldsymbol{u_0}\|_2^2 + \lambda_r \|\boldsymbol{\psi} \boldsymbol{u_f}\|_2^2, \end{aligned} \tag{3.24}$$

where

$$\boldsymbol{\psi} = \begin{bmatrix} -1 & 1 & 0 & \cdots & 0 \\ 0 & -1 & 1 & \ddots & \vdots \\ \vdots & \ddots & \ddots & \ddots & 0 \\ 0 & \cdots & 0 & -1 & 1 \\ 0 & \cdots & 0 & 0 & 0 \end{bmatrix}. \tag{3.25}$$

Here, $\boldsymbol{y_0} = [y_0(1) \quad y_0(2) \quad \cdots \quad y_0(N)]^T$ and $\boldsymbol{u_0} = [u_0(1) \quad u_0(2) \quad \cdots \quad u_0(N)]^T$ denote the time-series raw data vector of the output and the input of the controlled object with noise. $\boldsymbol{y_f} = [y_f(1) \quad y_f(2) \quad \cdots \quad y_f(N)]^T$ and $\boldsymbol{u_f} = [u_f(1) \quad u_f(2) \quad \cdots \quad u_f(N)]^T$ denote the denoised time-series data vector of the output and the input of the controlled object. N is the length of the raw data. $\boldsymbol{\psi}$ is a matrix with size $N \times N$. The first term of Equation (3.24) is used to find the data $\boldsymbol{y_f}$ or $\boldsymbol{u_f}$, which are close to the observed raw data $\boldsymbol{y_0}$ or $\boldsymbol{u_0}$ with noise. The second term (total variation) indicates that the adjacent data about $\boldsymbol{y_f}$ or $\boldsymbol{u_f}$ must not change considerably. The strength of relative smoothing can be adjusted using the design parameter λ_r. The optimal solutions of Equation (3.24) can be obtained using the least-squares method as follows:

$$\begin{aligned} \boldsymbol{y_f^*} &= (I + \lambda_r \boldsymbol{\psi}^T \boldsymbol{\psi})^{-\mathbf{1}} \boldsymbol{y_0}, \\ \boldsymbol{u_f^*} &= (I + \lambda_r \boldsymbol{\psi}^T \boldsymbol{\psi})^{-\mathbf{1}} \boldsymbol{u_0}, \end{aligned} \tag{3.26}$$

where I is the identity matrix with size $N \times N$.

Summarizing the aforementioned equations as Step 0 in the algorithm, the denoising process is as follows:

[Step 0-1] Measure the input/output data of the controlled object

The raw input/output time-series data is obtained via an experiment.

[Step 0-2] Perform the denoising process

The denoised input/output time-series data measured in Step 0-1 is obtained using Equation (3.26).

This algorithm provides the denoised input/output data, which are used in the control parameters optimization.

Remark 3.4. In the previous literature [60], a denoising method on the data in the frequency domain by Fourier transforming the time series data has been proposed, and a significant noise removal effect has been obtained. However, the conditions for executing the Fourier transform are that data is absolutely integrable and is periodic. The step response is not a periodic signal and cannot be directly Fourier transformed, so some measures are required. On the other hand, the proposed method removes noise directly from the time series data, and only the above algorithm needs to be applied.

3.4 **Parameter tuning for the reference model**

Conventionally, the reference-model parameters are tuned by the designer in a trial-and-error manner because performance degradation can be observed when using an inappropriate reference model [61]. The characteristics, including the gain and phase margins of the system and those of the reference model, are considered to be almost identical when model matching is realized. In other words, the gain and phase margins can be indirectly considered before implementing the controller by realizing model matching. Herein, a technique to optimize the reference-model parameters is proposed for model matching using dead times. First, dead times are identified from the

input/output data acquired in Step 0 of the algorithm. Next, a variable reference model in which dead time is considered as a tuning parameter is introduced as follows:

$$\begin{aligned} M_d(z, L_{est}) &= z\big(M_d(s, L_{est})\big), \\ M_d(s, L_{est}) &= M_{d0} e^{-L_{est}s} \\ &= \frac{\omega_0^n}{s^n + \gamma_{n-1}\omega_0 s^{n-1} + \cdots + \gamma_1 \omega_0^{n-1} s + \omega_0^n} e^{-L_{est}s}, \end{aligned} \tag{3.27}$$

where s is the Laplacian operator, L_{est} is a tuning parameter related to the dead time, ω_0 is a design parameter related to responsiveness, γ is a design parameter for determining the characteristics of the reference model, and $z()$ is an operator for converting from the continuous time domain to the discrete time domain. The controller parameters and dead time can be estimated by replacing the reference model of the cost function in Equation (3.18) with a variable reference model and minimizing the cost function

$$J^*(\rho, L_{est}) = \frac{1}{N}\sum_{k=1}^{N} \varepsilon^*(\rho, L_{est}, k)^2, \tag{3.28}$$

$$\varepsilon^*(\rho, L_{est}, k) = y^*(\rho, k) - M_d(L_{est}, z) r(k). \tag{3.29}$$

At this time, the controller parameters and reference-model dead time that minimize the cost function of Equation (3.28) are obtained via optimization calculation. If the obtained reference-model dead time coincides with the identified controlled-object dead time, then the parameters for which model matching can be realized using a controller of the specified order are found. However, if the reference-model dead time does not coincide with the identified one, then either the order of the controller must be increased or the target reference response must be decelerated. Thus, the appropriate reference-model parameters are tuned automatically. The algorithm is as follows.

[Step 2-1] Dead times are identified from the input/output data acquired in advance.

[Step 2-2] Controller parameters and reference-model dead time are estimated that minimize the FRIT cost functions considering the detection of destabilization

(i.e., ID-FRIT proposed in Step 1), including variable reference models, as shown in Equation (3.28).

[Step 2-3] Tuning of parameters related to the responsiveness of the reference model.

(a) Estimated reference model dead time > identified dead time: (a-1) or (a-2)

(a-1) Increase the reference-model responsiveness parameter as $\tau_M \leftarrow \tau_M + \Delta\tau_M$

(a-2) Increase the order of the controller.

(b) Estimated reference model dead time <= identified dead time: End

Else: Return to Step 2-2.

Remark 3.5. ID-FRIT needs to be used in this algorithm. In the case where the conventional FRIT is used, we may not obtain an appropriate responsiveness parameter in Step 2 because the closed-loop system may become unstable when the cost function based on conventional FRIT (see Equation (2.29)) is minimized. Thus, Step 2 requires the ID-FRIT proposed in Step 1.

Remark 3.6. This algorithm aims to bring the system closer to the reference model. However, it does not explicitly consider model matching; thus, it does not always provide model matching. To ensure model matching, the tracking error can be treated as a constraint condition [62].

Remark 3.7. In this study, we considered the problem of model matching; however, because the output from the Step 1 algorithm can be predicted, the cost function can be set without using the reference model. The reason for setting the model matching problem in this study is to reflect the characteristics of the reference model to the closed-loop system by realizing model matching.

3.5 **Simulation verification**

The proposed method was verified via two numerical simulations. One numerical simulation is a process system without and with noise, whereas the other is a spring-mass system with noise. The formulation of a reference model and the controller used in this

section are described. Similar to that in previous studies [33] [35] [63], the reference model is a second-order binomial-coefficient standard form in which no overshoot occurs, i.e.,

$$\begin{aligned} M_d(z) &= z\big(M_d(s)\big), \\ M_d(s) &= \frac{1}{(\tau_M s+1)^2}, \end{aligned} \tag{3.30}$$

where τ_M is a parameter related to the responsiveness of the system. The controller $C(z,\rho)$ is the PID controller and can be given as

$$C(z,\rho) = \rho^T \phi(z) \tag{3.31}$$

with

$$\rho = [K_p \quad K_i \quad K_d]^T, \tag{3.32}$$

$$\begin{aligned} \phi(z) &= z\big(\phi(s)\big), \\ \phi(s) &= \left[1 \quad \frac{1}{s} \quad \frac{s}{\tau_d s+1}\right]^T, \end{aligned} \tag{3.33}$$

where K_p, K_i, and K_d are the proportional, integral, and differential gains, respectively. In this study, because a PID controller is used, Step 2-3(a-1) of increasing the responsiveness parameter of the reference model is performed instead of changing the order of the controller. The controller and controlled object are discretized by a zero-order hold.

3.5.1 **Application to system 1: Process system**

The controlled object P is an actual process system [35] [36] [63] often considered to be a numerical example or benchmarking problem of data-driven control. Moreover, the dead time L is added to the system [63]. Many industrial systems involve dead times, as indicated by the delays in the transport of materials and the transmission of signals, making it considerably difficult to obtain stable parameters. Therefore, the effectiveness

of the proposed method is shown for a system with added dead time. The controlled object is

$$\begin{aligned} y(k) &= P(z)u(k) + n(k), \\ P(z) &= z\big(P(s)\big), \\ P(s) &= \frac{12s + 8}{20s^4 + 113s^3 + 147s^2 + 62s + 8} e^{-Ls}, \end{aligned} \tag{3.34}$$

where L is the dead time and n is the white noise. The sampling period is 100 ms. The parameter sets are presented in Table 3.1, and the simulation is performed for conditions 1 and 2. In condition 1, by assuming that model matching is possible, the controlled object has no dead time and the responsiveness parameter of the reference model is set to a large value. In condition 2, by assuming that model matching cannot be performed, the controlled object has a dead time and the responsiveness parameter of the reference model is set to a small value. The dead time values are the same as those in the literature [63] [64], and the conventional and proposed methods are compared in simulations under these two conditions.

Table 3.1. System and control parameters for the process system.

Symbol	Value	
	Condition 1	Condition 2
L	0	5
τ_M	5	1
K_p (initial)	0.5	0.5
K_i (initial)	0.05	0.05
K_d (initial)	0.01	0.01
τ_d	0.1	0.1
L_{est}	0	0

3.5.1.1 **Simulation results**

[Case 1: Ideal condition]

The proposed method is verified by considering the ideal condition; thus, the variance of white noise shown in Equation (3.34) is zero.

First, we confirm the effectiveness of ID-FRIT using Step 1 of the algorithm. Figure 3.1 shows the time history when the initial parameter values are used. Figure 3.2 shows the time history of the input/output data with the conventional FRIT and the proposed method when the step input under condition 2 is applied to the closed-loop system. Figure 3.3 shows the values of the cost function for a particular number of PSO iterations. Although Figure 3.3 shows that the cost functions of the standard FRIT converge, the output data of the standard FRIT shown in Figure 3.2 are divergent. In contrast, in the proposed method, the controller parameters that stabilize the closed-loop system are obtained even when model matching cannot be realized. The simulation results are presented in Table 3.2, which is used in the discussion section.

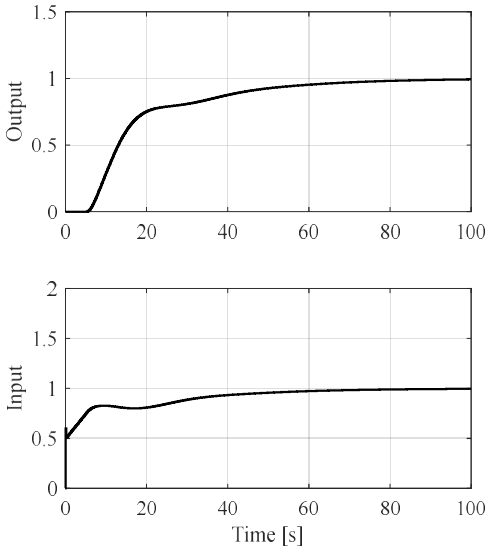

Figure 3.1. Input and output time series data with the initial PID gain for the ideal process. Dead time is 5.0 s.

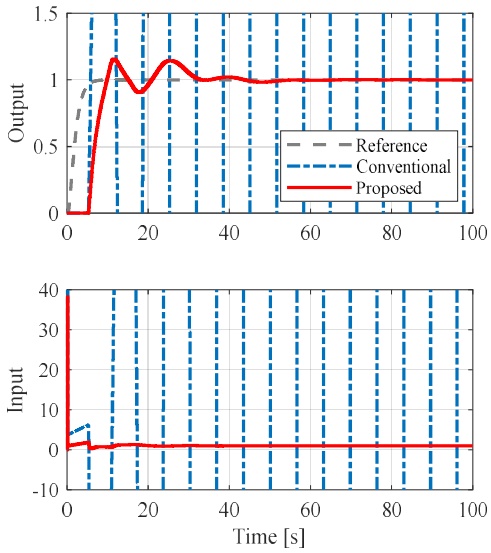

Figure 3.2. Input and output time series data with the conventional and proposed methods under condition 2 for an ideal process.

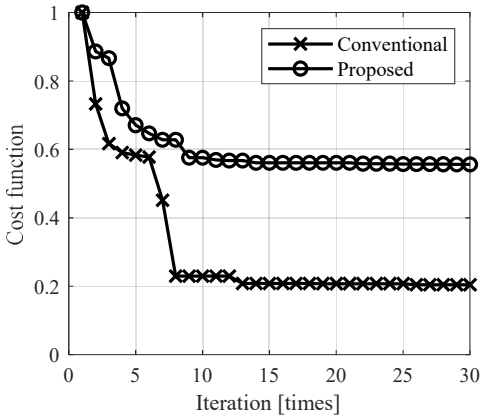

Figure 3.3. Relationship between the normalized cost function and optimization iterations.

Table 3.2. Tuned parameters in all conditions with the conventional and proposed method for the ideal process system.

Symbol	Condition 1		Condition 2	
	Conventional	Proposed	Conventional	Proposed
K_p	0.3711	0.3734	3.7406	0.9879
K_i	0.1008	0.1009	0.4876	0.1671
K_d	0.0094	0.0064	20.064	3.7261
J_{FRIT}	1.0781×10^{-6}	-	1.8223×10^{-4}	-
J^*	-	1.0693×10^{-6}	-	3.6590×10^{-2}
J_0	1.3820×10^{-5}	1.5066×10^{-5}	6.2087×10^{13}	3.6649×10^{-2}
Stability	Stable	Stable	Unstable	Stable

Next, we confirm the effectiveness of the reference-model optimization method by applying Step 2 of the algorithm. The reference model with a tunable parameter L_{est}, which is added to Equation (3.30), is used as described in Section 3.4. The controlled-object dead time is 5.0 s from Table 3.1. Figure 3.4 shows the time histories of the closed-loop system using the parameters obtained before and after applying Step 2 of the algorithm. The dead time of the variable reference model before optimization is fixed to 5.0 s to match the conditions before and after the application of Step 2 of the algorithm. Figure 3.4(a) shows the time-series data obtained before applying the optimization algorithm, and Figure 3.4(b) shows the time-series data obtained after optimizing the responsiveness parameter. In Figure 3.4(a), the responsiveness parameter is not optimized and the response is vibrational. In contrast, Figure 3.4(b) shows that the parameter related to the responsiveness of the reference response is optimized. Further, the actual response can follow the reference response under a controller of the specified order. Thus, a response close to the characteristics desired by the designer can be realized. The simulation results are summarized in Table 3.3, which is used in the discussion section.

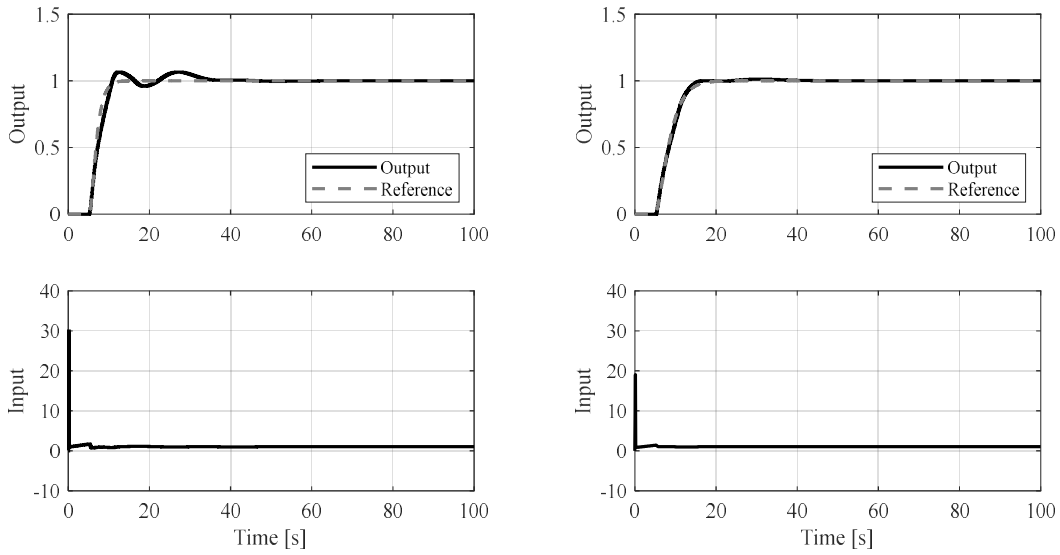

Figure 3.4. Input and output time series data for the ideal process (a) before and (b) after tuning by Step 2.

Table 3.3. Tuned parameters including the reference model for an ideal process system.

Symbol	Before tuning	After tuning
τ_M	1.0 (given by designer)	2.0
L_{est}	5.0 (identified by Step 2-1)	4.6997
K_p	0.9563	0.8719
K_i	0.1440	0.1155
K_d	2.9003	1.8231
J^*	1.5321×10^{-3}	5.6789×10^{-5}
J_0	9.9596×10^{-4}	7.8718×10^{-5}

[Case 2: Noisy condition]

The proposed method is verified for the process system with noise by assuming a real environment; therefore, the variance of white noise shown in Equation (3.34) is 5×10^{-3}.

First, we confirm the effectiveness of ID-FRIT with respect to Step 1 of the algorithm. Figure 3.5(a) shows the time history of the raw and denoised input/output data of the closed-loop system when the initial parameter values are used, and λ_r is set to 10. The denoised data is obtained using Equation (3.26). Figure 3.5(b) shows the enlarged view of the output. From the figure, we can obtain the identified dead time of 6.5 s, and this value is used in Step 2 of the algorithm. The denoising method is confirmed to work effectively. Figure 3.6 shows the time history of the input/output data with the conventional FRIT and the proposed method when the step input under condition 2 is applied to the closed-loop system. The output data of the standard FRIT shown in Figure 3.6 are divergent. In contrast, in the proposed method, controller parameters that stabilize the closed-loop system are obtained even when model matching cannot be realized. The simulation results are summarized in Table 3.4, which is used in the discussion section.

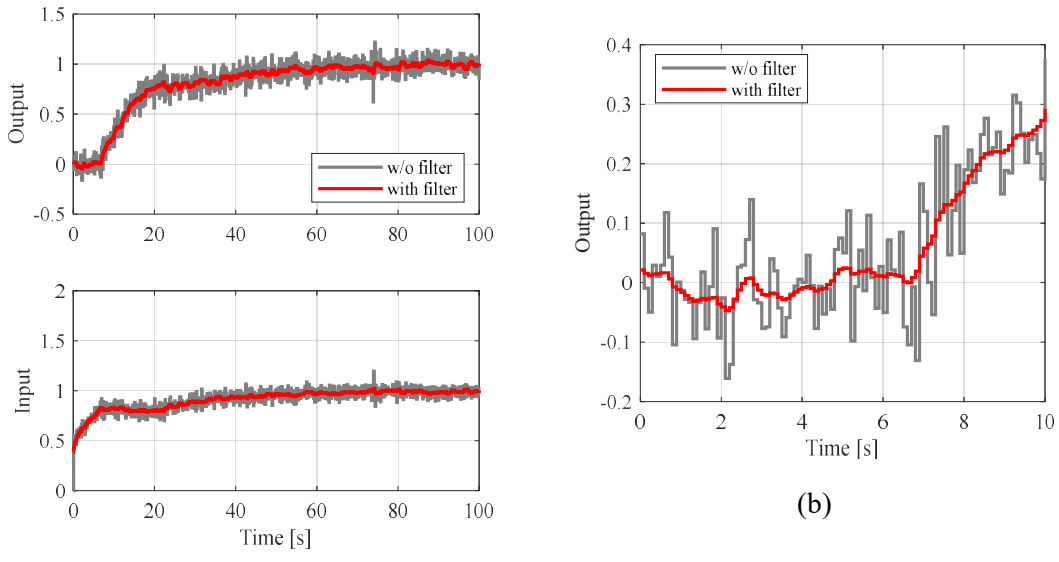

Figure 3.5. Time-series data without and with the filter using the initial PID gain (λ_r = 10). (a) Overview of the input and output. (b) Enlarged view of the output.

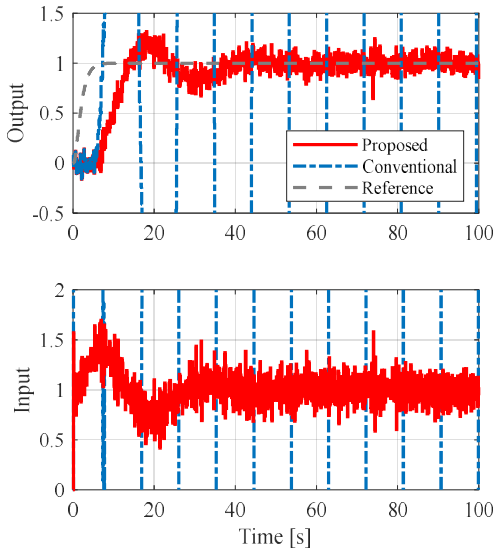

Figure 3.6. Input and output time series data with the conventional and proposed methods under condition 2 for the process with noise.

Table 3.4. Tuned parameters in both conditions with conventional and proposed methods for the process system with noise.

Symbol	Condition 1		Condition 2	
	Conventional	Proposed	Conventional	Proposed
K_p	0.3538	0.3442	5.6971	0.8730
K_i	0.1001	0.1006	0.4065	0.0915
K_d	0.0989	0.0223	3.1632	0.0857
J_{FRIT}	4.1164×10^{-4}	-	9.8933×10^{-4}	-
J^*	-	2.9524×10^{-4}	-	6.1928×10^{-2}
J_0	5.2281×10^{-3}	5.2539×10^{-3}	1.1385×10^{10}	6.6092×10^{-2}
Stability	Stable	Stable	Unstable	Stable

Next, we confirm the effectiveness of the reference-model optimization method with respect to Step 2 of the algorithm. The reference model with a tunable parameter L_{est}, which is added to Equation (3.30), is used as described in Section 3.4. Here, we assume that the controlled-object dead time is identified in Step 2-1 as 6.5 s from Figure 3.5(b). Figure 3.7 shows the time histories of the closed-loop system using the parameters

obtained before and after applying Step 2 of the algorithm. The dead time of the variable reference model before optimization is fixed to 6.5 s to match the conditions before and after applying the optimization algorithm. Figure 3.7(a) shows the time-series data before applying Step 2 of the algorithm, and Figure 3.7(b) shows the time-series data obtained after optimizing the responsiveness parameter. In Figure 3.7(a), the responsiveness parameter is not optimized and the response is vibrational. In contrast, Figure 3.7(b) shows that the parameter related to the responsiveness of the reference response is optimized. The actual response can follow the reference response under the controller of the specified order. Thus, a response close to the characteristics desired by the designer can be obtained. The simulation results are summarized in Table 3.5, which is used in the discussion section.

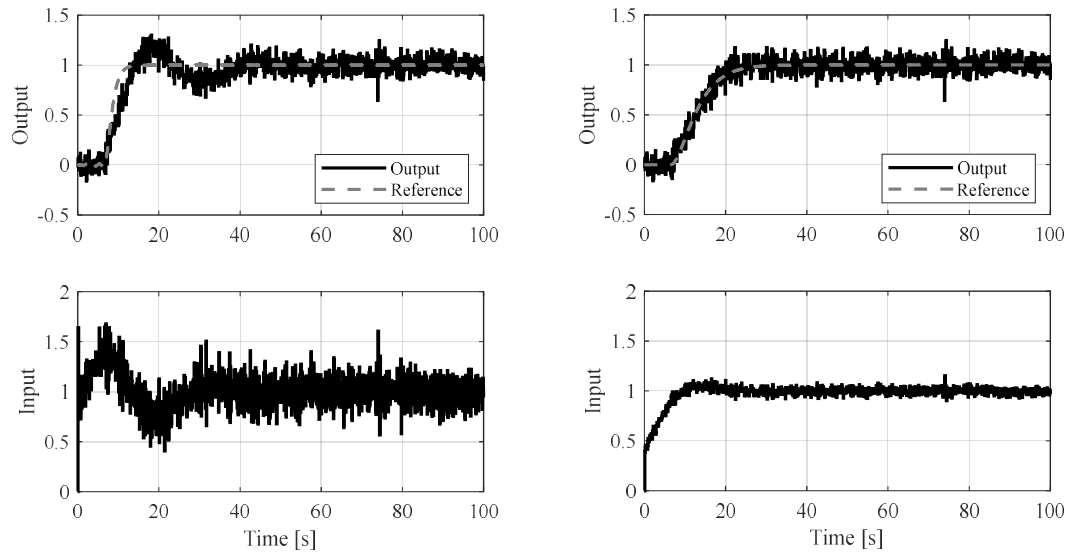

Figure 3.7. Input and output time series data for the process with noise (a) before and (b) after tuning by Step 2.

Table 3.5. Tuned parameters including the reference model for the process system with noise.

Symbol	Before tuning	After tuning
τ_M	1 (given by designer)	3.5
L_{est}	6.5 (identified by step2-1)	6.3781
K_p	0.8538	0.4210
K_i	0.0942	0.0745
K_d	0.0933	0.0005
J^*	6.1938×10^{-2}	5.5985×10^{-4}
J_0	1.1907×10^{-2}	5.4505×10^{-3}

3.5.1.2 **Discussion about system 1**

From Table 3.2 and Table 3.4, the conventional and proposed methods almost provide the same performance when comparing the cost function J_0 values under condition 1. This is because the reference model that can easily realize model matching is provided. Under condition 2, model matching cannot be realized because the responsiveness parameter of the reference model is considerably small for the system and the closed-loop system based on the parameters obtained using the standard FRIT is divergent. In contrast, the proposed method results in parameter values that stabilize the closed-loop system. Thus, the proposed method, i.e., ID-FRIT, can effectively obtain parameters that can ensure the closed-loop BIBO stability. From Table 3.3 and Table 3.5, the PID gains after Step 2 of the algorithm are smaller than those before the application of this step of the algorithm, and the cost function after Step 2 of the algorithm is better than that before the application of this step of the algorithm. Thus, the control performance and stability can be improved by optimizing the reference model. If the ID-FRIT that considers the detection of the destabilization shown in Step 1 is not used, instability may be encountered in the middle of the algorithm.

Thus, the proposed method is effective because the (i) controller parameters (PID gains) are obtained, which makes the closed-loop BIBO stable. Also, (ii) the characteristics of

the closed-loop system are similar to those of the reference model because model matching is realized. Hence, the gain and phase margins of the reference model and the closed-loop stability are almost identical. By obtaining the loop transfer function for the reference model, the gain and phase margins can be predicted even if the controlled-object characteristics are unknown; therefore, the gain and phase margins can be considered. For instance, if the reference model is a binomial-coefficient standard form, a Butterworth standard form, an integral of time weighted absolute error (ITAE) minimum standard form, or the like, then the reference model has a constant phase margin, gain margin, and overshoot rate regardless of the responsiveness parameters. Therefore, the designer can positively consider the gain and phase margins. In this simulation, the reference model is selected to the binomial-coefficient standard form, the poles of which have a real part, as shown in Equation (3.30). Thus, the designer demands characteristics with no overshoot, and the characteristics are realized after Step 2 of the algorithm. With respect to the results obtained using the controlled object without noise, the gain and phase margins of the reference model are 8.301 dB and 63.71°, respectively. In addition, the gain and phase margins of the closed-loop system using the obtained parameters by applying the proposed method are 7.913 dB and 64.63°, respectively. In case of the results obtained with respect to the controlled object with noise, the gain and phase margins of the reference model are 9.867 dB and 65.78°, respectively. Further, the gain and phase margins of the closed-loop system using the obtained parameters by applying the proposed method are 9.811 dB and 64.70°, respectively. Thus, a controller equivalent to the user-defined reference model characteristics can be obtained.

In addition, some supplementary contents are provided. The difference between the proposed method and the previous study [63] is presented. In the literature, the controller parameters, the reference-model parameters, and the dead time are tuned without considering BIBO stability. Thus, we cannot predict whether the closed-loop system is stable until the controller is implemented. On the other hand, the proposed method provides BIBO stability and model matching before the controller is implemented. The identification of dead time is not necessary when considering only BIBO. If we consider model matching along with BIBO, we must know the dead time used in Step 2 of the algorithm. However, the proposed method does not require any design parameters except for the dealing noise. Previous studies have not described how to deal with noise. Also,

the responsiveness parameter of the reference model in the proposed method is smaller than that in the literature. This is because the low-pass filter of the differential term is different. The set value is considered to be appropriate from the results with the noisy condition and previous studies [33] [35].

3.5.2 **Application to system 2: Spring-mass system**

In this section, the proposed method is applied to a spring-mass system with a response lag and dead time; this system has a time constant faster than that of the process system. Spring-mass systems are often used in many industries. A system with noise is only described because the principle of the proposed method has been confirmed under the ideal process system. The controlled object can be given as follows:

$$\begin{aligned} y(k) &= P(z)u(k) + n(k), \\ P(z) &= z\big(P(s)\big), \\ P(s) &= \frac{1}{(0.01s+1)(0.1s^2+0.5s+5)}e^{-Ls}. \end{aligned} \tag{3.35}$$

The variance of white noise n is 5×10^{-3} when assuming a real environment. The sampling period is 4 ms. The parameter sets are given in Table 3.7, and the simulation is performed for conditions 1 and 2. In condition 1, model matching is assumed to be possible, whereas in condition 2, model matching is assumed to be not achieved. The conventional and proposed methods are compared in simulations under these two conditions.

Table 3.6. System and control parameters for the spring-mass system.

Symbol	Value	
	Condition 1	Condition 2
L	0	0.1
τ_M	1	0.005
K_p (initial)	1.0	1.0
K_i (initial)	0.5	0.5
K_d (initial)	0.02	0.02
τ_d	0.01	0.01
L_{est}	0	0

3.5.2.1 **Simulation results under noisy condition**

First, we confirm the effectiveness of ID-FRIT with respect to Step 1 of the algorithm. Figure 3.8(a) shows the time history of the raw and denoised input/output data of the closed-loop system when the initial parameter values are used, and λ_r is set to 10. The denoised data is obtained using Equation (3.26). Figure 3.8(b) shows the enlarged view of the output. From the figure, the identified dead time is 0.2 s, and this value is used in Step 2 of the algorithm. Figure 3.9 shows the time history of the input/output data with the conventional FRIT and the proposed method when the step input under condition 2 is applied to the closed-loop system. From this figure, the output data of the standard FRIT can be confirmed to be divergent. In contrast, in the proposed method, controller parameters that stabilize the closed-loop system are obtained even when model matching cannot be realized. The simulation results are summarized in Table 3.7.

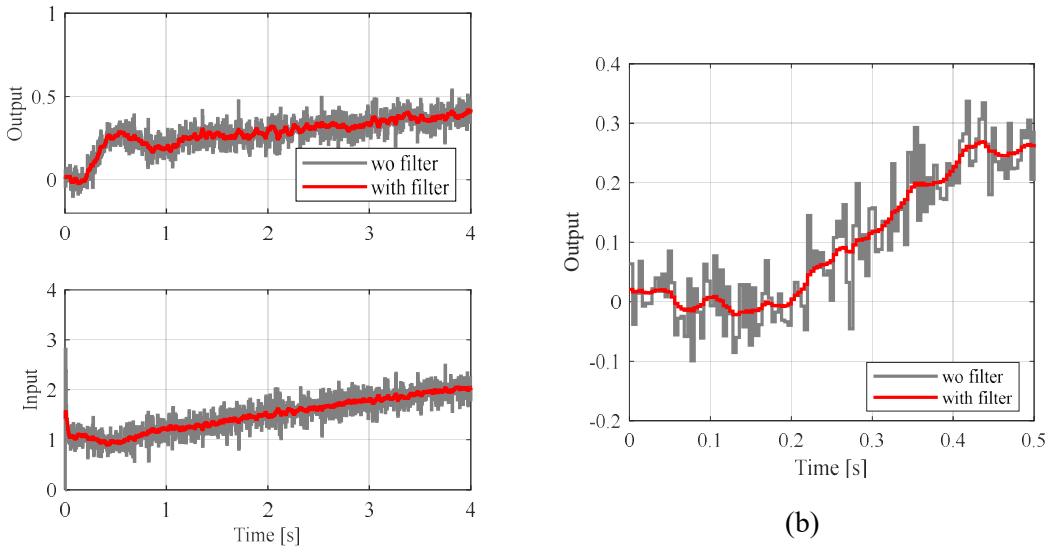

Figure 3.8. Time-series data used in the optimization without and with the filter under the initial PID gain (λ_r = 10). (a) Overview of the input and output. (b) Enlarged view of the output.

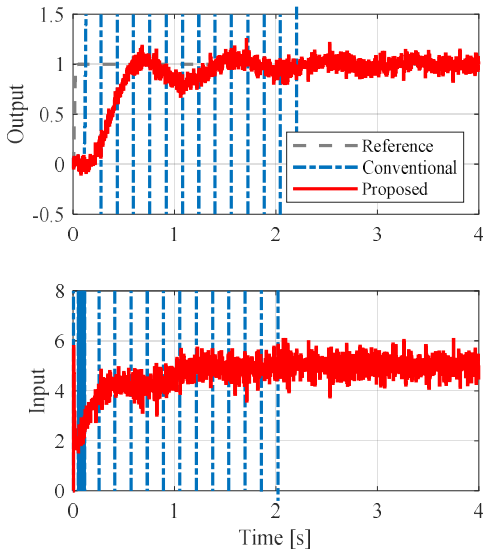

Figure 3.9. Input and output time series data with the conventional and proposed methods under condition 2.

Table 3.7. Tuned parameters in all condition with conventional and proposed method for the spring-mass system.

Symbol	Condition 1		Condition 2	
	Conventional	Proposed	Conventional	Proposed
K_p	0.0311	0.0003	106.61	1.4505
K_i	2.4431	2.4320	117.14	11.103
K_d	0.0447	0.0095	22.917	0.0471
J_{FRIT}	6.4984×10^{-4}	-	8.8166×10^{-5}	-
J^*	-	1.3647×10^{-3}	-	3.3616×10^{-2}
J_0	3.8648×10^{-3}	3.8958×10^{-3}	1.0761×10^{195}	2.6731×10^{-2}
Stability	Stable	Stable	Unstable	Stable

Next, the effectiveness of the reference-model optimization method using Step 2 of the algorithm is confirmed. The reference model with a tunable parameter L_{est} is used as described in Section 3.4. Here, we assume that the controlled-object dead time is identified in Step 2-1 as 0.2 s from Figure 3.8(b). Figure 3.10 shows the time histories of the closed-loop system using the parameters obtained before and after applying Step 2 of the algorithm. The dead time of the variable reference model before optimization is fixed to 0.2 s to ensure that the conditions before and after the application of Step 2 of the algorithm match. Figure 3.10 (a) shows the time-series data before applying the optimization algorithm, and Figure 3.10(b) shows the time-series data after optimizing the responsiveness parameter. In Figure 3.10(a), the responsiveness parameter is not optimized and the response is vibrational. In contrast, Figure 3.10(b) shows that the parameter related to the responsiveness of the reference response is optimized. Further, the actual response can follow the reference response under the controller of the specified order. Thus, a response exhibiting characteristics close to those desired by the designer can be realized. The simulation results are summarized in Table 3.8.

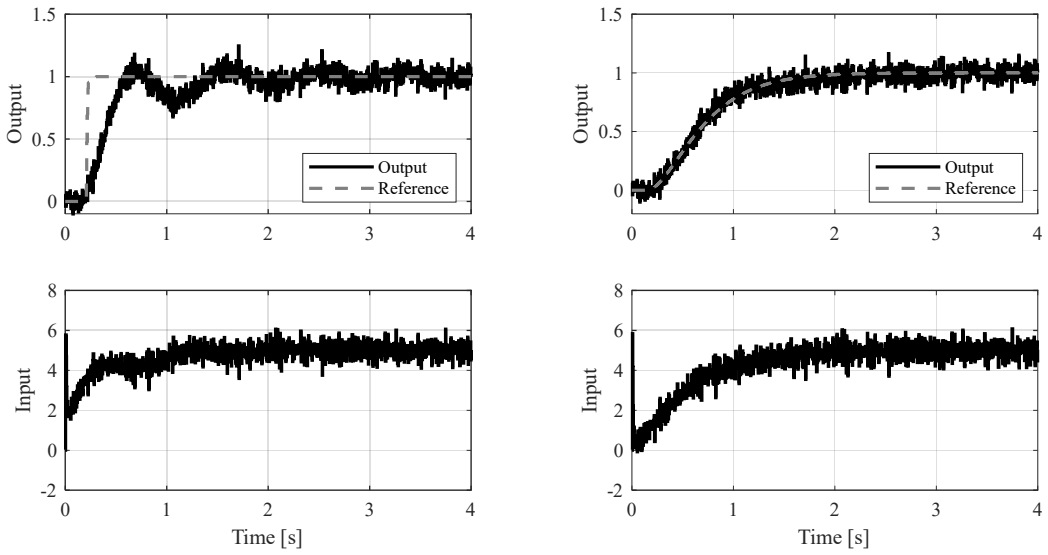

Figure 3.10. Input and output time series of the experimental data for spring-mass system (a) before and (b) after tuning by Step 2.

Table 3.8. Tuned parameters including reference model for the spring-mass system.

Symbol	Before tuning	After tuning
τ_M	0.005 (given by designer)	0.3
L_{est}	0.20 (identified by Step 2-1)	0.1607
K_p	1.4585	0.0024
K_i	11.077	6.1933
K_d	0.0472	0.0145
J^*	1.3664×10^{-2}	3.8396×10^{-4}
J_0	1.1578×10^{-2}	3.2622×10^{-3}

3.5.2.2 **Discussion about system 2**

The proposed method is effective with respect to the results obtained by its application to the system because (i) controller parameters (PID gains) are obtained, causing the closed-loop system to become stable. Also, (ii) the characteristics of the closed-loop system coincide with those of the reference model when model matching is realized. After Step 2 of the algorithm, the gain and phase margins of the reference model are 14.67 dB and 70.34°, respectively. Further, the gain and phase margins of the closed-loop system using the obtained parameters by applying the proposed method are 18.00 dB and 84.32°, respectively. The gain and phase margins before the application of Step 2 are 1.676 dB and 22.82°, respectively. Thus, a controller with characteristics equivalent to those of the user-defined reference model can be obtained.

3.6 **Experimental result and discussion**

The proposed method is experimentally verified. The controlled object is a DC motor, and we obtain the PID gain for speed control. The experimental system is shown in Figure 3.11. The motor and generator are connected by a rubber. The control input is calculated using a PID controller, and the controlled variable is the rotational speed (generator voltage) of the generator. The sampling period is 40 ms, and the time constant of the derivative filter is 100 ms. The initial PID gains and the dead time of the reference model are $K_p = 2.0$, $K_i = 0.1$, and $K_d = 0.005$. The dead zone is compensated because the rotation is controlled from the stopped state.

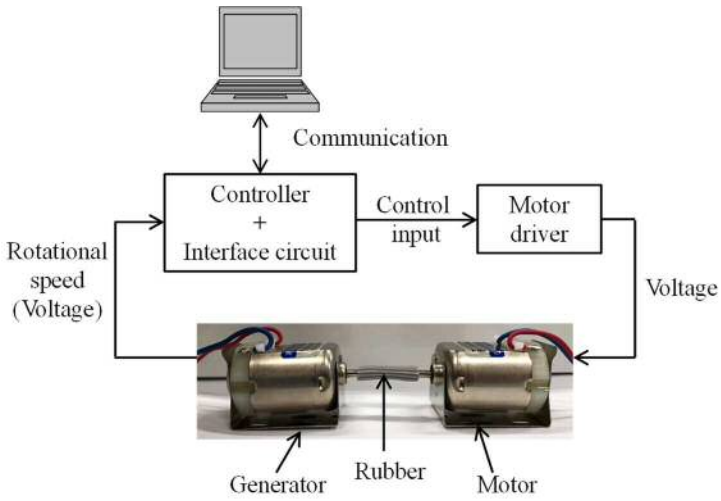

Figure 3.11. Experimental setup with the motor and generator connected by rubber.

First, we confirm the effectiveness of the ID-FRIT with respect to Step 1 of the algorithm. Figure 3.12(a) shows the time history of the raw and denoised input/output data of the closed-loop system when the initial parameter values are used, and λ_r is set to 5. The denoised data is obtained using Equation (3.26). Figure 3.12(b) shows the enlarged view of the output. From the figure, we can obtain the identified dead time as 0.12 s, and this value is used in Step 2 of the algorithm. From Step 1 of the algorithm, the PID gains obtained by conventional FRIT are $K_p = 17.8881$, $K_i = 20.4399$, and $K_d = 9.4438$. Also, the PID gains obtained by ID-FRIT are $K_p = 5.1579$, $K_i = 4.6819$, and $K_d = 9.4438$. Figure 3.13 shows the time history of the output (generator voltage) and input calculated by the PID controller with the conventional FRIT and proposed method. In this figure, in the proposed method, the closed-loop system is stable even when model matching cannot be realized. In the conventional FRIT, the closed system seems to be not divergent because of the input voltage limitation of the hardware from −5 to +5 V; however, the control input is very large and the PID gains are not appropriate.

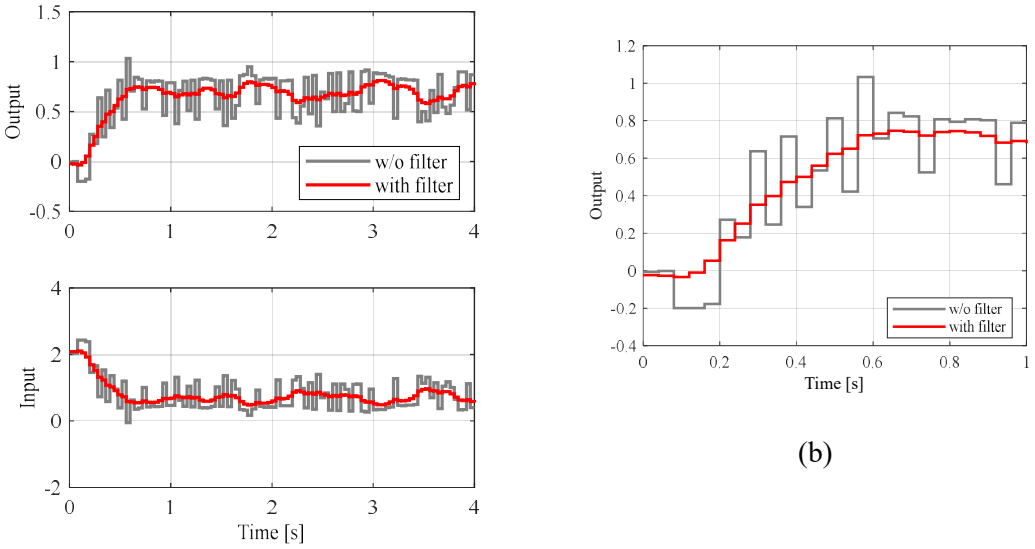

(a) (b)

Figure 3.12. Time-series of the experimental data used in the optimization without and with the filter under the initial PID gain (λ_r = 5.0). (a) Overview of the input and output. (b) Enlarged view of the output.

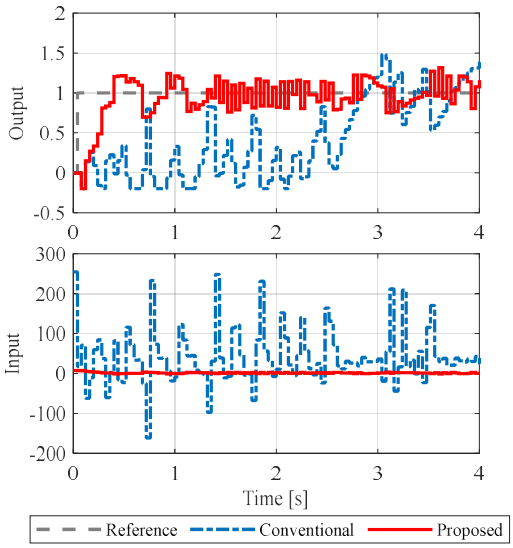

Figure 3.13. Input and output time series of the experimental data with the conventional and proposed methods under condition 2.

Next, we confirm the effectiveness of the reference-model optimization method using Step 2 of the algorithm. The reference model with a tunable parameter L_{est} is used as described in Section 3.4. Here, we assume that the controlled-object dead time is identified in Step 2-1 as 0.12 s from Figure 3.12(b). The tuned PID gains before applying Step 2 of the algorithm are $K_p = 2.7890$, $K_i = 4.2147$, and $K_d = 0.2823$. The dead time of the variable reference model before optimization is fixed to 0.12 s to ensure that the conditions before and after applying Step 2 of the algorithm match. Also, the PID gains and estimated dead time after applying Step 2 are $K_p = 1.3251$, $K_i = 1.8455$, $K_d = 0.0010$, and $L_{est} = 0.1198$. Figure 3.14 shows the time histories of the closed-loop system using the parameters obtained before and after applying the above algorithm. Figure 3.14(a) shows the time-series data before applying Step 2 of the algorithm, and Figure 3.14(b) shows the time-series data after the optimization of the responsiveness parameter. In Figure 3.14(a), the responsiveness parameter is not optimized and the response is not close to the reference response. In contrast, Figure 3.14(b) shows that the parameter related to the responsiveness of the reference response is optimized, and the actual response can follow the reference response. Thus, the parameters obtained using the proposed method provide BIBO stability and model matching.

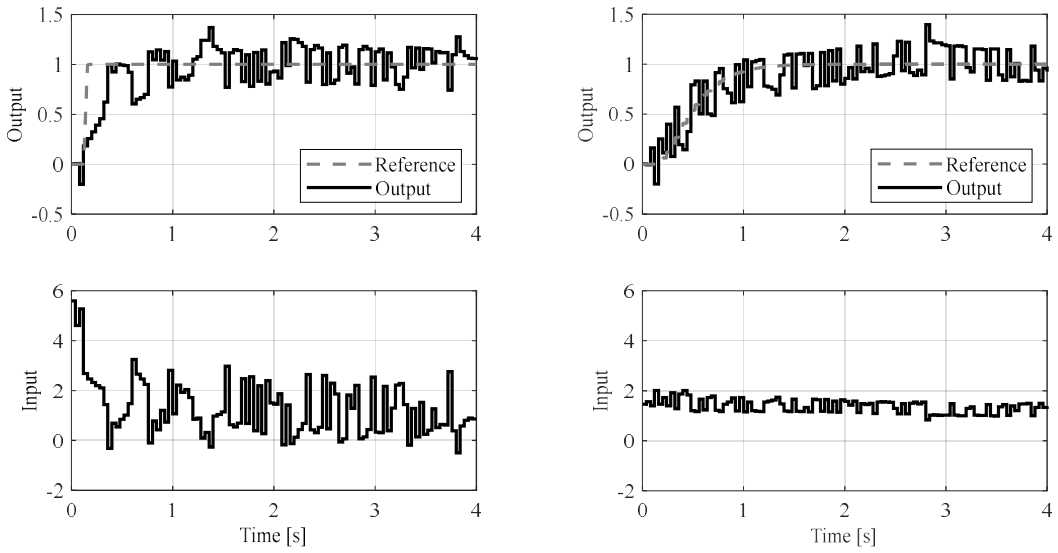

(a) (b)

Figure 3.14. Input and output time series of the experimental data (a) before and (b) after tuning by Step 2.

3.7 **Conclusion**

In this chapter, a direct tuning method for the feedback controller parameters based on a fictitious reference signal that ensures BIBO stability and an auto-tuning method of the reference model for model matching from single-experiment data were proposed. First, the BIBO stability of closed-loop system is satisfied. A transfer function, the input and output of which are a fictitious reference signal and a controlled-object response, respectively, is identified in the time domain to obtain pole information. Thus, we can obtain the parameters that make the closed-loop system BIBO stable. Next, the reference model parameters are automatically tuned using the proposed algorithm for model matching. Thus, BIBO stability and model matching can be considered in the algorithms. Moreover, the design parameters are not influential apart from noise. These features allow the easy application of this method. Thus, many engineers can easily use this method. Two simulations and an experiment were performed on a system with dead time to verify the effectiveness of the proposed method. Results showed that the conventional FRIT and the proposed method result in optimal controller parameters when model matching is possible. However, when model matching is impossible because of an inappropriate reference model, the closed-loop system using the controller parameters obtained with the standard FRIT is unstable, whereas the proposed method can be used to obtain optimum control parameters without destabilizing the system. In addition, the reference-model parameters can be optimized for model matching. Thus, the parameters obtained using the proposed method provide BIBO stability and model matching.

Chapter 4
Direct tuning for gain-scheduled sparse controllers

In this chapter, a direct tuning method for nonlinear systems is proposed. In industry, gain-scheduled PID control is carried out for nonlinear systems using a look-up table (LUT) that is easy to understand. Compared with the fixed PID, the scheduler has many more parameters; tuning them is time-consuming. The ROM storage area also increases. To address these problems, a gain-scheduled control law using the sparse polynomial functions and a direct parameter tuning method without system identification are proposed. The polynomial functions are used instead of a LUT to reduce the ROM area. For direct tuning, data-driven control is formulated so that it can be applied to the gain-scheduled control; the optimal parameters are obtained by least absolute shrinkage and selection operator (LASSO) regression, where the small contributing parameters of the scheduler become zero, and a sparse controller is obtained. The effectiveness of this method was examined via simulations for two systems. The results revealed that a sparse controller with a low calculation cost and a reduced ROM area can be directly obtained without knowing the characteristics of the controlled object for a large number of control parameters of the gain scheduler. The contents of this chapter are based on the literature [65].

4.1 Introduction

Over 90% of the closed-loop control methods in industrial systems use PID control because the perspective is easy to understand and the calculation cost is low [7], as mentioned in Chapter 1. The desired control performance can be obtained if the controlled object has strong linearity, but in the case of a nonlinear system, it is difficult to obtain sufficient control performance with PID control with fixed gains [66]. The nonlinear control theory and robust control can be applied, but the hurdles of nonlinear control

applications are high because the theory is complicated and the calculation load is often large. In addition, it is generally difficult to address a robust controller for a system whose characteristics significantly change. Against this background, the gain-scheduled control is one of the most popular approaches to nonlinear control design [40] [67], and it is well-known as an effective and economical method for actual nonlinear control designs [41]. The gain-scheduled control is a method that realizes the desired control performance by changing the controller parameters according to the state of the controlled object and the external environment. This approach is intuitively understandable and easy to accept in many industries. In addition, the gain-scheduled PID control, which uses a look-up table (LUT), is often used in many industries [68] [69]. At the same time, a large number of control parameters must be tuned to obtain the desired control performance. The fixed PID control has three tuning parameters, but the gain-scheduled control with LUT has a much greater number of parameters that must be tuned. Hence, it takes a lot of time for parameter tuning. The model-based design of the LPV (Linear Parameter-Varying) controller has been proposed, but it may still be difficult to obtain highly accurate models because industrial systems are often complicated [70], so the controller may not be fully performed.

In recent years, direct controller design methods that do not need controlled object models or system identification have attracted extensive attention. We focused on data-driven control methods such as VRFT [20] [21] and FRIT [22] [23] because the controller parameters can be obtained offline from a set of input/output data without repeated experiments (see Chapter 1). Meanwhile, these methods are based on a linear control system. Because many complex nonlinear systems exist in industrial systems, a data-driven control system that enables nonlinear control is required. There are applications to nonlinear systems, such as DD-PID [71] and DD-FRIT [72] [73], FRIT for feedback linearization [74], and VRFT for LPV systems [75] [76] [77]. The DD-PID and DD-FRIT have relatively high storage capacity and computational cost when a controller is implemented. In FRIT for feedback linearization, it is necessary to know the model structure in advance, and it is not possible to directly obtain the PID controller parameters, which are mostly used in many industries. In the VRFT for the LPV system, the gain-scheduled controller is obtained, which has a small calculation cost and storage capacity at implementation. In addition, it is possible to interpret and understand the same, as the

gain-scheduled PID control uses the described LUT at the beginning by visualizing the schedulers for each of the obtained PID gains. Therefore, it is desirable to obtain the parameters for the gain-scheduled PID control by the VRFT.

In the gain-scheduled control, the selection process of the scheduling parameters is also important. For example, the position control for the spring-mass system is very important, and it is combined with different states, such as the position, velocity, or acceleration. If the selected scheduling parameters do not affect the change in the characteristics of the controlled object, the calculation cost and ROM area would increase for unnecessary parameters. In the regression problem of machine learning, to prevent overlearning, a method called LASSO (least absolute shrinkage and selection operator) regularization, in which the L_1 norm is added to the cost function is performed. Mainly, this is a method for extracting essential low-dimensional information with high accuracy from high-dimensional information. In the model obtained by LASSO, the elements with little information representing the feature are zero, and such a property is called sparseness.

In this chapter, the author proposes a method that automatically tunes the parameters of the scheduling function (scheduler) for gain-scheduled PID control while considering the sparseness property of LASSO. The gain-scheduled PID controller is defined by expressing the scheduling function as a polynomial that consists of weight coefficients, which are the tuning parameters. By using a polynomial instead of the LUT, the tuning parameters can be reduced. Next, the cost function of the VRFT for the gain-scheduled PID controller is derived. Additionally, the value of the optimum control parameters is calculated by LASSO so that the cost function becomes minimum. In addition, the gain scheduler with the high sparseness can be constructed by LASSO. As a result, trial and error parameter tuning and system identification are not needed. Moreover, the ROM area of the controller and the calculation cost are reduced. In other words, the controller with the high sparseness and reduced parameter tuning man-hours can be obtained. Studies [75] [76] [77] for applying the VRFT to the LPV system have been previously proposed. In comparison with those studies, the main features of this study are as follows. For industrial applications, the PID controller is assumed as a control law, the gain scheduler adopts a quadratic polynomial, and the sparse controller can be obtained.

The structure of this chapter is as follows. In Section 4.2, the problem formulation is described. Section 4.3 describes the proposed method and the direct tuning method of the gain-scheduled control parameters using the VRFT. In Section 4.4, two types of nonlinear systems are controlled using the proposed method by numerical simulation, the correspondence of the controller parameters to the characteristic fluctuations is revealed, and the desired control performances are obtained. Section 4.5 provides a summary of this chapter.

4.2 **Problem formulation**

The model-referenced gain-scheduled control problem and the controlled objects are explained. In this chapter, VRFT shown in Section 2.2 is used.

4.2.1 **Model-referenced gain-scheduled control problem**

When the controlled object has complicated characteristics, such as nonlinearity or time-varying, the performance deterioration cannot be avoided with a time-invariant fixed controller, whereas a gain-scheduled controller can be an effective method for realizing good control performance. The gain-scheduled control system shown in Figure 4.1 is considered the control law. In the figure, $u \in R$ is the control input, $y \in R$ is the output, r is the set-point, e is the error, and P is the controlled object. The gain-scheduled control is constructed from the controller $C(z, \rho)$, the controller parameter vector ρ, the rational function vector $\psi(z)$, the scheduling parameter $\theta \in \Theta$, the parameter vector w, and the scheduling function (scheduler) $f(\theta, w)$. The controller is described as

$$C(z, \rho) = \rho^T \psi(z) = f(\theta)^T \psi(z), \tag{4.1}$$

where

$$\begin{gathered} \rho = [\rho_1 \quad \rho_2 \quad \cdots \quad \rho_n]^T, \\ f(\theta, w) = [f_1(\theta, w_1) \quad f_2(\theta, w_2) \quad \cdots \quad f_n(\theta, w_n)]^T, \\ \psi(z) = [\psi_1(z) \quad \psi_2(z) \quad \cdots \quad \psi_n(z)]^T, \\ w = [w_1 \quad w_2 \quad \cdots \quad w_n]^T, \end{gathered} \tag{4.2}$$

where z is the shift operator, and w_i is a parameter vector that constructs the *i*-th scheduling function $f_i(\theta, w_i)$. The controller parameter vector ρ changes according to the scheduling function $f(\theta, w)$. The detailed settings of the rational function vector $\psi(z)$ are described in Section 4.3.1.

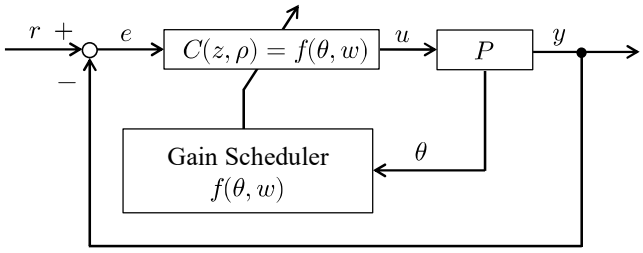

Figure 4.1. Gain-scheduled control system.

We considered the model reference control as well as the previous studies of the data-driven control [21] [23]. Figure 4.2 shows a block diagram of the model reference gain-scheduled control. The problem setting is to acquire the sparse controller by automatically tuning the control parameters of the gain scheduler so that the transfer characteristics from the set-point to the output can match the reference model M_d, which is determined by the designer. In other words, our aim is to obtain the optimum parameters that make up the sparse gain-scheduled controller that minimizes the following cost function.

$$J_{MR}(w) = \|y(t, w) - M_d(z)r(t)\|_2^2 + \lambda\|w\|_1, \tag{4.3}$$

where λ denotes the weight coefficients, and the second term is the weight-related to w. The details are provided in Section 4.3.3.

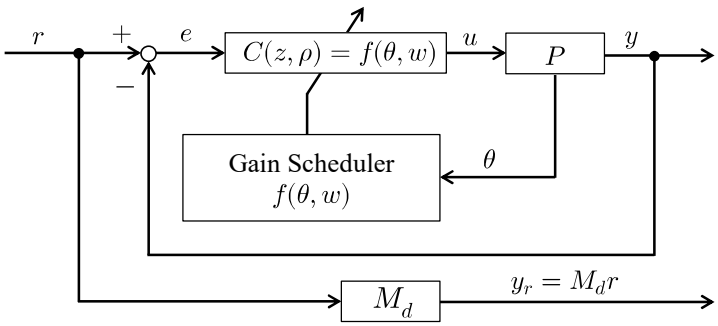

Figure 4.2. Gain-scheduled control system and reference model.

4.2.2 **Controlled object**

The LPV system whose characteristics are changed by the scheduling parameters was used in many previous studies. However, the target system is unknown if it is strictly the LPV system or not. Hence, the controlled objects are unknown two-type nonlinear single-input single-output (SISO) systems, which are an explicit LPV system and a system that is not explicitly described as an LPV system. The first system, the LPV system, is described as

$$\begin{cases} x(t+1) = A_d(\theta)x(t) + B_d(\theta)u(t) \\ y(t) = C_d(\theta)x(t) \end{cases}, \tag{4.4}$$

where $u \in R$ is the control input, $y \in R$ is the output, $x \in R^n$ is the state, and θ is the scheduling parameter. The matrices A_d, B_d, and C_d are bounded and unknown functions that are continuous with respect to θ, and the candidates of the scheduling parameters are associated with the controlled object output or state. We assumed that this system is stable. The second system is often used in the numerical example of the database control [71] [78] as

$$y(t) = f_p(y(t-1), \ldots, y(t-n_y), u(t-1), \ldots, u(t-n_u)), \tag{4.5}$$

where f_p is an unknown nonlinear function, and n_u and n_y denote the unknown orders of the input and output, respectively. We assumed that this system is stable and can be linearized at an equilibrium point. The candidates of the scheduling parameters are associated with the controlled object output. Thus, in general, it is necessary to linearize

the nonlinear system to design a gain scheduler, but this study aims at designing the gain scheduler without system identification and linearization.

4.3 Direct tuning of the PID gain scheduler

4.3.1 Gain-scheduled PID control

In the gain-scheduled PID control, the closed-loop system may become unstable due to the sudden change in the gain. As a countermeasure, the velocity form of the PID controller and the described scheduling function in the polynomial are adopted.

4.3.1.1 Velocity form of the PID controller

The velocity form of the PID control law that is suitable for the gain-scheduled control is adopted. This has the advantage that the integral term does not need to be reset, and the control input does not rapidly change even when the gain rapidly changes [79] [80]. If the gain abruptly changes, the control input changes over time, causing disturbance to the system. Figure 4.3 shows a block diagram of the velocity form of the PID control. An integral element appears just before the control input, and the time change can be reduced. Furthermore, an integral element is used after the K_i element, and the K_d element is used after the difference element. However, it is not preferable when these orders are reversed, as the time change of the control input at the time of switching becomes large [81]. The velocity form of the PID control that is shown in Figure 4.3 is expressed by the following equation.

$$u(t) = u(t-1) + C_v(z,\rho)e(t) \tag{4.6}$$

with

$$\begin{aligned} C_v(z,\rho) &= K(t)\psi(z), \\ K(t) &= [K_p(t) \quad K_i(t) \quad K_d(t)]^T, \\ \psi(z) &= [(1-z^{-1}) \quad 1 \quad (1-z^{-1})^2]^T, \end{aligned} \tag{4.7}$$

where $e(t)$ is the error that is given by $e(t) = r(t) - y(t)$, and $r(t)$ is the set-point. $K_p(t)$, $K_i(t)$, and $K_d(t)$ denote the proportional gain, integral gain, and derivative gain,

respectively, and Δ represents the difference operator, which is expressed as $\Delta = 1 - z^{-1}$ using the backward operator z^{-1}, where $z^{-1}y(t) := y(t-1)$.

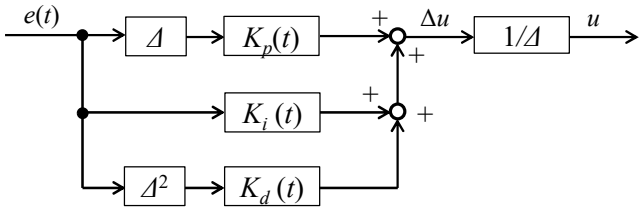

Figure 4.3. Block diagram of the velocity form of the PID controller.

As a supplement, based on the literature [79] [80], the advantage of the velocity form of the PID controller, also known as the incremental PID controller, is explained. The velocity form of the PID controller has two main features.

First, the velocity form of the PID controller has a bumpless transfer feature. The bumpless means that the control input changes continuously even when the controller is switched. For example, bumpless is often used when switching from automatic to manual operations or in override control (mode switching control). In the position form, switching the controller may result in system instability because of the rapid change of control input. On the other hand, the velocity form of the PID controller calculates the derivative control input, and the control input is obtained by integrating the derivative control input; thus, the control input is continuously changed because of the integration of the derivative control input. The difference between the PID controller's position form and velocity form is described. Figure 4.4 shows the time series data with the position form and velocity form of the PID controller when the controller is switched at 15s, indicating that PID gains are switched to different gains. From the figure, the control input is switched in the case of the position form and the response is not preferred. However, the control input in the velocity form is smoothly changed and the effect of switching the controller is almost negligible. In gain-scheduled control, the rapid time change of control input due to variable PID gains may occur. Therefore, we consider the velocity form of the PID controller suitable for gain-scheduled control. In addition, this form has also been used in the literature [81].

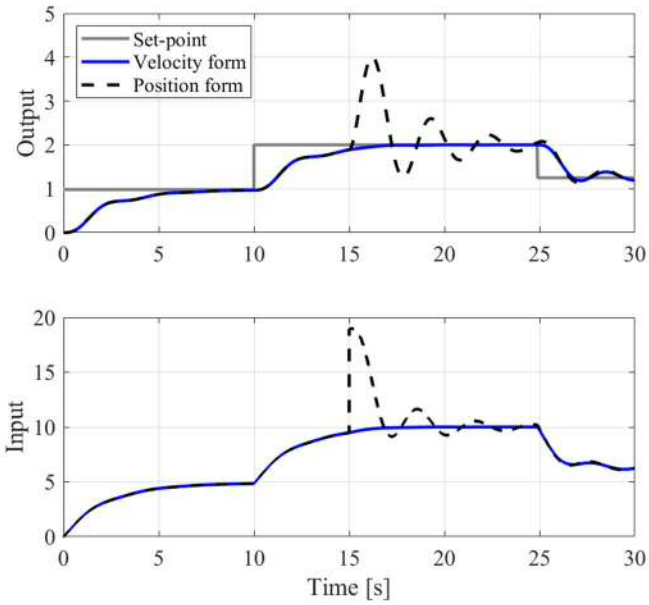

Figure 4.4. Time series data when PID gain is switched at 15 s.

Second, no special anti-windup measure is required. This is not directly relevant to this study, but the outline will be introduced. We consider the case in which the range of the control input for the actuator is limited. When the steady error cannot be reduced to zero because of the limitation, the integral term continues to accumulate the error. As a result, the subsequent response is delayed, decreasing the system's control performance. A process that cancels out the effect of the integral term should be added. An anti-windup measure should be added in the position form of the PID controller. However, that is not necessary for the velocity form of the controller. The difference between the position form and velocity form of the PID controller is demonstrated. Figure 4.5 shows the time series data of the PID controller in the position form and velocity form when the actuator range is limited. The control input is limited up to 4.0 and the response does not reach the set-point value of 1.0. In the position form, the integral term continues to accumulate the error, known as windup, from approximately 10 to 30 s (see position form before limitation line). As a result, the response is delayed when the set-point is changed at 30 s. This is because the integral term has a large value. Thus, we need to add some anti-windup measure. On the other hand, the velocity form does not require an anti-windup measure, as shown in Figure 4.5.

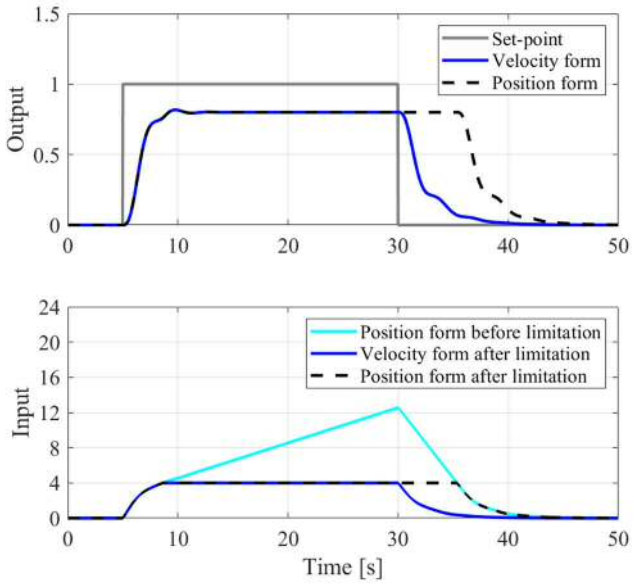

Figure 4.5 Time series data when the actuator range is limited.

4.3.1.2 **PID gain scheduler**

In this chapter, the gain scheduler in Equation (4.2) uses a polynomial. The use of the Just-In-Time method [78], database control [71], and neural network [82] is difficult to install in mass product controllers due to the limitations of the calculation cost and ROM area. The gain schedulers that use the LUTs have been used for a long time in many industries, especially in automobile control. However, the ROM capacity and tuning parameters increase. Furthermore, as a concern of the gain-scheduled control in which the gain that is designed for each operating point is directly expressed by the LUT, there is a possibility that the PID gain rapidly fluctuates and that the system becomes unstable. Therefore, in this chapter, the scheduling function is represented by the quadratic polynomial shown in Equation (4.8). As a result, in addition to reducing the number of stored parameters, the gain continuously changes so that the sudden gain changes are less likely to occur.

$$
\begin{gathered}
K_j(\theta) = w_j^T \theta_{sf}, \\
w_j = \begin{bmatrix} w_{j0} & w_{j1} & w_{j2} & w_{j3} & w_{j4} & w_{j5} \end{bmatrix}^T, \\
j \in \{p, i, d\}, \\
\theta_{sf}(\theta) = [1 \quad \theta_1 \quad \theta_2 \quad \theta_1\theta_2 \quad \theta_1^2 \quad \theta_2^2]^T, \\
\theta = [\theta_1 \quad \theta_2]^T,
\end{gathered}
\tag{4.8}
$$

where $K_j(\theta)$ is the PID gain scheduler, which is the scheduling function. θ_l is the scheduling parameter ($l = 1, 2$), and θ_{sf} is the function vector, which is the base function that is composed of the scheduling parameters. In addition, w_j is the weight coefficients vector, which is the regression coefficient vector of the PID gains, which are the tuning parameters. As scheduling parameters, the signals of the external environment, such as the temperature, or the states, such as the position and speed of the controlled object, are generally used. In Equation (4.8), the number of scheduling parameters is two, and the scheduling function is a quadratic polynomial, but it is not limited to this order.

4.3.2 **Derivation of the cost function**

Herein, a cost function that finds the optimum values of the weight coefficients of the gain scheduling function is derived. From the cost function of the VRFT (see Equations (2.10)) and Equations (4.6)–(4.8), which are related to the gain-scheduled PID control, the weight coefficient of the gain scheduler can be obtained. The cost function is

$$
J(w) = \|d(t) - w^T \xi(t)\|_2^2 \tag{4.9}
$$

$$
\begin{gathered}
d(t) = L\Delta u(t) \\
\xi(t) = X(M_d^{-1}(z) - I)Ly(t)
\end{gathered}
\tag{4.10}
$$

with

$$
w = \begin{bmatrix} w_p & w_i & w_d \end{bmatrix}^{\mathrm{T}}, \tag{4.11}
$$

$$
X = \begin{bmatrix} \theta_{sf}^T \psi_1(z) & \theta_{sf}^T \psi_2(z) & \theta_{sf}^T \psi_3(z) \end{bmatrix}^{\mathrm{T}}, \tag{4.12}
$$

where ψ_i is the *i*−th element of the vector ψ, as shown in Equation (4.7). Since the cost function is linear with respect to the weight coefficients vector w, the optimal solution w^* can be obtained by the following equation using the least-squares (LS) method.

$$w^* = (Z^T Z)^{-1} Z^T D, \tag{4.13}$$

where

$$Z = [\xi(1) \quad \xi(2) \quad \cdots \quad \xi(N)]^{\mathrm{T}}, \tag{4.14}$$

$$D = [d(1) \quad d(2) \quad \cdots \quad d(N)]^{\mathrm{T}}. \tag{4.15}$$

4.3.3 **Automatic tuning by LASSO**

LASSO is a method for extracting essential low-dimensional information from high-dimensional information with high accuracy. By introducing the L_1 regularization term, the weight coefficients with less influence are set to zero. This property is called sparseness. In the field of machine learning, it is used to reduce the prediction error of the model by preventing overfitting. In this chapter, LASSO is applied to find the optimal solution of Equation (4.9). As a result, it can be expected to suppress the overfitting of the weight coefficients and to obtain a controller with high sparse.

The cost function obtained by adding the L_1 regularization term to Equation (4.9) is

$$J(w) = \|d(t) - w^T \xi(t)\|_2^2 + \lambda \|w\|_1, \tag{4.16}$$

where λ is a positive constant and a parameter that tunes the relative strength between the regularization term and the sum of the squared error terms. The sparsity can be tuned by changing the value of λ. In this study, cross-validation is used to automatically determine the optimal regularization parameter λ from the multiple λ, which is set by the designer. The cross-validation can be explained using Figure 4.6.

[Step 1] Divide the data into k (=5) blocks. This is called a fold.

[Step 2] Fold 1 and the others (folds 2–5) are used as the test and training sets, respectively. Then, the learning and evaluation of the model are performed, and the cost function value J_1 is obtained.

[Step 3] Fold 2 and the others (folds 1, 3–5) are used as the test and training sets, respectively. Then, the learning and evaluation of the model are performed, and the cost function value J_2 is obtained.

[Step 4] This process is repeated until fold 5 becomes the test set, and the cost functions J_1–J_5 can finally be obtained. Also, the cost value J, which is the average value of J_1–J_5, can be calculated.

By performing cross-validation for multiple λ values, which are set by the designer, and by obtaining the cost function value J for each λ, the optimum λ and the optimum parameters with the smallest cost functions are obtained. Python is used as the programming language, and cross-validation is performed by LASSO CV, which is included in the package scikit-learn to determine λ and to find the optimal solution.

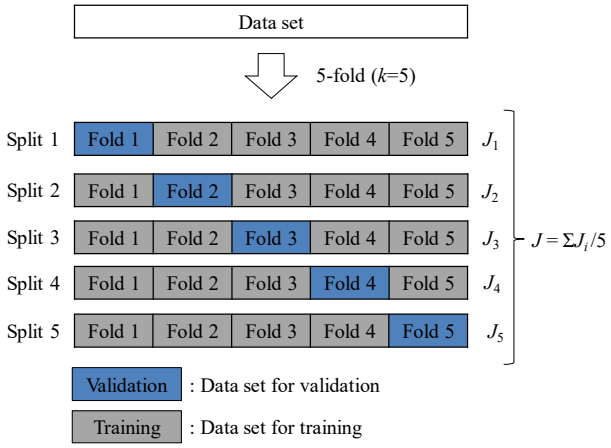

Figure 4.6. k-fold cross-validation. k is five in the figure.

4.3.4 **Algorithm**

Using the VRFT, the algorithm for the direct tuning method of the weight coefficients of the PID gain scheduling function is shown below.

[Step 1] Measure the input and output data $u(t)$, $y(t)$, $t = 1, \ldots, N$ in the test. The data set is *Z* and *D* described in Equations (4.14) and (4.15), respectively.

[Step 2] Set the reference model.

[Step 3] Decide the scheduling parameter candidates and the scheduling function for each PID gain.

[Step 4] Design the prefilter for the VRFT.

[Step 5] Obtain the weight coefficients, which are the scheduling parameters, of the scheduling function that minimizes the cost function by LASSO.

Remark 4.1. In Step 4, by applying a strict prefilter in the study [75] [76], the original cost function and the VRFT cost function can be matched. However, additional experiments are required. In this study, we consider the practical application and use the prefilter of the following filter [28]:

$$L(z) = M_d(z). \tag{4.17}$$

Remark 4.2. This algorithm is based on VRFT, where an open-loop test has been adopted, as in many studies [21] [27] [28] [29] [75] [76] [77]. This algorithm faces the same theoretical problem as the general system identification and the previous studies [75] [76] [77] when using closed-loop test data. For practice use, we could obtain controller parameters realizing model-matching if the noise is of an acceptable magnitude. The literature [27] shows that optimized parameters can be obtained using closed-loop data for an industrial system with the standard VRFT. If the observed noise is large, a filtering process is required similar to the common machine learning process. In addition, in FRIT, which has a lot of achievements using closed-loop test data, a filtering process is performed for noisy data [83]. In Section 4.4, the results when using the initial data of open-loop and closed-loop tests will be shown. The results show that good performance was achieved in both cases.

Remark 4.3. The feature of this method is summarized. The advantages of the proposed method are described as follows: (i) The gain-scheduled controller parameters can be

obtained without the controlled object model. (ii) ROM area and calculation cost can be reduced using LASSO. In addition, LASSO prevents overlearning. (iii) Many engineers can easily understand the controller structure, as industrial engineers are familiar with gain-scheduled control and PID control. On the other hand, the disadvantage is that stabilization is not completely guaranteed; however, this is a common issue with direct data-driven control methods [21] [23] [27] [28] [66] [71] [72] [73] [81]. This will be one of our future works.

4.4 **Simulation verification**

The controlled objects are two nonlinear systems. The first one is a nonlinear dynamic system described in the LPV system, and it is a spring-mass system that is often used in industrial systems, where each parameter is time-varying. The second system is the Hammerstein model [84], in which a linear dynamic system is connected in series to the output of the static nonlinear function, and it is widely used as a model for describing the nonlinear system [85]. This model is also used as numerical examples for data-driven control [71] [72] [73] [86]. We use open-loop and closed-loop data to verify the effectiveness of the proposed method for these systems.

4.4.1 **Application to LPV systems**

It is applied to a controlled object whose system parameters change according to the state of the controlled object. In other words, the target is a nonlinear dynamic system.

4.4.1.1 **System formulation**

The controlled object, reference model, and controller used in this section are formulated. The controlled object is a spring-mass system with time-varying parameters, as shown in Figure 4.7. Here, m, c, k, and y denote the mass, viscosity coefficient, spring stiffness, and system response (position), respectively. The mass, spring stiffness, and viscosity coefficient change depending on the system response and the controlled object is a system in which the following equation of motion is discretized.

$$m(y,t)\frac{d^2y(t)}{dt^2}+c(y,t)\frac{dy(t)}{dt}+k(y,t)=u(t)+v(t), \tag{4.18}$$

where

$$\begin{aligned} m(y,t)&=1+0.2y(t),\\ k(y,t)&=5+2y+y^2(t),\\ c(y,t)&=2+0.5y(t). \end{aligned} \tag{4.19}$$

v is the white noise with the variance 1×10^{-4}, and the set-point at each time is given as

$$r(t)=\begin{cases} 0.75 & (0<t\le 10)\\ 2.0 & (10<t\le 25)\\ 1.25 & (25<t\le 40)\\ 0.5 & (40<t\le 50) \end{cases}. \tag{4.20}$$

The reference model is a first-order system with a time constant of 1 s as

$$\begin{aligned} M_d(z)&=z\big(M_d(s)\big),\\ M_d(s)&=\frac{1}{s+1}, \end{aligned} \tag{4.21}$$

where $z(\cdot)$ represents the discretization, s is the Laplace operator, and the sampling period of the controller is 10 ms. The gain scheduler uses Equation (4.8), and the scheduling parameters are the position and its derivative as

$$\theta_1(t)=y(t),\theta_2(t)=y(t)(1-z^{-1}). \tag{4.22}$$

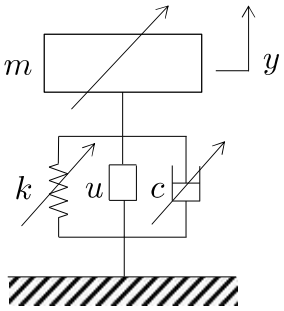

Figure 4.7. Controlled object with time-varying parameters.

4.4.1.2 **Result**

Figure 4.8 shows the given input/output data in the open-loop test. The input signal is given to the staircase signal to obtain the input/output data that represents the characteristics around the equilibrium points, and the step width is 3.0. From the figure, it can be seen that the system becomes difficult to move with the increase in the position. Figure 4.9 shows the time series data when the gain scheduling parameters were obtained from the input/output data in the open-loop test. For comparison, the data when using the fixed PID gain (VRFT), the VRFT by GS (using the least-squares method (GS-VRFT-LS)), and the VRFT by GS (using LASSO regression (GS-VRFT- LASSO)) are shown. The fixed PID gains obtained by the VRFT are $K_p = -0.0340$, $K_i = 0.0605$, and $K_d = 0.0070$, respectively. From the top of the figure, the output, input, proportional gain, integral gain, and derivative gain are shown. Table 4.1 shows the MSE (mean squared error) of the tracking error performance, which is $\mathrm{MSE} = \frac{1}{N}\sum_{t=1}^{N}\big(y(t) - M_d(z)r(t)\big)^2$, of VRFT, GS-VRFT-LS, and GS-VRFT-LASSO, also shown in the figure and table, the GS-VRFT-LS has a better tracking performance than the standard VRFT. This is because the PID gain changes appropriately according to the state of the controlled object in the GS-VRFT-LS. Next, by comparing GS-VRFT-LS and GS-VRFT-LASSO, it can be seen that they have the same tracking characteristics. Table 4.2 shows the operation counts and weight coefficients obtained by the GS-VRFT-LS and GS-VRFT-LASSO for calculating PID gains from the gain scheduler in Equation (4.8). The total counts of multiplication and addition in the scheduler obtained using LASSO are less than those obtained using the least-squares method. In the scheduler obtained by LASSO, the 18 weight coefficients that make up the PID gain scheduler are reduced to 9, and the same performance is obtained when using 18 weight coefficients. The weight coefficients $w_2, w_3,$ and w_5 of

the PID gain scheduler became zeros. In other words, the gain-scheduled PID controller with high sparsity is obtained. The optimum value of λ for the L_1 regularization was 1×10^{-7} because of the cross-validation for multiple λ, which is described in Section 4.3.3.

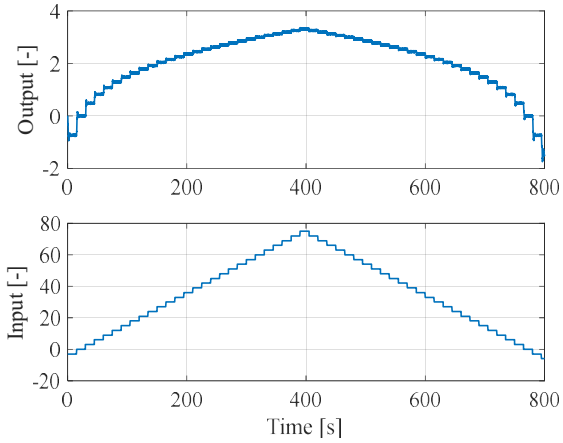

Figure 4.8. Time series data of the initial input and output under open-loop test.

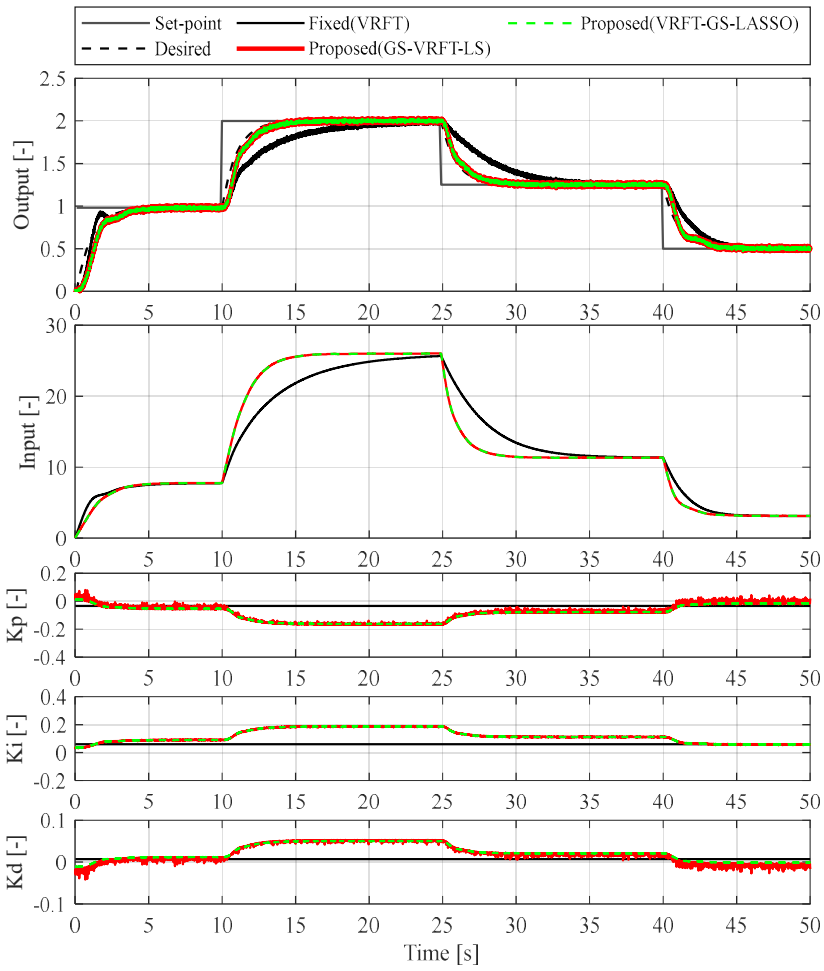

Figure 4.9. Time series data with the proposed method and fixed PID gain using open-loop data. The GS-VRFT-LS and GS-VRFT-LASSO are almost overlapped.

Table 4.1. Results of the tracking error for the spring-mass model for open-loop test.

	Fixed (VRFT)	GS-VRFT-LS	GS-VRFT-LASSO
MSE	1.918×10^{-2}	4.149×10^{-3}	4.178×10^{-3}

Table 4.2. Operation counts and parameters of gain scheduler for spring-mass system.

	GS-VRFT-LS	GS-VRFT-LASSO	Efficiency [%]
Multiplication	33	12	36.4
Addition	15	6	40.0
Total	48	18	37.5
Weight coefficients	18	9	50.0

Figure 4.10 shows the given input/output data in the closed-loop test. The set-point signal is given to the staircase signal of which step width is 0.25, and the input/output data is measured. The fixed PID gains are set to $K_p = 0.0$, $K_i = 0.3$, and $K_d = 0.0$. Figure 4.11 shows the time series data obtained from the closed-loop test input/output data when gain scheduling parameters are used. For comparison, the data when using the fixed PID gain (VRFT), VRFT by the GS (using the least-squares method (GS-VRFT-LS)), and VRFT by GS (using LASSO regression (GS-VRFT- LASSO)) are shown. The fixed PID gains obtained using VRFT are $K_p = -0.0651$, $K_i = 0.0684$, and $K_d = 0.0212$. Table 4.3 shows the MSE of the tracking error performance of VRFT, GS-VRFT-LS, and GS-VRFT-LASSO. From the figure and table, we can see that the performance using closed-loop experiment data is good as well as the results using open-loop experiment data. In addition, the operation counts and weight coefficients obtained using the GS-VRFT-LS and GS-VRFT-LASSO are the same as those shown in Table 4.2. The total counts of multiplication and addition in the scheduler obtained using LASSO are less than those obtained using the least-squares method. In the scheduler obtained using LASSO, the 18 weight coefficients that make up the PID gain scheduler are reduced to 9, and the same performance is obtained when using 18 weight coefficients. The weight coefficients $w_2, w_3,$ and w_5 of the PID gain scheduler became zeros. In other words, a gain-scheduled PID controller with high sparsity was obtained. The optimum value of λ for the L_1 regularization was 1×10^{-7}.

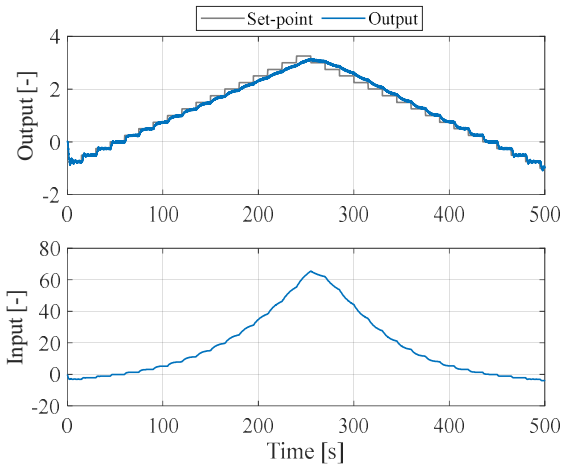

Figure 4.10. Time series data of the initial input and output under closed-loop test.

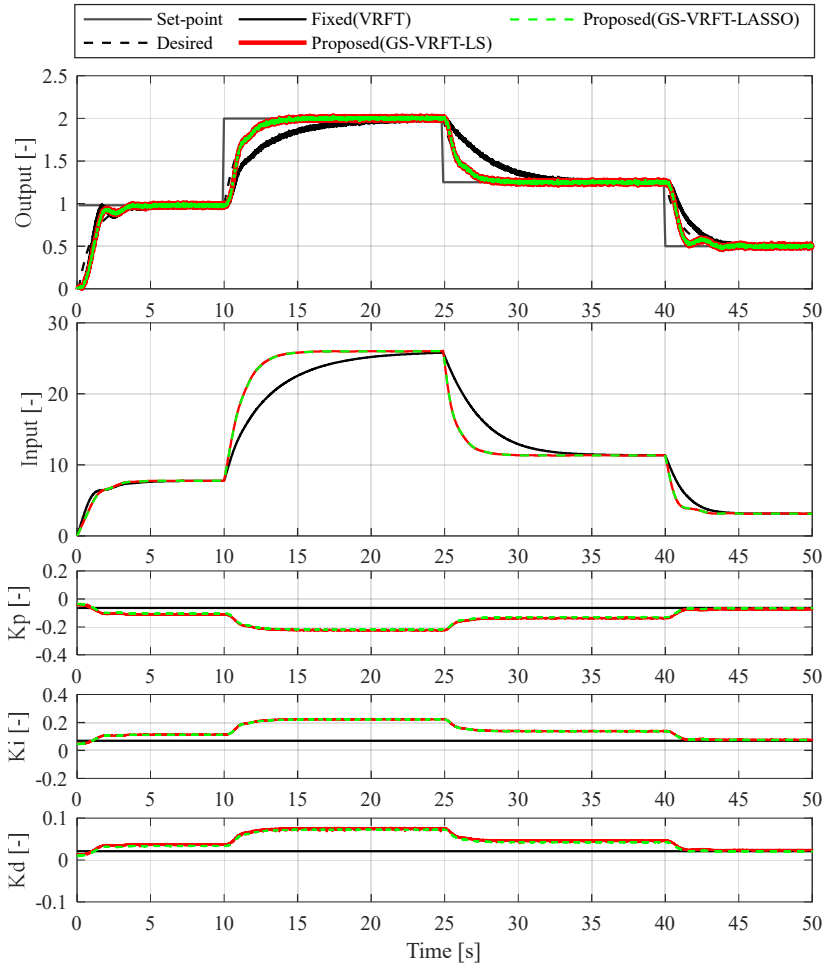

Figure 4.11. Time series data with the proposed method and fixed PID gain using closed-loop data. The GS-VRFT-LS and GS-VRFT-LASSO are almost overlapped.

Table 4.3. Results of the tracking error for the spring-mass model for closed-loop.

	Fixed (VRFT)	GS-VRFT-LS	GS-VRFT-LASSO
MSE	1.474×10^{-2}	2.846×10^{-3}	2.834×10^{-3}

4.4.2 **Application to the Hammerstein model**

The Hammerstein model, which is widely used as a model for describing nonlinear systems, is the controlled object. Figure 4.12 shows the block diagram of the Hammerstein model, which consists of a nonlinear static function and a linear model.

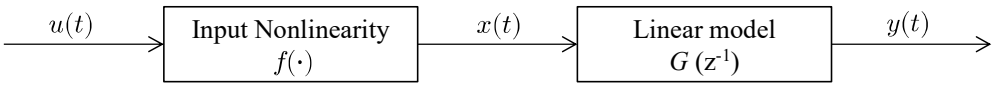

Figure 4.12. Block diagram of Hammerstein model.

4.4.2.1 **System formulation**

The system formulation in this section is the same as that in the previous literature [71] [72] [73] [84]. The sampling period of the simulation, which includes the controller, is 1s, and the Hammerstein model is the control target, as shown in the following equation.

$$\begin{aligned} y(t) &= 0.6y(t-1) - 0.1y(t-2) + 1.2x(t-1) \\ &\quad -0.1x(t-2) + v(t), \\ x(t) &= 1.5u(t) - 1.5u^2(t) + 0.5u^3(t), \end{aligned} \tag{4.23}$$

where v is the white noise with the variance 1×10^{-3}. Figure 4.13 shows the static characteristics of this system.

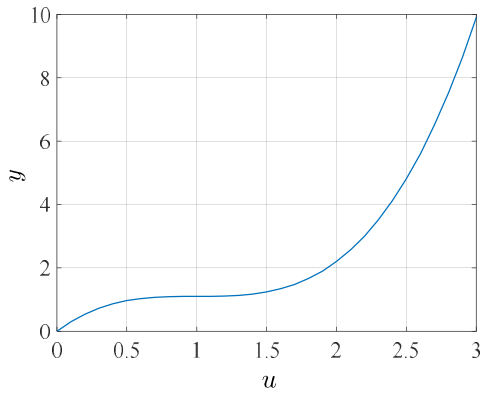

Figure 4.13. Static characteristic of the Hammerstein model.

The set-point at each time is

$$r(t) = \begin{cases} 1.0 & (0 < t \leq 100) \\ 3.0 & (100 < t \leq 200) \\ 0.5 & (200 < t \leq 300) \\ 2.0 & (300 < t \leq 400) \end{cases}. \tag{4.24}$$

The reference model uses the following equation [71] [72] [73].

$$M_d(z^{-1}) = \frac{0.399z^{-1}}{1 - 0.736z^{-1} + 0.135z^{-2}} \tag{4.25}$$

The gain scheduler uses Equation (4.8), and the scheduling parameters are the output and its second derivative:

$$\theta_1(t) = y(t), \theta_2(t) = y(t)(1 - z^{-1})^2. \tag{4.26}$$

In Section 4.4.1, we adopted the derivative as a scheduling parameter. In Section 4.4.2, we adopted the second derivative, which is more susceptible to noise, as another candidate.

4.4.2.2 **Result**

Figure 4.14 shows the given input/output data in the open-loop test. A chirp sin signal (frequency 0 to 1 Hz, amplitude 1.75, offset 1) is applied to the input, and the input/output data is measured. Figure 4.15 shows the time series data after the gain scheduling parameters are obtained from the measured input/output data. For comparison, this figure shows the time series data when using the CHR method, the standard VRFT (fixed PID gain), the VRFT by GS (applying the least-squares method (GS-VRFT-LS)), and the VRFT by GS (applying LASSO (GS-VRFT-LASSO)). The PID gains by the CHR method are K_p = 0.059, K_i = 0.058, and K_d = 0.0038, which were obtained from previous studies [71] [72] [73] . The fixed PID gains obtained by VRFT are K_p = 0.0655, K_i = 0.1744, and K_d = 0.0166. From the top of the figure, output, input, proportional gain, integral gain, and derivative gain are shown. Table 4.4 shows the MSE of the tracking error performance of CHR, VRFT, GS-VRFT-LS, and GS-VRFT-LASSO. In addition, as shown in the figure and the table, the response was very slow in the classical CHR method. By comparing the standard VRFT and GS-VRFT-LS, we can confirm that the GS-VRFT-LS has a PID gain that changes according to the state of the controlled object and that follows the target response. Also, by comparing the GS-VRFT-LS and GS-VRFT-LASSO, it can be seen that they have the almost same followability. Table 4.5 shows operation counts and weight coefficients obtained using the GS-VRFT-LS and GS-VRFT-LASSO for calculating PID gains from the gain scheduler shown in Equation (4.8). The total

counts of multiplication and addition in the scheduler obtained using LASSO are less than those obtained using the least-squares method. In LASSO, two weight coefficients became zero. In other words, the gain scheduling was performed with 18 weight coefficients for the LS and 16 weight coefficients for LASSO. The optimum value of λ for the L_1 regularization was 0.002 because of the cross-validation for multiple λ, which is described in Section 4.3.3.

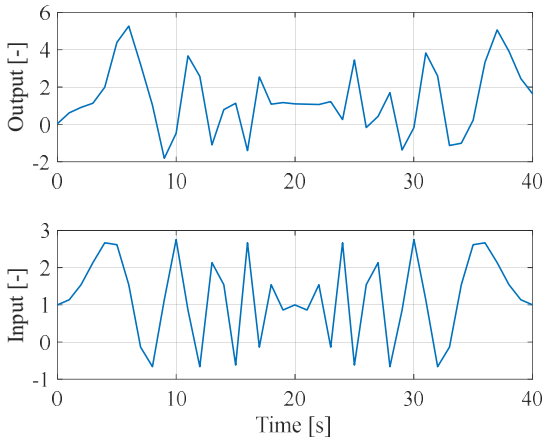

Figure 4.14. Time series data of the initial input and output under open-loop test.

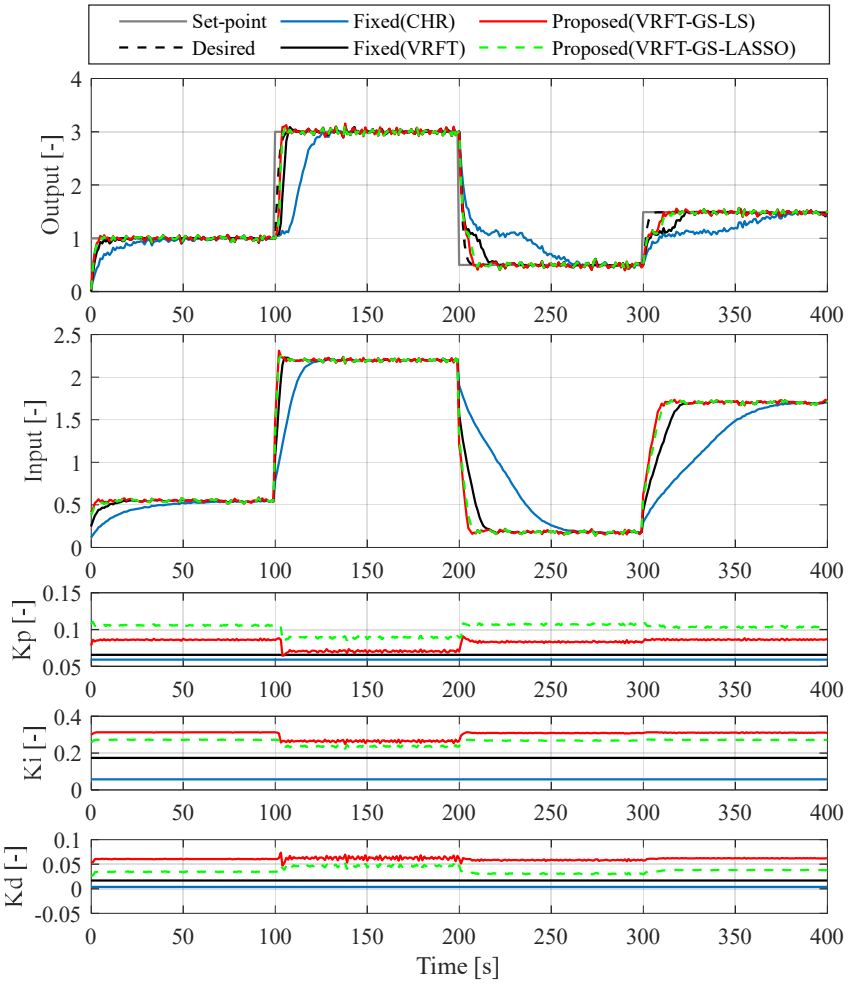

Figure 4.15. Time series data with the proposed method and fixed PID gain using open-loop data. GS-VRFT-LS and GS-VRFT-LASSO are overlapped.

Table 4.4. Results of the tracking error for the Hammerstein model for open-loop test.

	Fixed (CHR)	Fixed (VRFT)	GS-VRFT-LS	GS-VRFT-LASSO
MSE	1.548×10^{-1}	2.830×10^{-2}	8.121×10^{-3}	1.053×10^{-2}

Table 4.5. Operation counts and parameters of gain scheduler for Hammerstein model using open-loop data.

	GS-VRFT-LS	GS-VRFT-LASSO	Efficiency [%]
Multiplication	33	30	90.9
Addition	15	13	86.7
Total	48	43	89.6
Parameters	18	16	88.9

Figure 4.16 shows the given input/output data in the closed-loop test. The set-point signal is given to the random signal of which range is from −1 to 5, and the input/output data are measured. The fixed PID gains are set to $K_p = 0.059$, $K_i = 0.058$, and $K_d = 0.0038$, which were obtained using the CHR method in previous studies [71] [72] [73]. Figure 4.17 shows the time series data when gain scheduling parameters were obtained from the input/output data in the closed-loop test. For comparison, the data obtained when using the fixed PID gain (VRFT), the VRFT by GS (using the least-squares method (GS-VRFT-LS)), and the VRFT by GS (using LASSO regression (GS-VRFT- LASSO)) are shown. The fixed PID gains obtained using VRFT are $K_p = 0.0206$, $K_i = 0.1246$, and $K_d = 0.0229$. Table 4.6 shows the MSE of tracking error performance of CHR, VRFT, GS-VRFT-LS, and GS-VRFT-LASSO. Table 4.7 shows the operation counts and weight coefficients obtained using GS-VRFT-LS and GS-VRFT-LASSO for calculating PID gains from the gain scheduler shown in Equation (4.8). The total counts of multiplication and addition in the scheduler obtained by LASSO are less than those obtained using the least-squares method. In LASSO, one weight coefficient became zero. In other words, the gain scheduling was performed with 18 weight coefficients for the LS and 17 weight coefficients for LASSO. The optimum value of λ for the L_1 regularization was 1×10^{-5} because of the cross-validation for multiple λ, which is described in Section 4.3.3.

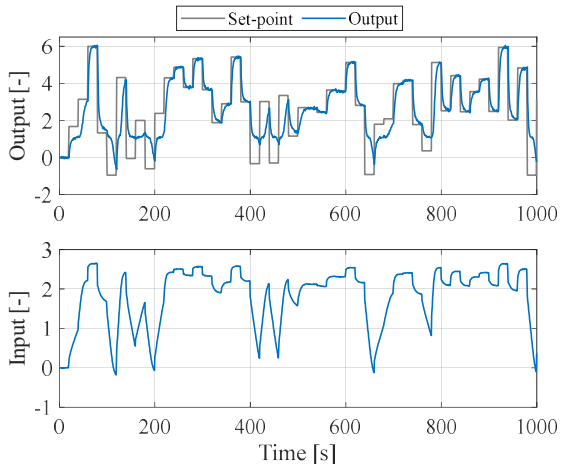

Figure 4.16. Time series data of the initial input and output under the closed-loop.

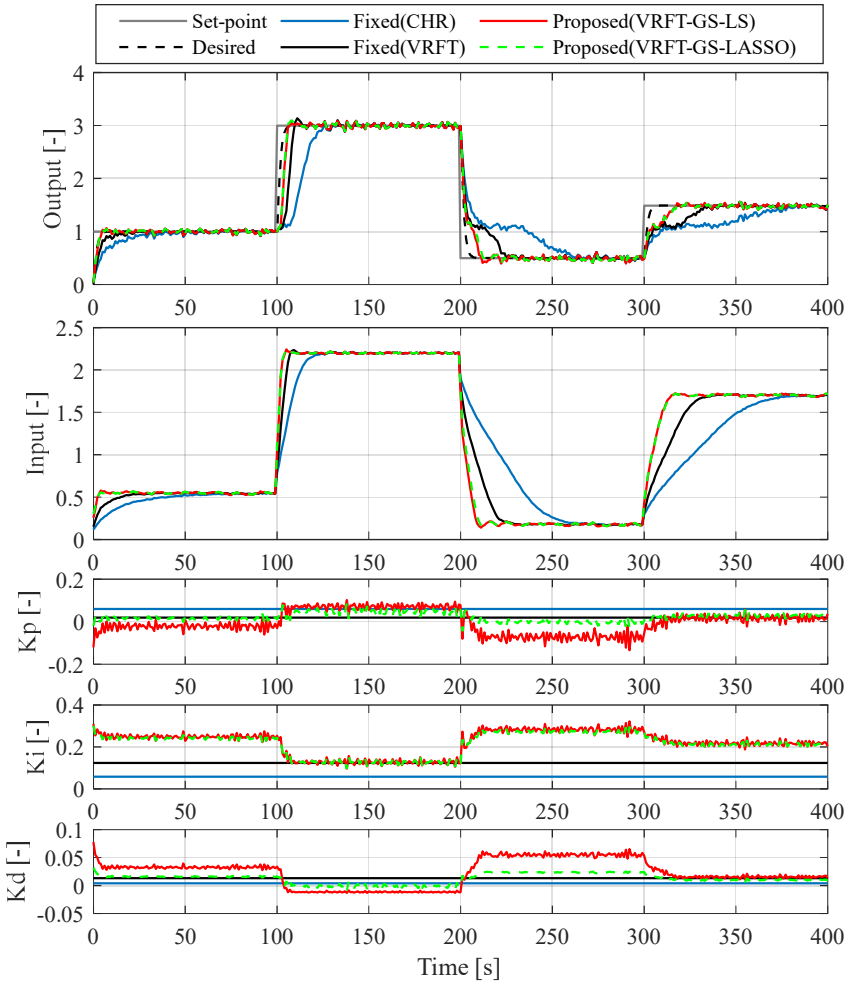

Figure 4.17. Time series data with the proposed method and fixed PID gain using closed-loop data. GS-VRFT-LS and GS-VRFT-LASSO are overlapped.

Table 4.6. Results of the tracking error for Hammerstein model for closed-loop test.

	Fixed (CHR)	Fixed (VRFT)	GS-VRFT-LS	GS-VRFT-LASSO
MSE	1.548×10^{-1}	5.562×10^{-2}	1.884×10^{-2}	1.908×10^{-2}

Table 4.7. Operation counts and parameters of gain scheduler for Hammerstein model using closed-loop data.

	GS-VRFT-LS	GS-VRFT-LASSO	Efficiency [%]
Multiplication	33	31	93.9
Addition	15	14	93.3
Total	48	45	93.8
Parameters	18	17	94.4

4.4.3 **Discussion**

When applied to System 2, the number of reductions of the weight coefficients by LASSO was low. However, System 1 was an LPV system whose characteristics changed because of the position. Therefore, it is considered that the velocity, which is the first derivative of the position used as the scheduling parameter, has little effect on the system characteristic fluctuation and that the number of weight coefficients is reduced. As a result, the calculation cost of the controller and the ROM area can be reduced, which is a significant result for the implementation in the mass product controllers. In System 1, the closed-loop system became unstable when the weight coefficients were obtained by the LS method under the simulation condition that scheduling parameters are positions and acceleration without the white noise. However, it was stable when LASSO was used. This is because overlearning occurred due to the unnecessary weight coefficients related to the acceleration when the LS method was used; however, in LASSO, the weight coefficients for acceleration were zero, implying that overlearning was suppressed. Regarding the use of open-loop and closed-loop test data, the tracking performance of the proposed method was shown to be significantly better than those of the conventional fixed gain tuning methods in both cases. However, in system 2, the trajectory of PID gains between open-loop and closed-loop is different. This is because initial input/output data are different between open-loop and closed-loop tests. We consider that multiple candidates exist for the controlled variable to be close to the reference. In Section 4.4, we used the position as one of the scheduler parameters, and another was velocity and acceleration for system 1 and system 2, respectively. Contrary to the above cases, it was confirmed that the same performance can be obtained when acceleration and velocity are used as scheduler parameters for system 1 and system 2, respectively.

4.5 **Conclusion**

In this chapter, a direct design method of a gain-scheduled PID controller that considers sparseness without system identification was presented for two types of nonlinear systems. In this method, to reduce the tuning parameters, a polynomial was used as the scheduling function, and the weight coefficients of the scheduling function, which are the tuning parameters, were obtained based on the data-driven control. By applying the VRFT, a

gain-scheduled PID controller could be directly designed from a set of input/output data without system identification. Furthermore, in the optimization, LASSO was used to further reduce the controller parameters and prevent overfitting. The effectiveness of this method was examined by simulation for two types of nonlinear systems. As a result, it was revealed that a controller with high sparse can be obtained without knowing the characteristics of the controlled object for a large number of control parameters of the gain scheduler. In summary, it was possible to realize gain-scheduled PID control with a low computational calculation cost and ROM area and without trial and error parameter tuning. It is considered that the proposed control law and tuning method can easily be accepted in many industries.

Chapter 5
Slip control during inertia phase using model-free self-tuning control

In this chapter, shift control of transmissions using model-free self-tuning control is proposed. Transmissions require a good shift feeling and improved fuel efficiency. In state-of-the-art stepped automated transmissions, the number of gear stages is increased and the lock-up area is expanded to improve fuel efficiency. However, a large number of stages and large lock-up area make obtaining a good shift feeling difficult and result in a transmission that requires a large number of man-hours for calibration. Therefore, to reduce the number of man-hours required for calibration and improve the shift feeling, a slip control law between the engine and the clutch, which is composed of a PID controller and a disturbance observer, is proposed. Moreover, PID gain is tuned online by installing an automatic tuning method that does not require a controlled object model. The effects of the proposed method are verified in an experiment using an actual vehicle. The experimental results show that the proposed method is effective for automatically tuning the PID gain and improving the shift feeling of the stepped automated transmission. The contents in this chapter are based on the literature [32].

5.1 **Introduction**

As components of automobiles, transmissions are required to have a good shift feeling and increasingly good fuel efficiency. To improve fuel efficiency, the number of gear stages of stepped automated transmissions with clutch-to-clutch shifting, such as automatic transmissions (ATs) and dual clutch transmissions (DCTs), has been increased, and in vehicles with torque converters, the area of the lock-up, which directly transfers engine power to the transmission without oil, has been expanded. As the shifting frequency in automated transmissions increases to become more multistage, a slight shift

shock causes discomfort to the driver and leads to deterioration of the durability of the product. In conventional shift control, the shift shock is absorbed by the fluid of the torque converter without lock-up, but in recent years, slip control law of the torque converter using the lock-up clutch has been studied to achieve both improvements in fuel efficiency and reduction in shift shock [87] [88] [89] [90] [91]. To realize slip control of the torque converter by implementing a lock-up mechanism, in addition to the multiplication of the lock-up clutch, changing the piston chamber and damper, and adding a proportional valve, a new configuration of the control system is required, which increases cost. Moreover, some vehicles are not equipped with a torque converter. Therefore, it is desirable to reduce the transmission shock by clutch control of the transmission without relying on slip control of the torque converter by the lock-up clutch. Figure 5.1 shows a shift process during an upshift. If the clutch is contacted when the angular acceleration of the engine is high, a shift shock occurs, as shown in Figure 5.1 (broken line). To reduce transmission shock, the engine angular acceleration must be reduced during the synchronization between the engine and the clutch output shaft rotational speed (i.e., when the differential rotation speed between the engine and clutch output shaft becomes zero). However, to reduce the contact shock, if the shift time is simply lengthened, as shown in Figure 5.1 (dotted line), slow feeling shift occurs, which leads to discomfort to the driver and a decrease in clutch life. These problems arise when the engine speed or the differential speed between the engine speed and the clutch output shaft speed cannot achieve the target value. Hence, by realizing control system design that follows the target value, it is possible to realize a shift without the slow sense or shock. In addition to the target value shown in Figure 5.1, when the clutch capacity is sufficient, slip control [92] is also performed in which the vehicle travels while generating the differential rotation speed to avoid a shift shock.

Control law during the inertia phase of an automated transmission has been studied in various ways by using model-based control [93] [94] [95] [96] [97] [98] [99]. For example, it is possible to study differential rotation speed control by using robust control such as H_∞ control. Although H_∞ control can ensure stability by considering the error in advance, it is usually necessary to estimate the error when a multi-domain complex system like an automatic transmission, which includes hydraulic, electric, and mechanical domains, is targeted. Thus, the designed controller becomes conservative. Further, the order of the

controller must be lowered so that it can be mounted on the mass production controller. Know-how is required to achieve good performance. It should be noted that a reduction in number of development man-hours is required, but it takes man-hours to obtain an accurate mathematical model. Also, it may be difficult to obtain highly accurate models in real systems in the industry. In commercial systems, most control systems are feed-forward control and PID control, which are easy to understand. In particular, PID control is used in more than 90% of industrial control loops [7]. However, PID control requires calibration to tune the control parameters. In recent years, the rapid increase of electronic control has caused a problematic increase in the number of calibration man-hours [87]. Considering this background, studies have been carried out on model-free control and reducing the number of calibration man-hours [13] [17] [19] [21] [22] [33] [34].

This study proposes a differential rotation speed control law (in other words, a slip control law) that realizes reduced shock during the inertia phase by slip control of a transmission for a stepped automated transmission with clutch-to-clutch shifting. Automatic PID gain tuning uses online FRIT based on recursive least square (RLS) [35] [36] that do not require a controlled object model. There have been no prior studies on applying FRIT to automotive systems, particularly automated transmissions and their experimental verification, because FRIT is a relatively new technique. Most FRIT applications involve simple experimental equipment and plants in which PID controllers are used in large quantities as mentioned in the Chapter 1. The conventional slip control law for an automated transmission does not cooperatively control the engine and automated transmission. Such conventional control systems have not been designed to be suitable for applying FRIT to tune the feedback linear controller parameters. Particularly, because the clutch torque is operated according to the conventional slip control law, a trade-off with drivability occurs, and complicated modeling of the clutch is required. In light of these factors, linear feedback control cannot be constructed, and it is difficult to automatically tune all the parameters. Furthermore, experimental verification using actual industrial machines is also a hurdle and is likely the reason why there has been no automotive application. This study proposes a linear feedback control law in which the engine torque is used as the manipulated variable by performing cooperative control of the engine and the automated transmission; this allows the slip control law to be implemented in a linear controller, which facilitates the application of FRIT. A reduction

in the number of calibration man-hours and a good shift feeling are expected by automatically tuning the controller parameters of the proposed control law.

The structure of this chapter is described as follows. Section 5.1 describes the necessity of the stepped transmission, its problems, and the importance of the control method without using a model. Section 5.2 explains the controlled object by using a simple model of the automated transmission with clutch-to-clutch shifting. In Section 5.3, a closed-loop system is constructed by using a PID controller and a disturbance observer for slip control. That is, the cooperative control of the engine and the automated transmission is constructed. Further, the FRIT–RLS technique [35] [36] for automatically tuning the PID gain is briefly described. Section 5.4 experimentally verifies the effect of the control law constructed in Section 5.3 by using an actual vehicle. The results show that clutch control of the transmission according to the proposed method can realize slip control and shifting without extension or shock. Section 5.5 discusses the conclusions of this chapter.

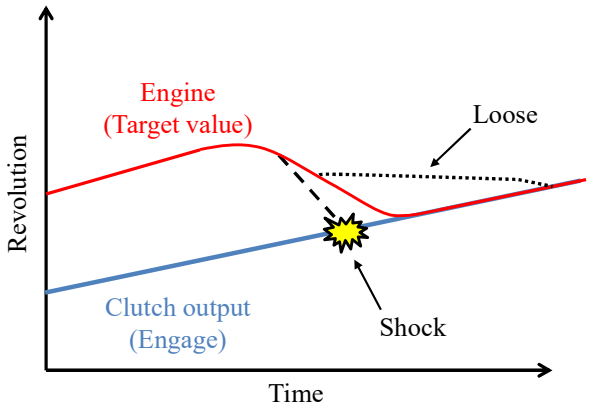

Figure 5.1. The cause of shift shock.

5.2 System overview

5.2.1 Controlled object

Figure 5.2 shows a simplified model of a controlled object. The controlled object includes an engine, a plurality of clutches, and gears. T_e, T_{clt}, T_o, ω_e, ω_{clt}, and ω_o are the engine torque, the clutch torque, the output shaft torque of the automated transmission, the engine rotation speed, the clutch output rotation speed, and the output

shaft rotation speed of the automated transmission, respectively. Subscripts A and B represent clutches A and B, respectively. Next, the shift process during an upshift is shown in Figure 5.3. There is a torque phase in which the clutch is replaced during an upshift, and there is an inertia phase during which a change in the engine speed takes place [100]. In the inertia phase, it is important to reduce the slow feeling and shock that occur when the engine and clutch output shaft rotation speed are synchronized (i.e., when the differential rotation speed between the engine rotation speed and the clutch output shaft rotation speed becomes zero). As shown by the broken line in Figure 5.1, a shock occurs when the engine rotation angular acceleration at the differential rotation speed 0 is large. Note that the torque converter is not shown in Figure 5.2 because it is in the lock-up state during the shift.

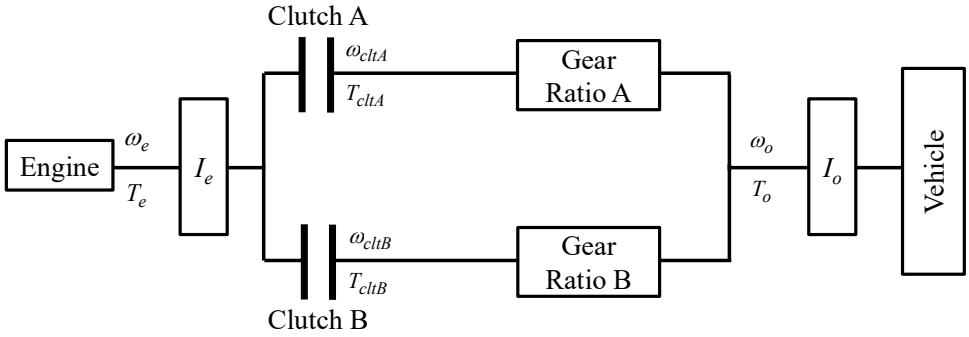

Figure 5.2. Simplified vehicle system with a stepped transmission.

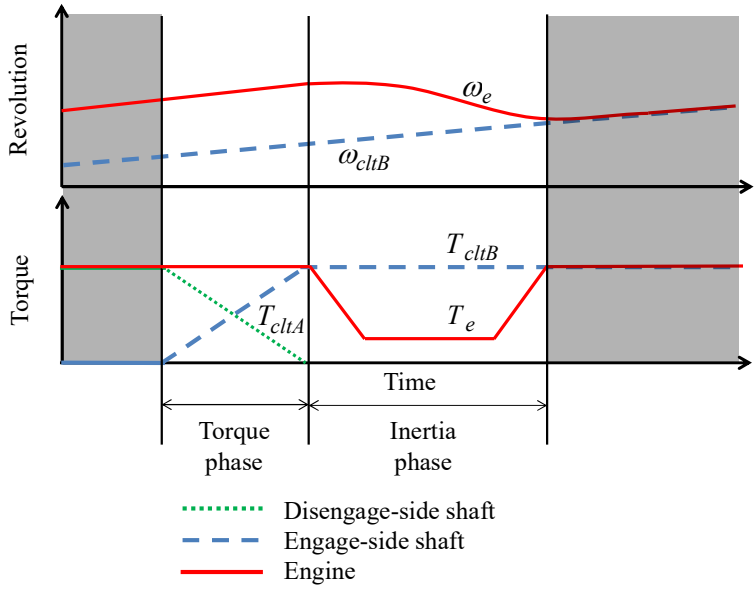

Figure 5.3. Shift process.

5.2.2 **Motion model during the inertia phase**

During the inertia phase, the clutches A and B are in a slip state. The equations of motion of the engine shaft and the clutch output shaft are expressed by Equation (5.1). The shift is realized by generating engine and clutch torque. Note that the actual drivetrain model is more complicated, but a very simplified model is described because the on-line automatic PID tuning method subsequently described in Section 5.3 does not require a controlled object model.

$$\begin{cases} I_e \dfrac{d\omega_e}{dt} = T_e - T_{cltB} \\ I_{in} \dfrac{d\omega_{cltB}}{dt} = T_{cltB} - T_L \end{cases}, \tag{5.1}$$

where I_{in} is the equivalent moment of inertia of the vehicle (the sum of the vehicle-side rotation inertia converted on the clutch), T_L is the driving resistance torque, and F_L is the driving resistance. T_L and F_L are expressed as

$$
\begin{aligned}
T_L &= \frac{F_L r_w}{G_r G_f}, \\
F_L &= \frac{1}{2}\rho_0 C_d A_f {v_x}^2 + mg(\mu_r + \sin\beta) + F_{wd},
\end{aligned}
\tag{5.2}
$$

where G_r, G_f, r_w, ρ_0, C_d, A_f, m, g, μ_r, β, and F_{wd} are gear ratio, final stage gear ratio, tire dynamic radius, air density, resistance coefficient, projected area on the front surface, vehicle weight, gravitational acceleration, rolling resistance coefficient, road gradient, and disturbance, respectively. T_{cltB} is the clutch torque acting on the engaging-side shaft and is expressed as

$$
\begin{aligned}
T_{cltB} &= \mu R N (A P_{cB} - F_{rtrn}), \\
P_{cB} &= f(i_{vlvB}),
\end{aligned}
\tag{5.3}
$$

where μ, R, N, A, P_{cB}, F_{rtrn}, and i_{vlvB} are clutch frictional coefficients, clutch effective radius, the number of clutch contacting surfaces, piston pressure receiving area, hydraulic pressure in the clutch piston chamber, clutch spring reaction force, and the current of the pressure proportional valve, respectively; note that f represents a function. The clutch torque is correlated with the pressure in the clutch piston chamber. The pressure in the piston chamber is generated by applying current to the pressure proportional valve. That is, clutch torque is generated by applying current to the pressure proportional valve. The relationship between the current and pressure is nonlinear, and the characteristic differs depending on each pressure proportional valve.

5.2.3 **Relationship between the controllers and a controlled object**

The vehicle system comprises a plurality of controllers. The respective controllers exchange various signals by controller area network (CAN) communication. The relationship between the transmission control module (TCM), engine control module (ECM), transmission, and engine can be described as follows. Figure 5.4 shows the main component of the shift control during the inertia phase. Q_{fuel} is the fuel injection quantity, ^ represents the estimated value, and the subscript *cmd* represents an instruction value. The content described in Section 5.3 is implemented in the TCM. The engine

torque is sent by the TCM to the ECM by CAN communication. The engine torque is generated by informing the engine of the fuel injection quantity calculated by the engine torque controller in the ECM. Further, the engine torque estimated by the torque estimator in the ECM is transmitted to the TCM. The engine speed obtained by the sensor and the electronic circuit in the ECM is transmitted to the TCM by CAN communication. The engine torque commanded by the TCM is sent to the ECM by CAN communication. This engine torque is obtained by the proposed slip speed controller in the TCM described later. The clutch output shaft speed is generated by informing the transmission of the clutch valve current calculated in the TCM. The clutch output shaft speed is obtained by the sensor and the electronic circuit in the TCM. The clutch valve current is calculated to meet the driver requested torque, which is calculated from the driver's accelerator pedal position and engine speed.

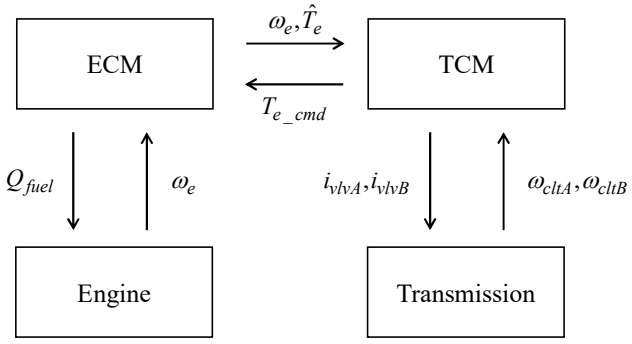

Figure 5.4. Vehicle system controllers and controlled objects.

5.3 **Slip speed control**

After introducing an outline of the shift control during the inertia phase, the feedback control system using a PID controller that is constructed to realize the differential rotation speed control of the clutch and engine is described. In addition, we discuss a disturbance observer and self-tuning PID control that are introduced to cope with changes in the clutch characteristics and reduce the number of calibration man-hours.

5.3.1 **Outline of shift control during inertia phase**

The outline of the basic control of the engine and clutch in the inertia phase is described here. Figure 5.5 shows the process of generating the clutch and engine torque; α is the driver's accelerator pedal position, $\Delta\omega$ is the amount of slip rotation between the engine rotation speed and clutch output engage-side shaft rotation speed. First, the driver requested torque is calculated from driver's accelerator pedal position and engine speed. The driver requested torque is the target clutch torque on the engine shaft. A current to be applied to the valve is calculated from the driver requested torque by using the equation correlating the clutch torque and the pressure (Equation (5.3)). The clutch torque is then generated by applying the calculated valve current. This enables the driver to generate the intended driving force. Becuase the clutch torque generates the driver demand torque, the engine torque is used as a manipulated variable to control the engine speed or the differential speed; i.e., the engine speed control or the differential rotation speed control are performed using the engine torque as a control input to the engine.

In the differential rotation control law proposed by the literatures [96] [97] [98], the driver requested torque cannot be generated by the clutch torque because the valve current that manipulates the clutch torque is used in the manipulated variable for slip control. Thus, the output shaft torque of the transmission fluctuates, and a favorable transmission feeling cannot be obtained. To reduce the torque fluctuation, the engine torque is given as a feed-forward term [97] [98]. However, the logic is not explained, and if the feed-forward term is not appropriate, the driver's intended acceleration will not be achieved. In comparison, in the method proposed in this chapter, the driver-required torque is generated by the clutch torque, and the differential rotation speed control is performed by using the engine torque as the manipulated variable; the shift leading to the driver's intended acceleration can be realized during the inertia phase.

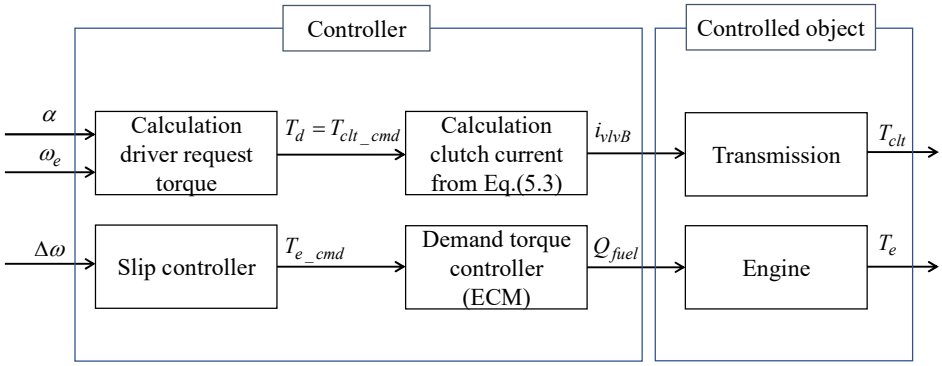

Figure 5.5. Overview of shift control during the inertia phase.

5.3.2 **Slip speed control law between engine and clutch**

A feedback control law for realizing differential rotation control is derived. When Equation (5.1) is rearranged, the equation of motion for the differential rotational speed is as follows:

$$I_e \frac{d\,\Delta\omega}{d\,t} = T_e - T_d \tag{5.4}$$

with

$$T_d = T_{cltB}\left(1 + \frac{I_e}{I_{in}}\right) - \frac{I_e}{I_{in}} T_L, \tag{5.5}$$

$$\Delta\omega = \omega_e - \omega_{cltB}, \tag{5.6}$$

where T_d can be regarded as a disturbance torque. Therefore, let the right side of Equation (5.4) be the control input of the PID controller, according to Equation (5.7):

$$\begin{aligned} I_e \frac{d\,\Delta\omega}{d\,t} &= u \\ &= T_e - T_d. \end{aligned} \tag{5.7}$$

The PID controller $C(s,\rho)$ is given by

$$C(s,\rho) = \rho^T \varphi(s) \tag{5.8}$$

with

$$\begin{aligned} \rho &= [\rho_p \quad \rho_i \quad \rho_d]^T, \\ \varphi(s) &= \left[1 \quad \frac{1}{s} \quad \frac{s}{\tau_d s + 1}\right]^T, \end{aligned} \tag{5.9}$$

where ρ, ρ_p, ρ_i, ρ_d, and τ_d are control parameter vectors, proportional gains, integral gains, differential gains, and time constants of an approximate differentiator, respectively, and the symbol s represents a Laplace operator. The information sent to the engine is the required value of engine torque and is expressed as

$$T_{e\_cmd} = u + T_d. \tag{5.10}$$

Therefore, it is necessary to know the disturbance torque T_d. Here, the disturbance torque is estimated using the disturbance observer [101] [102] [103], as shown in the following equation:

$$\hat{T}_d = \frac{T_e - I_e \Delta\omega s}{\tau s + 1} = \frac{T_e + I_e \Delta\omega/\tau}{\tau s + 1} - \frac{I_e}{\tau}\Delta\omega, \tag{5.11}$$

where τ is the low-pass filter time constant. First, the methods to determine the parameter by the general theory are described. The time constant should be small based on the estimated velocity. However, possibly, the correct estimation cannot be performed owing to the influence of observation noise. In other words, there is a trade-off to determine the time constant. Next, the method to determine the parameter for the proposed slip controller is explained. When the differentiation is performed with a small time constant, the estimated disturbance torque becomes oscillatory for the observation noise. Thus, the engine command torque also becomes oscillatory; this leads to driver discomfort. However, the estimation must follow changes in the disturbance torque including the driver requested torque and the load torque. In practice, the time constant should be chosen so that the estimated disturbance torque does not oscillate.

We can see that by using the disturbance observer in Equation (5.11), calibration parameters significantly reduce and the disturbance torque can be estimated more simply. If the disturbance observer is not adopted, disturbance torque is obtained from Equation (5.5), which includes engine inertia, vehicle-side rotational inertia, clutch torque, and driving resistance. Therefore, there is substantial calibration cost requirement for the system identification to obtain parameters in Equation (5.5). Moreover, methods to estimate the clutch torque and the driving resistance must be established. Therefore, the disturbance observer is effective to simplify the estimation of the disturbance torque.

As described in Equations (5.8) and (5.11), the three parameters required for the design of the slip control law are the PID gain ρ, the low-pass filter time constant τ of the disturbance observer, and the engine inertia I_e. However, the PID gain is automatically tuned (as described later), and the time constant used in the disturbance observer is easily determined. The engine inertia is readily obtained by checking the design information or system identification.

The control structure is shown in Figure 5.6. The PID gain is optimized by the automatic tuning mechanism described in Section 5.3.3.

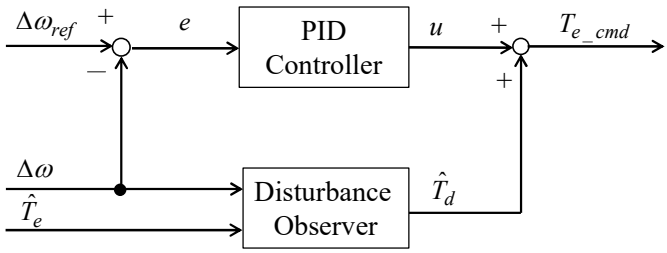

Figure 5.6. Block diagram of the slip controller.

5.3.3 **Automatic PID gain tuning mechanism**

An automatic PID gain tuning mechanism is introduced to cope with characteristic variations caused by aging or temperature changes as well as to reduce the number of calibration man-hours. FRIT has been proposed as a method for automatically tuning control parameters off-line without a controlled object model using only a set of input/output data. This feature implies that using this method can reduce the number of

calibration man-hours. Furthermore, an on-line FRIT based on RLS has been applied [35] [36].

5.3.3.1 **FRIT for slip control**

We consider the case where the FRIT content shown in Chapter 2 is replaced with slip control, as shown in Figure 5.7. Thus, we obtain next equation:

$$J(\rho) = \sum_{k=1}^{N} (\Delta\omega_{yr}(k) - \Delta\omega(k))^2 \tag{5.12}$$

with

$$\Delta\omega_{yr}(k) = M_d(z)\Delta\omega_{ref}(k). \tag{5.13}$$

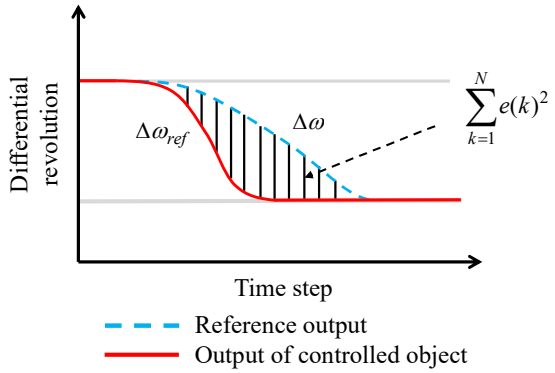

Figure 5.7. Time series of the slip control using FRIT.

5.3.3.2 **On-line FRIT**

Because standard FRIT has a nonlinear cost function, the computational cost of performing on-line calculations is high. In on-line FRIT, the computational cost is reduced by transforming the optimization problem to be solved into a least squares problem and solving the optimization problem by the RLS method. To make the cost function a least squares problem, Equation (2.30) is modified.

Considering the ideal case where the cost function is zero, Equation

$$y_0(k) - M_d(z)\tilde{r}(\rho, k) = 0. \tag{5.14}$$

is obtained. Substituting this equation into Equation (2.28) yields:

$$C(\rho)y_0(k) - M_d(z)u_0(k) - C(\rho)M_d(z)y_0(k) = 0 \tag{5.15}$$

Focusing on Equation (5.15), a cost function such as Equation (5.16) is minimized:

$$\hat{J}(\rho) = \sum_{k=1}^{N} \hat{e}(k)^2 \tag{5.16}$$

with

$$\hat{e}(k) = C(\rho)\big(1 - M_d(z)\big)y_0(k) - M_d(z)u_0(k). \tag{5.17}$$

We replace the initial input/output data u_0 and y_0 with the input/output u and y (sequentially measured) and organize Equation (5.17) as following:

$$C(\rho) = \rho^T \varphi(z), \tag{5.18}$$

$$\xi(k) = \varphi(z)\big(1 - M_d(z)\big)y(k), \tag{5.19}$$

$$d = M_d(z)u(k), \tag{5.20}$$

where $\varphi(z)$ is obtained by discretizing $\varphi(s)$. Then, Equation (5.17) is as follows:

$$\hat{e}(k) = \rho^T \xi(k) - d(k). \tag{5.21}$$

We can see that the error $\hat{e}$ can be expressed in a linear form with respect to ρ. The RLS with the forgetting factor is implemented to minimize the linearized cost function for on-line calculation. The RLS algorithm [104] with forgetting factor is found in Equations

$$\hat{\rho}(k) = \hat{\rho}(k-1) + K(k)\Big(d(k) - \xi^T(k)\hat{\rho}(k-1)\Big), \tag{5.22}$$

$$K(k) = \frac{\boldsymbol{P}(k-1)\xi(k)}{\lambda + \xi^T(k)\boldsymbol{P}(k-1)\xi(k)}, \tag{5.23}$$

$$P(k) = \frac{1}{\lambda}\left\{P(k-1) - \frac{P(k-1)\xi(k)\xi^T(k)P(k-1)}{\lambda + \xi^T(k)P(k-1)\xi(k)}\right\}, \tag{5.24}$$

where P is the covariance matrix, and λ is the forgetting factor. In the on-line FRIT, to prevent instability of the system due to a rapid parameter change of the controller, it has been proposed that an implemented controller parameter is updated by Equation (5.25), which is also used in this study:

$$\rho(k) = (1-\gamma)\rho(k-1) + \gamma\hat{\rho}(k-1), \tag{5.25}$$

where γ is a small positive number.

Remark 5.1. The relationship between online FRIT and VRFT is described. Equation (5.17) is equivalent to the cost function of VRFT when the prefilter L is M_d. That is, the online FRIT is equivalent to VRFT with $L = M_d$ under the assumptions that the cost function of FRIT is zero.

5.3.3.3 **Design of the reference model for slip control**

The design of the reference model for slip control is described. A designer determines an ideal response. For the slip control, a reference response without overshoot is recommended because the differential rotation speed between the engine and clutch output shaft should be zero to avoid transmission shock at the synchronization point. The *n*-order transfer function, shown in Equation (5.26), is known as the reference model that does not induce overshoot because all poles exhibit a negative real part [105].

$$M_d(s) = \frac{p^n}{(s+p)^n}, \tag{5.26}$$

where *p* is the parameter for determining the responsiveness. The design parameter *n* is chosen considering the computational cost; in a previous study [96], third order was used.

The parameter p is chosen considering the clutch durability and engine inertia, the maximum torque, etc. Moreover, we consider the case that the controlled object has dead time. It's impossible for the controlled object to track a reference response whose dead time is shorter than that of the controlled object. Because this limitation of dead time is related to the inherent characteristics that cannot be improved by controllers, the reference model, including the dead time, is used as [63]

$$M_d(s) = \frac{p^n}{(s+p)^n} e^{-sL}, \tag{5.27}$$

where L is the estimated dead time of the controlled object. In FRIT–RLS, the error $\hat{e}$ must be a linear form with respect to the optimizing parameters to use the RLS algorithm in Equation (5.21). However, when the optimizing parameters include dead time, the error $\hat{e}$ is not linear with respect to the optimizing parameters, including the dead time. Thus, we determine the dead time, included in Equation (5.27), in advance instead of including the dead time in the optimizing parameters. A designer needs to estimate the dead time to design the reference model. Hence, the transfer function form and the parameters n and p are determined without using a controlled object model. The parameter L should be determined based on information from the controlled object.

5.4 **Experimental verification**

5.4.1 **Outline of the experiment**

An overview of the system is shown in Figure 5.8. The test vehicle is a medium-sized truck (total vehicle weight is 8 tons), and the diesel engine used is a 4HK1-TCS (Type: 4 cylinders OHC direct injection diesel, displacement: 5193 cc, compression ratio: 16.5, maximum power: 154 kW/2400 rpm, maximum torque: 706 Nm/1400–1600 rpm). The transmission (T/M) is a stepped automated transmission with clutch change (torque converter is installed, wet multi-plate clutches are used). The ECM uses conventional controllers produced in large volumes, and the TCM uses dSPACE's Rapid Prototyping System (MABX and RapidPro). The created program is implemented in MABXII, and the programing language is MATALB®/Simulink. The sampling period of the TCM and ECM is 8 ms. Signals of various controllers are communicated by CAN. The transmission

of the engine torque from the TCM to ECM requires approximately 30 ms, and the engine speed is sent from the TCM to the ECM in 10 ms. Then, after the lock-up clutch of the torque converter is engaged, the upshift is performed. The time-series data sent from MABXII to the notebook PCs are measured for the various signals.

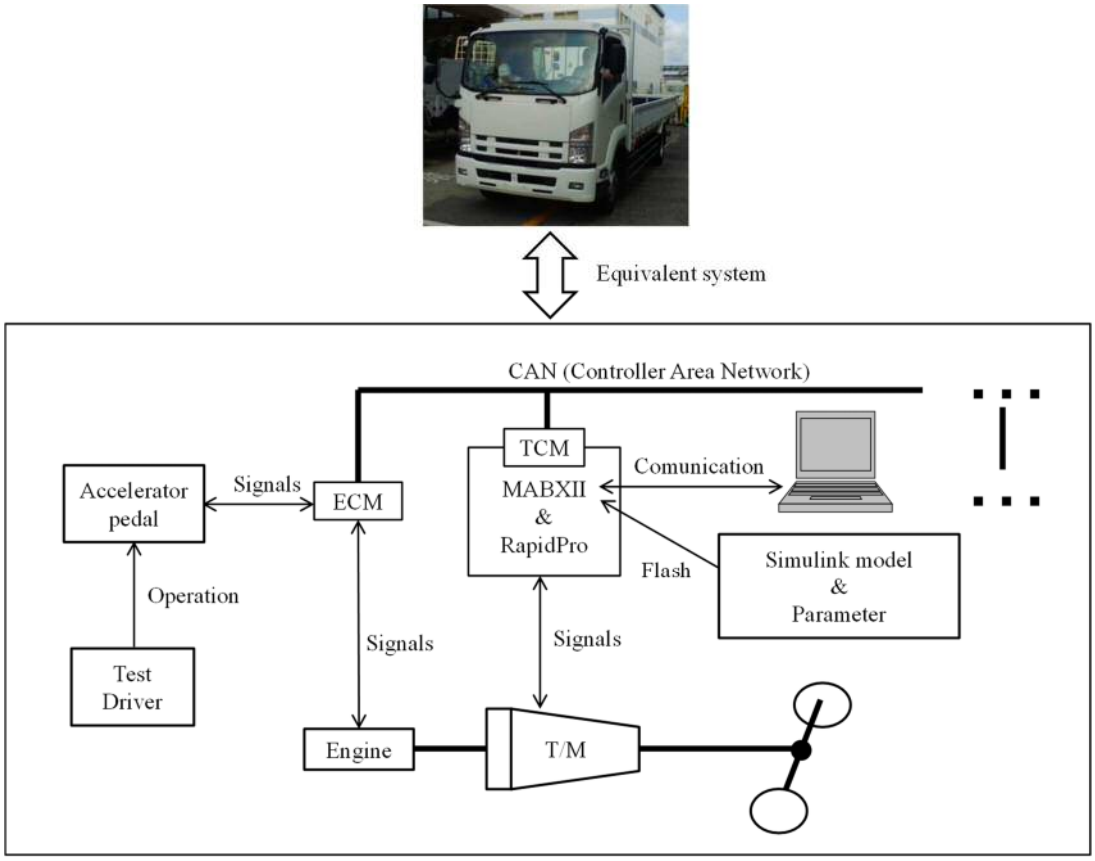

Figure 5.8. Overview of the experimental system.

The parameters for the reference model, RLS algorithm, and disturbance observer are shown in Table 5.1. The reference model uses the transfer function in Equation (5.27). We adopt the third order as performed in a previous study [96]. Regarding the dead time in Equation (5.27), see Figure 5.5; the engine torque is generated by providing the ECM with the value calculated by the TCM, calculating the fuel injection quantity for generating the requested torque in the ECM, and applying the calculated fuel injection value to the engine i.e., the requested engine torque and the actual torque are not completely the same. The actual engine torque generation mechanism is very complicated,

but in this study, the relationship between the requested engine torque value and the actual value is approximated by the dead time L in Equation (5.28):

$$T_e = T_{e\_cmd} e^{-Ls}. \tag{5.28}$$

Thus, a dead time occurs from the time when the engine torque value is requested to the time when the actual engine torque is generated. This approximation is reasonable from the experimental results described in Section 5.4.2.

Table 5.1. Design parameters.

Symbol	Value
p	30
L	0.03
$P(0)$	diag(1000,1000,1000)
λ	0.999
$\rho(0)$	[1.0, 0.3, 0.1]
γ	0.3
τ	0.2

5.4.2 **Experimental results and discussion**

Figure 5.9 shows time-series data obtained when the shift-up from the second to the third speed and the shift-up from the third to the fourth speed are performed under the condition that the target differential rotation speed is set to 200 rpm and the PID gain is set to an appropriate initial value. The horizontal axis represents time, and the temporal developments of the differential rotation speed, indicated torque, proportional gain, integral gain, and differential gain are shown in each plot. From the figure, we can see that the PID gain is automatically tuned and follows the target value in one shift. In Figure 5.10, time-series data is plotted for the clutch being smoothly engaged during the inertia phase with the tuned PID gain. The change in the differential rotation speed, rotational speed, and indicated torque and the transmission output shaft speed over time are shown in the plots. We see that the engine speed can be smoothly connected to the engage-side shaft, and the shift is completed without inducing a shock or a slow feeling. Moreover,

based on the rotation speed of the transmission output shaft, it is confirmed that no extreme fluctuation is present, and the fluctuation level is almost the same before and after synchronization. Therefore, we consider the shift shock to be extremely small. Table 5.2 shows the performance index that normalizes Equation (5.12) by the inertia phase time and maximum tracking error for the differential accelerator pedal position and shifting gear position. The conditions for accelerator pedal position are the low, middle, and high range, and for the gear shift speed, the conditions are from second to third, from third to fourth, and from fourth to fifth speed. Here, the second speed means the gear position in a commercial vehicle launch. Based on the results of the performance index, the proposed method realizes the same level of performance in every case with various accelerator pedal and shift positions. Also, the maximum tracking error in every case is 5.41 rad/s (51.7 rpm). Therefore, we consider that the proposed method realizes target slip control with approximately 50 rpm. Figure 5.11 shows the experimental result for a target differential rotation speed of 50 rpm. The horizontal axis represents time, and the temporal developments of the differential rotation speed, rotation speed, and torque are shown in each plot. The controlled object response can track the target response. Therefore, the results confirm that the constructed differential rotation speed control law with PID automatic tuning is capable of obtaining a good upshift feeling without prior calibration.

We consider the reasons for the automatically tuned differential and integral gains to approach almost zero. First, the integration approaches almost zero because of the effects of the disturbance observer and the dead time. Although the integral term of the PID controller is used to cancel the steady state deviation, the proposed method includes a disturbance observer; the removal of the steady state deviation is considered to be compensated by the disturbance observer rather than the integral term of the PID controller, i.e, all torques other than the nominal inertial acceleration/deceleration torque ($I_e \frac{d\Delta\omega}{dt}$) are regarded as equivalent disturbance, and the constructed disturbance observer simultaneously compensates them all [102]. Moreover, the control system, including the controlled object and the disturbance observer designed herein, has an integral factor, type 1 system, during the steady state (see Appendix). Thus, the steady state deviation theoretically becomes zero. As described above, because the disturbance observer cancels the steady state deviation, the integration gain becomes very small. Regarding the

influence of the dead time, if the integration term becomes large by integrating the error during the dead time, the control input becomes excessively large, and the control system becomes unstable in some cases. Because the reference model used in this experiment is a system with a relatively slow response, undershoot occurs with respect to the target response when the integral term excessively increases the control input. In addition, for systems in which phase lag occurs because dead time, it may be undesirable to further delay the phase from a stability standpoint because the integral term is a phase lag component. Considering why the differential gain approaches zero, it is important to remember that the differential term of the PID control is effective in improving the transient characteristic, i.e., although the differential term is used to improve the response in the high frequency region, the target response in this experiment exhibits a relatively gradual characteristic with respect to the target value, whereby the gain in the high frequency region does not need to be increased. Therefore, the differential gain becomes almost zero.

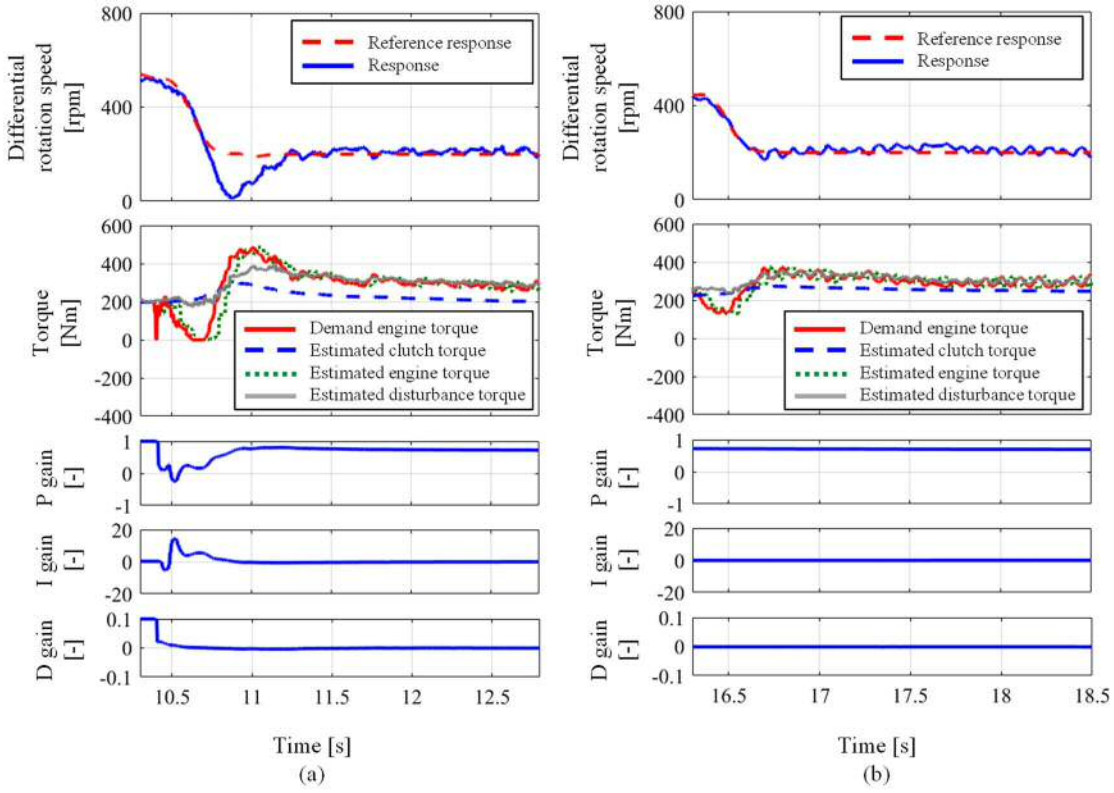

Figure 5.9. Results of upshift slip control. (a) Up shift (First time). (b) Up shift (Second time).

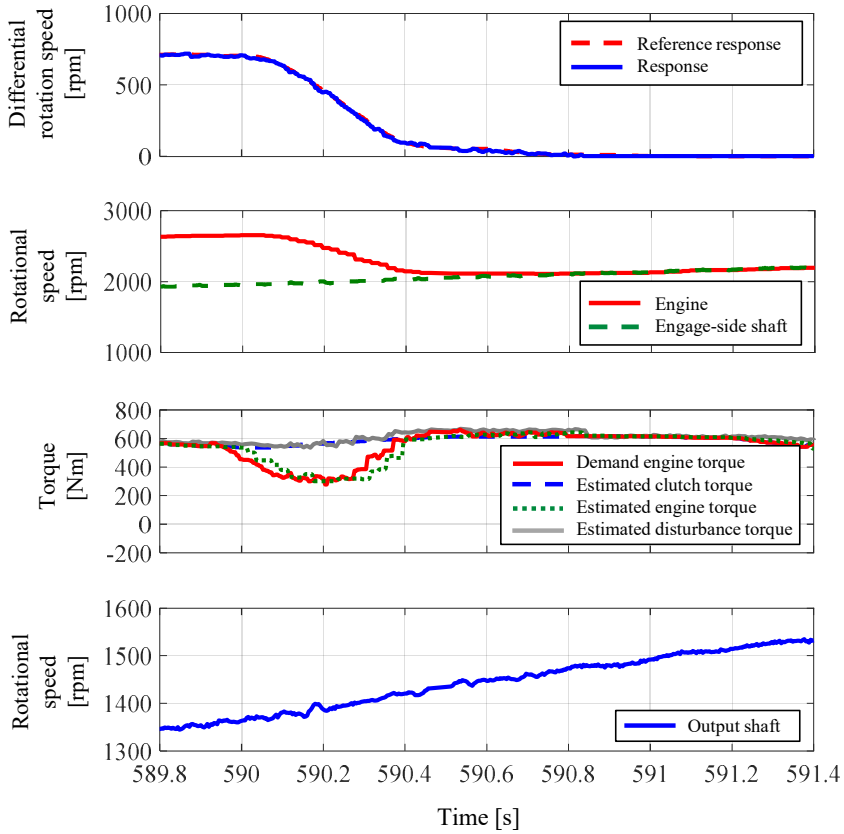

Figure 5.10. Results of ideal upshift control.

Table 5.2. Control results for different cases.

Accelerator pedal position [%]	Shifting gear position [speed]	Performance index [–]	Maximum tracking error [rad/s]
30–40	2nd to 3rd	4.74	+3.49
(Low range)	3rd to 4th	1.48	–2.61
	4th to 5th	2.43	+2.46
50–60	2nd to 3rd	5.43	–5.41
(Middle range)	3rd to 4th	3.25	–5.03
	4th to 5th	1.41	+2.52
80–90	2nd to 3rd	4.28	+4.83
(High range)	3rd to 4th	5.21	+4.59
	4th to 5th	2.23	+4.01

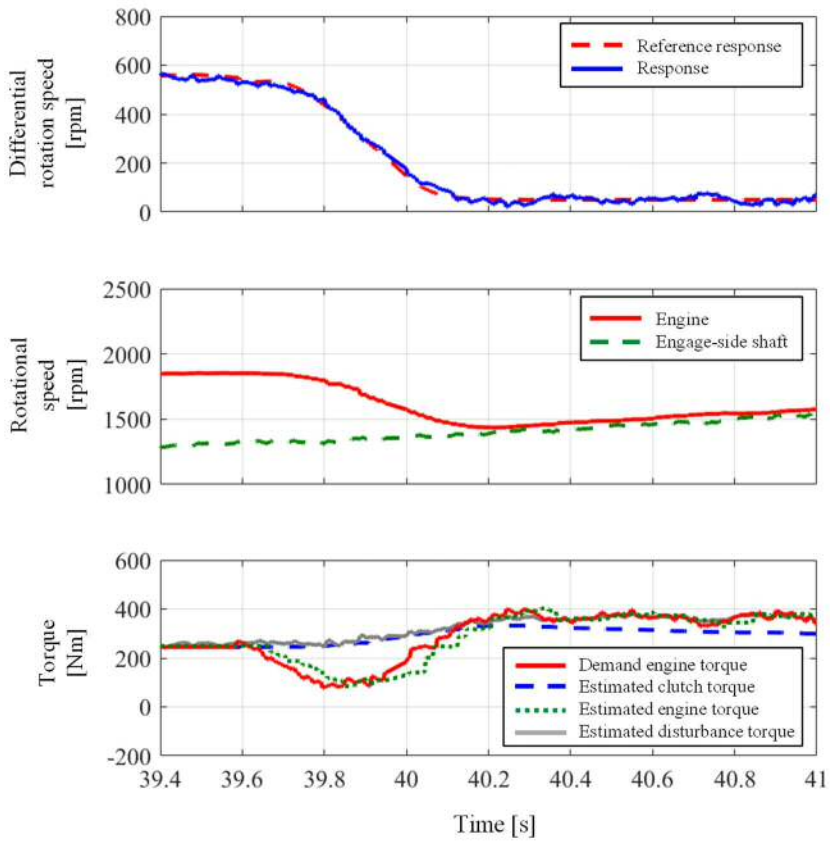

Figure 5.11. Shift-up control result under the condition with target differential rotation speed is 50 rpm.

5.5 **Conclusion**

A new slip control law is proposed for shifting during the inertia phase of a stepped automated transmission with clutch-to-clutch shifting. The proposed control law consists of a PID controller and a disturbance observer. The PID gain is automatically tuned by installing a FRIT–RLS method. The proposed method was experimentally verified by an actual vehicle test. The results confirmed that the PID gain can be tuned by one shift, and the amount of slip can achieve the target value. Also, the engine and clutch rotation speed on both sides are synchronized smoothly to realize the desired shift. Based on these results it can be concluded that the proposed method is effective in reducing the number of calibration man-hours and improving the shift feeling in a stepped automated transmission.

Appendix

The disturbance observer is described and the reason a system including controlled object and disturbance observer is a type 1 during the steady state is explained. Here, the type 1 system includes an integral factor [106]. The block diagram of the disturbance observer used in the slip control is shown in Figure 5.12. It's assumed that T_e, T_{e_cmd} and $\hat{T}_e$ are the same for a simple explanation. P is an actual controlled object, and F is a filter, such as a low-pass filter. P_m is a nominal model of P and can be expressed by Equation (5.29) based on Equation (5.4) or Equation (5.7):

$$P_m(s) = \frac{1}{I_e s}. \tag{5.29}$$

The relationship between the signals in Figure 5.12 is expressed as follows:

$$\Delta\omega = P(T_e - T_d), \tag{5.30}$$

$$T_e = u + \hat{T}_d, \tag{5.31}$$

$$\hat{T}_d = F\left(T_e - I_e \frac{d\Delta\omega}{dt}\right). \tag{5.32}$$

Organizing Equation (5.30), Equation (5.31), and Equation (5.32), Equation (5.33) can be obtained in Laplace space:

$$\begin{aligned}\Delta\omega(s) = &\frac{P(s)}{1 - F(s) + P(s)F(s)P_m^{-1}(s)}u(s) \\ &- \frac{\big(1 - F(s)\big)P(s)}{1 - F(s) + P(s)F(s)P_m^{-1}(s)}T_d(s).\end{aligned} \tag{5.33}$$

When the system shown in Equation (5.33) becomes steady state, $s = 0$ and $F(0) = 1$. Thus, we can obtain Equation (5.34):

$$\Delta\omega(0) = P_m(0)u(0). \tag{5.34}$$

Based on Equation (5.34), the characteristic of the system, including disturbance observer and controlled object, is the same as $P_m(s)$ during steady state. Therefore, this system guarantees a type 1 system that includes an integral factor.

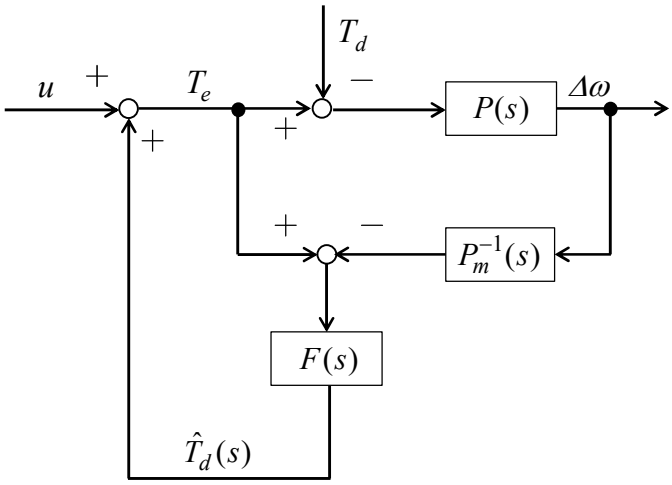

Figure 5.12. Block diagram of the disturbance observer.

Chapter 6
Direct tuning of electro-pneumatic clutch control

In this chapter, a gain-scheduled controller with direct tuning is proposed for the position control of a pneumatic clutch actuator installed in heavy-duty trucks. Pneumatic clutch actuators are highly nonlinear systems and cannot be easily controlled. Various industries require a simple controller design that is easy to understand and requires few trial-and-error calibrations. A gain-scheduled PID control law, which is a well-known and easy-to-understand nonlinear control method, is adopted. In this approach, a gain scheduler is expressed using polynomials composed of coefficient parameters and controlled object states as well as using the results from Chapter 4. To reduce trial-and-error tuning, the unknown coefficient parameters of the polynomials are directly tuned from the controlled object input/output data without requiring a controlled object model. The proposed controller design procedure is simple and does not require system identification or trial-and-error tuning. The effectiveness of the proposed method is verified via an experiment using an actual vehicle. The experimental results confirm the effectiveness of the proposed method for the position control of pneumatic clutch actuators. The contents in this chapter are based on the literature [107].

6.1 **Introduction**

The demand for driving comfort is increasing, with the automotive industry moving toward automatic transmissions not only for passenger vehicles but also for heavy-duty trucks. Automatic transmission (AT) and continuously variable transmission (CVT) are used in passenger cars but are unsuitable for heavy-duty trucks because of their high cost and low efficiency [108]. Automated manual transmission (AMT), which is manual transmission (MT) with electronic-controlled clutch and gear actuators, has advantages

such as low cost, high efficiency, and improved fuel efficiency, and is used in large trucks. An automatic control of the clutch connection plays an important role in AMT vehicles [43]. In general, a hydraulic system is preferred for position control [109] [110], whereas pneumatic clutch actuators are used in heavy trucks given that compressed air comes preinstalled in such vehicles. In addition, ON/OFF valves are used owing to their cost-effectiveness, compactness, and robustness. In a pneumatic clutch system, it is difficult to perform the desired and sensitive position control because of the compressibility of air, the nonlinearity in the clutch spring reaction force, and the use of ON/OFF valves.

The automobile industry uses control laws based on feedforward and PID control, which have low computational cost and are intuitive [32]. PID control is used in more than 90% of the control loops [7]. The control law often consists of a look-up table (LUT) tuned by trial and error [68] [69] because many automobile devices have nonlinearity. On the other hand, with the rapid adoption of electronic control in recent years, the time required for parameter tuning has increased [87]. To this end, model-free control and data-driven control have been explored [13] [17] [19] [21] [23] [27] [28] [47] [71] [75] [77] [111] and applied to automobile systems [30] [32] [49] [76].

Thus far, the control for pneumatic clutch actuators has been accomplished through use of model-based approaches, including H_∞ control [112], sliding mode control [113] [114], model predictive control [115] [116] [117] [118], adaptive control [119], state feedback control using feedback linearization [120], fuzzy control [121], and backstepping control [122]. In these methods, an observer is required to construct a state feedback controller; an observer for estimating the pressure inside a clutch piston has been proposed [123] [124]. Some previous studies reported satisfactory control performance; however, system identification was required for model-based control. As a pneumatic clutch actuator is a nonlinear system [108], a considerable amount of time is required to establish an accurate mathematical model. Identifying an accurate mathematical model remains a significant challenge. Additionally, neural networks have been investigated for PID control [125]. However, the calculation cost associated with neural networks is an issue.

Herein, a practical position control method is proposed to reduce calibration time for the tuning process and calculation cost for a pneumatic clutch actuator with strong nonlinearity. This method features a gain-scheduled control law with a polynomial as the

gain scheduler and enables direct tuning of the gain-scheduling parameters without use of a controlled model. Gain-scheduled control is an efficient and effective approach for actual nonlinear systems [41]. The design method can derive the Linear Matrix Inequality (LMI) using the Linear parameter-varying (LPV) model. Otherwise, the controller parameters need to be tuned at each operating point. In other words, tuning by trial and error or modeling of the nonlinear system is required. To deal with these issues, a method for automatically tuning the control parameters directly from the input/output data of the controlled object without system identification is constructed. This is expected to improve the development efficiency. In addition, gain-scheduled control using an LUT (which is often used in the automobile industry) can express the nonlinearity but is not preferred for mass production because the required ROM area is considerable. Therefore, a gain scheduler (scheduling function) with a polynomial composed of the controlled object states and coefficient parameters is constructed. This helps reduce the ROM area and vary the control parameters based on the clutch position and speed. A previous study [116] attempted to eliminate the nonlinearity between the valve signal and the amount of air by creating a correlation map between the duty ratio of the valve and the amount of air. However, it is generally difficult to measure the absolute amount of flow rate. Therefore, in this study, the duty ratio of the PWM (Pulse Width Modulation) control provided to the solenoid valves (i.e., the control input) is calculated directly from the clutch state quantity (i.e., position and speed) without having to establish a correlation map between the valve duty ratio and the flow rate. The direct tuning method is based on VRFT [21], which is a data-driven control method. Here, the coefficient parameters of the scheduling function and the basis function are linearly combined. This allows linear regression, which is a feature of VRFT, and the optimum solution of the coefficient parameters of the scheduler can be obtained using a linear regression algorithm such as the least-squares method. To the best of our knowledge, there have been no prior studies that applied a direct tuning method to gain-scheduled controllers for pneumatic clutch actuators.

This chapter is organized as follows. Section 6.2 briefly describes the pneumatic clutch actuator model which is the controlled object and the control system. Section 6.3 describes the direct tuning method for the gain-scheduled control based on VRFT. In Section 6.4, the effectiveness of the proposed method is verified through actual vehicle tests. The obtained results confirm that the automatically tuned gain-scheduled control

can achieve the desired position control. Section 6.5 presents the conclusions drawn from the study results.

6.2 Control system

6.2.1 Pneumatic clutch actuator system

Figure 6.1 shows the pneumatic clutch actuator system. The pneumatic clutch actuator system is the controlled object which is comprised of a valve system, a clutch actuator, and a clutch. The valve system has a supply side with two ON/OFF solenoid valves (valve 1 and valve 2). The exhaust side also has two ON/OFF solenoid valves (valve 3 and valve 4). The flow from the valve system enters chamber A and is converted to pressure. Under the pressure action on the piston, the piston moves, and a force acts on the spring, thereby generating a clutch torque. In other words, in a pneumatic clutch actuator, position control is performed to arrange the transmissible torque.

The model of the system is shown in Figure 6.1. Since no controlled object model is used in this study, the description of this system is simple. Note that the physical model shown in the figure can essentially express both the clutch actuators of which clutch spring is directly actuated by the pressure bearing and indirectly actuated by using a set of levers. The physical model of the clutch actuator can be expressed as follows:

$$\dot{y} = v, \tag{6.1}$$

$$\dot{v} = \frac{1}{M}\left(A_A p_A - A_0 P_0 - f_l(y) - f_f(v, z)\right), \tag{6.2}$$

$$p_A = \frac{RT_0}{V_A(y)} m_A, \tag{6.3}$$

$$\dot{m}_A = w_t(p_A, d), \tag{6.4}$$

$$w_t(p_A, d) = w_{v1}(p_A, d_1) + w_{v2}(p_A, d_2) - w_{v3}(p_A, d_3) - w_{v4}(p_A, d_4), \tag{6.5}$$

where y is the piston position, v is the velocity, p_A is the pressure in the chamber A, $w_t(p_A, d)$ is the flow rate for chamber A, and m_A is the mass of air in chamber A. d is the vector of the operation signal d_i (i = 1, 2, 3, 4) for each valve, and $w_{vi}(p_A, d_i)$ (i = 1, 2, 3, 4) is the flow rate generated at each valve. A_A is the area of chamber A. A_0 is the area of chamber A minus the area of the piston rod, M is the mass of the piston, P_0 is the atmospheric pressure, T_0 is the temperature, and R is the gas constant of air. $V_A(y)$, which is the gas constant for chamber A, is the volume, and $V_A y = V_{A0} + A_A y$, where V_{A0} is the dead volume of chamber A (volume in chamber A under atmospheric pressure). $f_l(y)$ and $f_f(v, z)$ are the clutch spring reaction force and frictional force, respectively. The mass flow rate w_{vi} of each valve formulated in ISO/DIS 6358 [126] and in literature [127] is as follows:

$$w_{vi} = A_{vi} C_i p_h \sqrt{\frac{T_0}{T_h}} d_i \quad (0.528 < z \leq 1), \tag{6.6}$$

$$w_{v_i} = A_{vi} C_i p_h \sqrt{\frac{T_0}{T_h}} \sqrt{1 - \left(\frac{z - 0.528}{1 - 0.528}\right)^2} d_i \quad (0 \leq z \leq 0.528), \tag{6.7}$$

$$z = \frac{p_l}{p_h}, \tag{6.8}$$

where A_{vi} is the orifice effective area, T_h is the supply-side temperature, T_0 is the standard temperature, p_h is the pressure on the high side, p_l is the pressure on the low side, and C_i is determined by the valve characteristics. Figure 6.2 shows an example of the relationship between the clutch position y and the clutch load $f_l(y)$, wherein the curve characteristic is linear to a certain position but thereafter becomes nonlinear, including hysteresis [128].

Next, the dead zone of the ON/OFF valve is described. In this study, the ON/OFF valve is driven by the PWM. In other words, the operation signal d_i for each valve is the duty ratio. When the duty ratio is low, there is a dead band width, wherein the valve is nonoperational. The dead zone $D_a(d_i)$ with the dead zone width $[0, a_i]$ is expressed as

$$D_a(d_i) = \begin{cases} d_i - a_i & d_i > a_i \\ 0 & 0 \le d_i \le a_i \end{cases}. \tag{6.9}$$

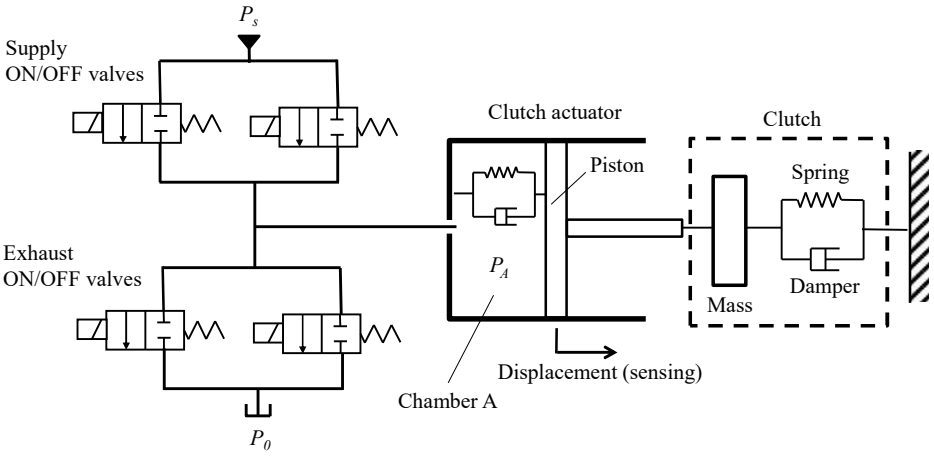

Figure 6.1. Layout of the electro-pneumatic clutch (EPC) system comprising three components.

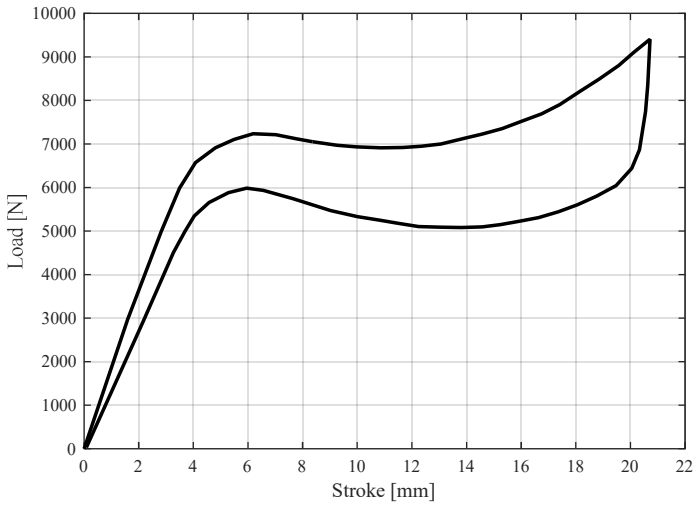

Figure 6.2. Characteristics of the spring used in the electro-pneumatic clutch (EPC) system [128].

6.2.2 **Control law**

From Section 6.2.1, we find that there are nonlinear elements such as the pneumatic cylinder, clutch spring characteristics, mass flow rate–valve input relationship, and ON/OFF valve. A control law to deal with these nonlinearities is constructed. Figure 6.3 shows the control law comprising gain-scheduled control, saturation, valve selection, and dead zone compensation. Here, *r* is the target value, y is the clutch position, u is the control input calculated by the gain-scheduled controller, u_s is the control input after saturation, $u_i(i = 1, 2, 3, 4)$ are the control input assigned to each valve that is the duty ratio, and $d_i(i = 1, 2, 3, 4)$ assigned to each valve are the duty ratio applied to the valve after dead zone compensation is performed.

The gain-scheduled control method achieves the desired control by changing the control parameters based on the environment and state of the controlled target. The gain-scheduled control is explained in detail in the next section. The saturation function $S(u)$ is expressed as

$$S(u) = \begin{cases} s_{ub} & u > s_{ub} \\ u & s_{lb} \leq u \leq s_{ub}, \\ s_{lb} & u < s_{lb} \end{cases} \tag{6.10}$$

where u is the control input, and s_{ub} and s_{lb} are the upper and lower limits of the control input, respectively. In other words, the range of the control inputs after saturation is $S(u) \in [s_{ub}, s_{lb}]$. For a total of four valves, when the duty ratio given to each valve is $u_i \in [0, 1]$ $(i = 1,2,3,4)$, the control input becomes $u \in [-2, 2]$. In other words, $s_{ub} = 2$, and $s_{lb} = -2$. Next, the method of selecting the valve to be driven is explained using Table 6.1. The control input of $u_s \in [-2, 2]$ is distributed to each valve. In this study, the orifice diameter of each valve is the same. Hence, if the control input is $u_s \in [0, 1]$, only valve 1 on the supply side is used, and if $u_s \in [1, 2]$, both valves 1 and 2 on the supply side are used. The same applies to the exhaust valve side. For the dead zone compensator $d_i(u_i)$, the minimum lower limit value $a_i(i = 1, 2, 3, 4)$ of the duty ratio at which the clutch position starts to operate for each valve is added.

$$d_i(u_i) = \begin{cases} (1-a_i)u_i + a_i & u_i > a_i \\ 0 & u_i = 0 \end{cases}, \tag{6.11}$$

where u_i is the duty ratio given to the valve before the dead zone compensation. To reduce valve operation as much as possible, the valves are switched off when the error in the clutch position with respect to the target value is within a predetermined threshold and remains in a predetermined duration.

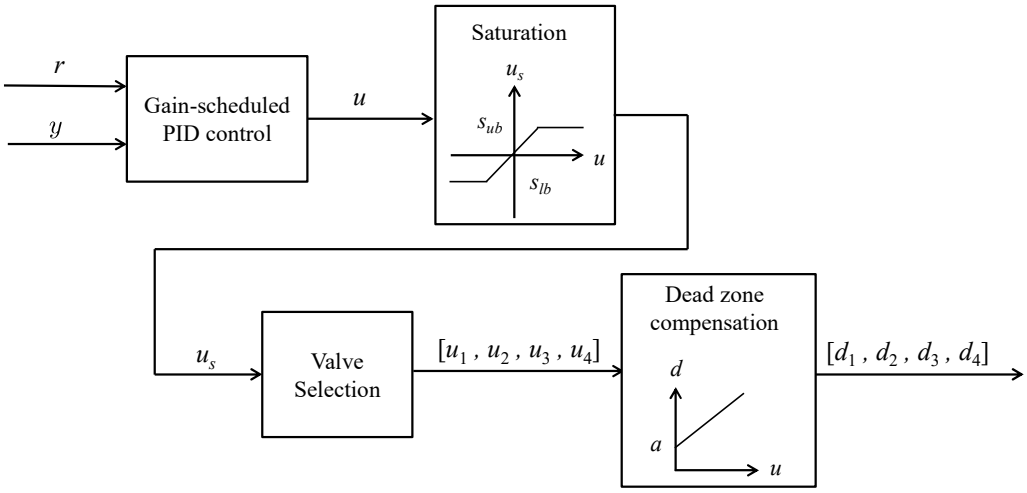

Figure 6.3. Control law for electro-pneumatic clutch actuator.

Table 6.1. Actuated valve selection.

	Duty ratio, u_s			
	$[-2, -1)$	$[-1, 0)$	$[0, 1]$	$(1, 2]$
Supply valve 1, u_1	0	0	$\lvert u_s \rvert$	1
Supply valve 2, u_2	0	0	0	$\lvert u_s \rvert - 1$
Exhaust valve 3, u_3	1	$\lvert u_s \rvert$	0	0
Exhaust valve 4, u_4	$\lvert u_s \rvert - 1$	0	0	0

6.2.3 **Gain-scheduled control**

We consider the application of the gain-scheduled PID controller to the position control of a pneumatic clutch actuator. First, the fixed PID control input is described as

$$u(t) = C_{pid}(z, x)e(t) \tag{6.12}$$

with

$$\begin{aligned} C_{pid}(z) &= K_{pid}^T \psi(z), \\ K_{pid} &= [K_p \quad K_i \quad K_d]^T, \\ \psi_{pid}(z) &= \left[1 \quad \frac{1}{(1-z^{-1})} \quad (1-z^{-1})\right]^T. \end{aligned} \tag{6.13}$$

Figure 6.4 shows a feedback control system comprising a feedback controller and the pneumatic clutch actuator system derived in Section 6.2.1. From Figure 6.4 and Equations (6.3) and (6.4), we see that the pneumatic clutch actuator includes an integral element between the control input and the mass of air. In other words, when the control input acts, the piston chamber pressure and clutch position vary. Considering the valve as a part of the controller, the integral term is already included in the controller. Therefore, the second term, which is the integral element of Equation (6.13), is no longer necessary, and PD control is used as the digital controller [80].

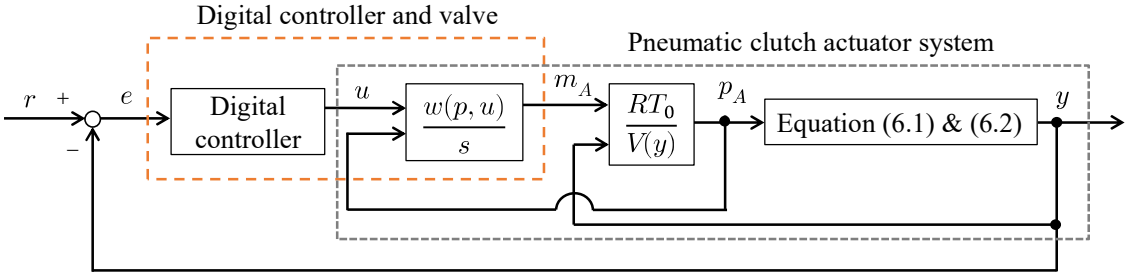

Figure 6.4. Block diagram of the feedback system for the pneumatic clutch actuator.

Figure 6.5 shows a block diagram of the gain-scheduled control system. The gain-scheduling PD control is as follows:

$$u(t) = C(z, x)e(t) \tag{6.14}$$

with

$$\begin{gathered} C(z,x) = K^T\psi(z) = f^T(x)\psi(z), \\ f(x) = [K_p(x) \quad K_d(x)]^T, \\ \psi(z) = [1 \quad (1-z^{-1})]^T, \end{gathered} \tag{6.15}$$

where $f(x)$ is the scheduling function vector, $K_j(x)$ $(j = p, d)$ is the PD gain scheduler (scheduling function), and x is the scheduling parameter vector. In this study, the gain scheduler in Equation (6.15) uses a polynomial. The just-in-time method [78], database control [71], and neural network [82] are difficult to implement in mass-produced controllers because of computational costs and ROM area limitations. Gain schedulers using LUTs have been used in industries, particularly for automobile control. However, the required ROM capacity is high, and the number of tuning parameters is considerable. Another concern in the gain-scheduled control with LUTs (which express the gain designed for each operating point) is the rapid fluctuation in the PD gain, which destabilizes the system. In this study, the scheduling function is represented by a quadratic polynomial, Equation (16). As a result, the number of storage parameters is reduced, and the gain varies continuously. The latter makes it difficult for sudden gain changes to occur.

$$\begin{gathered} K_j(x) = w_j^T x_{sf}, \\ w_j = \begin{bmatrix} w_{j0} & w_{j1} & w_{j2} & w_{j3} & w_{j4} & w_{j5} \end{bmatrix}^T, \\ j \in \{p, d\}, \\ x_{sf}(x) = [1 \quad x_1 \quad x_2 \quad x_1x_2 \quad x_1^2 \quad x_2^2]^T, \end{gathered} \tag{6.16}$$

where x_1 and x_2 are the scheduling parameters, which are the clutch position and speed, respectively. x_{sf} is the function vector (basis function) of the scheduling parameter, and w_j is the respective weight coefficient (regression coefficient) vector for the PD gain.

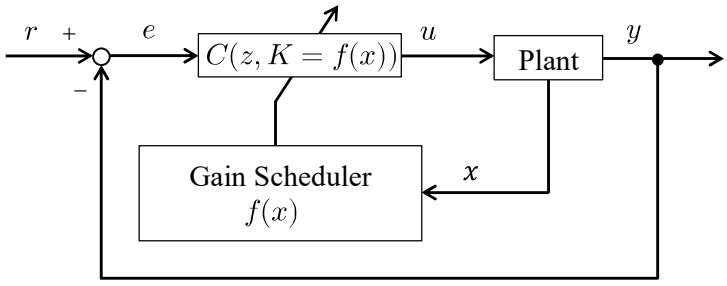

Figure 6.5. Gain-scheduled control system.

6.3 Automatic tuning method for gain-scheduling parameters

6.3.1 Optimization of gain-scheduling parameters by VRFT-GS

Herein, a new cost function to obtain the optimum value of the weighting coefficient of the gain-scheduling function is derived. From the cost function of VRFT (see Equation (2.10) and the Equations (6.14)–(6.16) related to the gain-scheduling PD control, the cost function for the gain-scheduling PD control using VRFT (GS-PD-VRFT) is as follows.

$$J(w) = \|d(t) - w^T \xi(t)\|_2^2 \tag{6.17}$$

$$\begin{aligned} d(t) &= Lu(t) \\ \xi(t) &= X(M_d^{-1}(z) - I)Ly(t) \end{aligned} \tag{6.18}$$

with

$$w = \begin{bmatrix} w_p & w_d \end{bmatrix}^{\mathrm{T}}, \tag{6.19}$$

$$X = \begin{bmatrix} x_{sf}^T \psi_1(z) & x_{sf}^T \psi_2(z) \end{bmatrix}^{\mathrm{T}}, \tag{6.20}$$

where ψ_i is the *i*-th element of the vector ψ. As the cost function is linear with respect to the control parameter vector w, the optimal solution can be obtained by the following equation using the least-squares method.

$$w^* = (Z^T Z)^{-1} Z^T D \tag{6.21}$$

with

$$Z = [\xi(1) \quad \xi(2) \quad \cdots \quad \xi(N)]^{\mathrm{T}}, \tag{6.22}$$

$$D = [d(1) \quad d(2) \quad \cdots \quad d(N)]^{\mathrm{T}}. \tag{6.23}$$

6.3.2 **Algorithm**

The algorithm for the weighting coefficient (control parameter) in the automatic tuning of the gain-scheduling function using VRFT is shown below.

[Step 1] Measure the input/output data of the controlled object.

[Step 2] Define the reference model.

[Step 3] Determine the candidates of the scheduling parameters and design the scheduling functions for each PD gain.

[Step 4] Design the VRFT prefilter.

[Step 5] Find the weighting coefficient (control parameter) of the scheduling function that minimizes the cost function.

Remark 6.1. In Step 1, the pneumatic clutch actuator includes an integral element between the control input and the clutch position (shown in Figure 6.1). The input/output data are acquired in a closed-loop manner in a system that includes this type of integral element [49]. In addition, the saturated input u_s is used to derive the control parameters that consider input saturation [111].

Remark 6.2. The reference model of Step 2 is described. The clutch position and torque are correlated. For example, if an undershoot occurs during half-clutch control, the torque fluctuates rapidly, and a shift shock occurs. Therefore, a response without over/undershoot is desirable. The *n*-order transfer function, expressed in Equation (6.24), is known as the reference model that does not induce overshoot because all the poles exhibit a negative real part. In addition, there is a dead time between the instruction

provided to the valve and the operation of the clutch. The reference model can be expressed by the following equation:

$$M_d(z) = \mathrm{c2d}\left(\frac{1}{(\tau s+1)^n}\right) z^{-L}, \tag{6.24}$$

where τ is a time constant that represents the response speed, n is the order, L is the lag step, and c2d is the conversion from the s region to the z region.

Remark 6.3. In Step 4, the original cost function and the cost function of the VRFT can be matched by applying a strict prefilter, as done in previous studies [75] [77]. However, the prefiltering requires multiple additional experiments. Herein, the prefilter described in Equation (6.25) is used for practical use [28].

$$L(z) = M_d(z). \tag{6.25}$$

6.4 Experimental verification

6.4.1 Outline of the experiment

Figure 6.6 shows the outline of the experimental system. The test vehicle is an actual heavy-duty truck (GVW class weighing approximately 25 ton), and the installed diesel engine is a 6UZ1-TCS model (type: six-cylinder OHC direct-injection diesel, displacement: 9839 cc, compression ratio: 16.2, maximum power: 279 kW/1800 r/min, maximum torque: 1814 N·m/1000–1200 r/min). The pneumatic clutch actuator used in this experiment was designed for heavy-duty trucks, similar to the one described above. The supply pressure is 850 kPa, and the battery voltage is 24 V. Table 6.2 shows the dead zone of the valves. The controller used is a rapid prototyping control system consisting of MABX and RapidPro from dSPACE. The proposed method was programmed in MATLAB®/Simulink® (ver. 2015a SP1) from MathWorks and implemented in MABX. The various signals were measured as time-series data sent from MABX to a notebook PC. The control law shown in Figure 6.3 is implemented on RCP, and the direct tuning procedure is performed by the PC in this study. Note that, at the time of commercialization, it is possible to perform all the procedures on the controller by measuring the input/output

data and solving the least squares problem shown in Equation (6.21) since the setting values for steps 2-4 of the proposed algorithm can be predetermined. The sampling period was 10 ms, and the PWM period was 20 ms. Table 6.3 shows the parameters of the reference model.

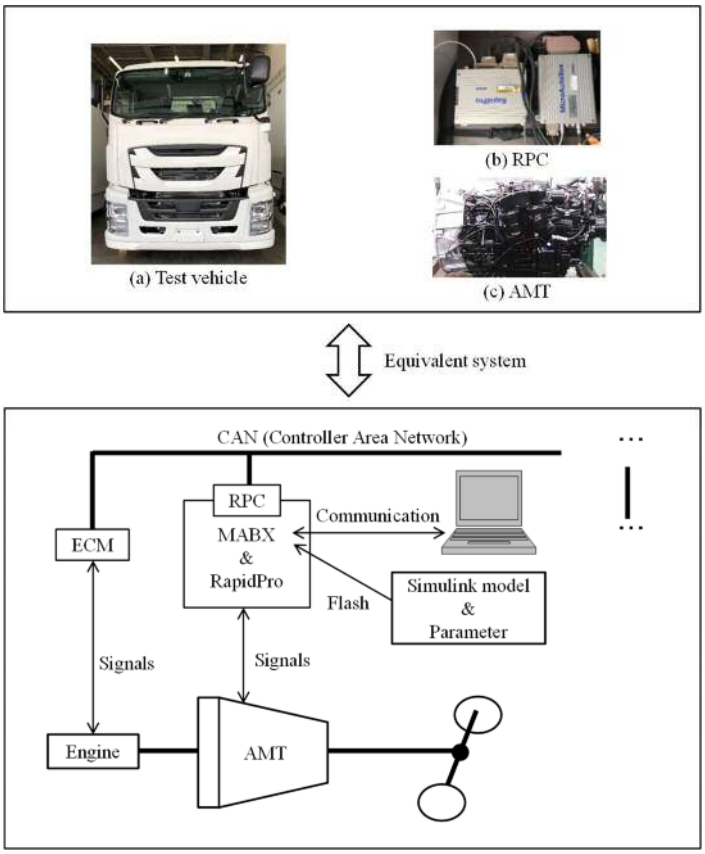

Figure 6.6. Experimental system. RPC: Rapid prototyping controller. ECM: Engine control module. TCM: Transmission control module. CAS: Clutch actuator system. CAN: Controller area network.

Table 6.2. Dead zone of valves.

Valve	Duty ratio [%]
Valve 1	25
Valve 2	26
Valve 3	15
Valve 4	15

Table 6.3. The parameters of reference model.

Symbol	Value
τ	0.025
n	3
L	2

6.4.2 **Experimental results and discussion**

As shown in Algorithm Step 1, the input/output data of the controlled object are acquired by conducting a closed-loop experiment. The PD controller was used, and the fixed PD gains were set to $K_p = 0.5$ and $K_d = 0.2$. The input/output data were acquired by setting the same target values as the actual vehicle launch and shift waveforms.

Figure 6.7 shows the time-series data when the closed-loop test was performed. The horizontal axis represents the time, while the vertical axis represents the clutch position, intake-side valve duty ratio, and exhaust-side valve duty ratio. When the clutch position is 0 mm, the clutch is fully engaged, and when it is 16 mm, the clutch is fully disengaged. When the clutch position is approximately 8 mm, it is in a half-clutch state. Figure 6.7(b) confirms that an undershoot occurred during the half-clutch control. This is undesirable because a sudden torque is generated due to the unintended clutch connection. The weight coefficient of the gain scheduler is calculated using the input/output data shown in Figure 6.7(a). Figure 6.8 shows the time-series data of the closed-loop system when the gain-scheduled control is applied. The target clutch position is the waveform calculated in the transmission control module. The horizontal axis represents the time, while the vertical axis represents the clutch position, valve duty ratio on the supply side, valve duty ratio on the exhaust side, proportional gain, and differential gain. Figure 6.8 shows that the response follows the target without any over/undershooting. The over/undershoot amounts prior and subsequent to direct tuning are 0.8/1.8 and 0.48/0.25 mm, respectively. This is the same characteristic as that of the defined reference model. Furthermore, it is considered that the response closer to the limit of the system can be achieved from the valve duty ratio. Regarding the proportional gain, the relationship between the clutch position and the load is nonlinear (see Figure 6.2). Hence, the proportional gain changes accordingly. The differential gain is lower than the proportional gain due to the fluctuation in the clutch position. This fluctuation is due to the eccentric movement of the clutch as

the engine rotates. Examination of Figure 6.8 indicates that the characteristics are close to the provided reference response because there is no over/undershooting. Conversely, as the control input is saturated, the system gives a reference response that cannot be achieved. In other words, the model matching is not possible due to physical constraints. To further confirm the matching between the reference model and the closed-loop characteristics, the response when the control input is not saturated is confirmed. Figure 6.9 shows the time-series data when the reference response that can be achieved in the system is given. The horizontal axis represents the time, whereas the vertical axis represents the clutch position and the tracking error. In the clutch position stage, the reference response is shown in addition to the target value and the actual response. Examination of Figure 6.9 confirms that the actual response follows the set reference response. In other words, the closed-loop system could approach the characteristics of the set reference model. Based on the above, the proposed gain-scheduled control and automatic tuning method were used to directly design a gain scheduler without system identification. Its effectiveness was confirmed by conducting actual vehicle tests. In addition, since the control method is practical and cost-effective, it can be easily implemented in mass-produced controllers and is expected to facilitate development due to the automatic parameter tuning feature.

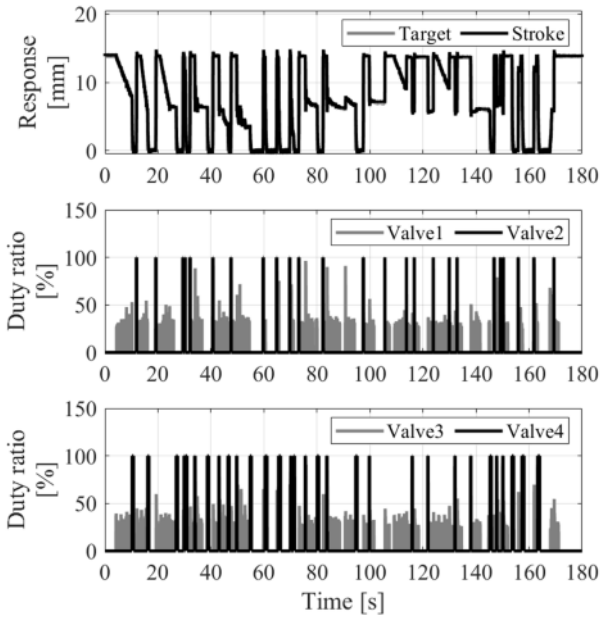

(a)

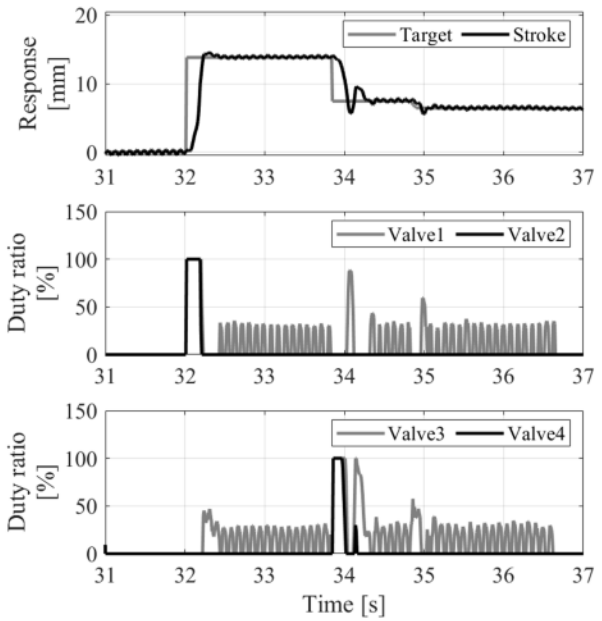

(b)

Figure 6.7. Closed-loop data with fixed PID gain. (a) Overview of time series. (b) Enlarged view of time series.

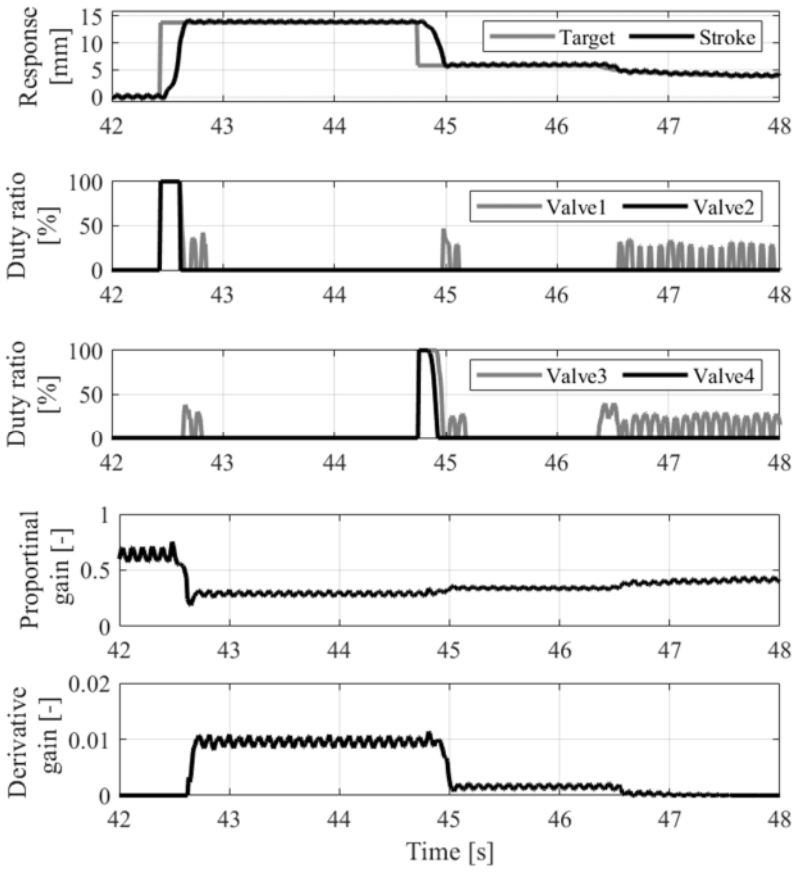

Figure 6.8. Closed-loop data with gain-scheduled PID control.

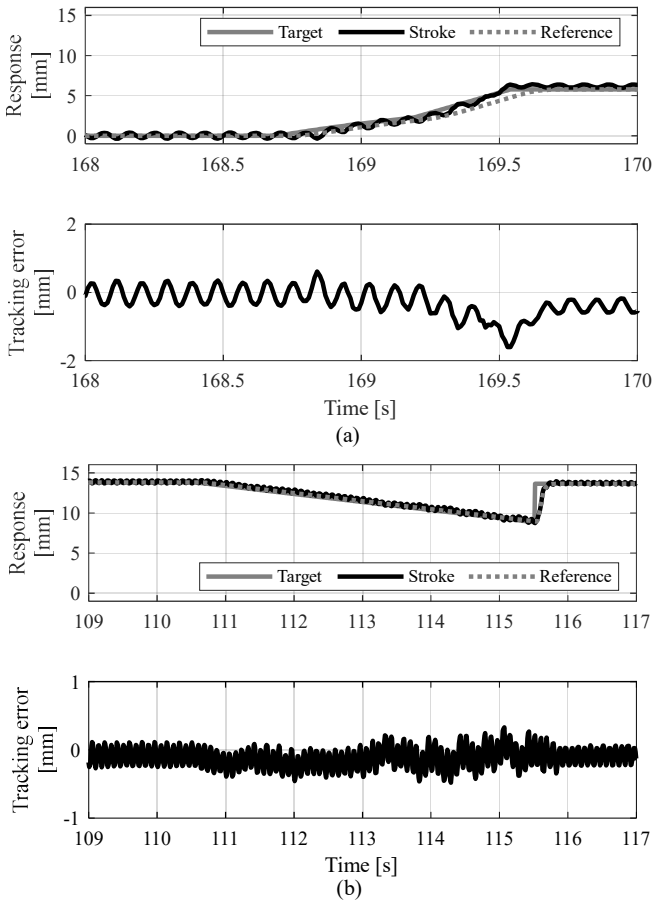

Figure 6.9. Closed-loop data with gain-scheduled PID control under no saturation of the valves. (a) Target of the clutch stroke moves from the engaged side to near the kiss point. (b) Target of the clutch stroke moves from disengaged side to near the kiss point and finally back to the disengaged side.

6.5 **Conclusion**

In this chapter, a control law and a direct tuning method for gain-scheduling control parameters were proposed for the position control of a pneumatic clutch actuator. The proposed direct tuning does not require a controlled object model. First, the pneumatic clutch actuator system was found to have strong nonlinearity in terms of the ON/OFF valve, pneumatic parameters, and spring characteristics. Next, a control law comprised of gain-scheduled control and a valve dead zone compensation are derived. In the gain-scheduled control, the gain scheduler was represented by a polynomial, and the number of tuning parameters was reduced compared to that in the gain scheduler with the LUT.

The LUT is often used in industries. Furthermore, an automatic tuning method for these parameters is derived and it is shown that the parameters can be obtained through use of optimization algorithms, such as the least-squares method. The effects of the control law and direct tuning method is experimentally confirmed. As a result, the controller parameters could be obtained directly from the input/output data of the controlled object. The PD gain was adapted based on the controlled object states, and good results were obtained for the target value. Thus, it was possible to achieve control with a small computational load and less calibration time required by the industry for pneumatic clutch actuators with nonlinearity. Future work will include the construction of reference response design methods that evaluate the saturation of the control inputs and online tuning methods.

Chapter 7
Conclusions

7.1 Conclusions

In this thesis, a theory for the direct data-driven control of industrial systems, especially automobile systems, was developed, and it was applied to automobile systems. In Chapter 1, the research background was stated, and the data-driven control method required for automobile systems was described. The difference between model-based control and data-driven control was explained. Model-based control was shown to be limited in its applicability to industrial systems for reasons such as the difficulty associated with modeling such systems. This difficulty is illustrated by the fact that more than 90% of the closed-loop controllers used in industry are PID control laws. By contrast, data-driven controls, which have been attracting attention in recent years, do not require modeling a controlled object. In this thesis, among the data-driven control methods, this thesis focused on VRFT/FRIT, which has the following features:

- Controller parameters are automatically tuned.
- A model of the controlled object is not required.
- Only a single experiment is needed.
- The method is applicable to a controller with the structure specified in advance, such as a PID controller.

It was considered that these properties make VRFT/FRIT highly suitable for industrial system control. However, in VRFT/FRIT, problems arise in that a linear system is assumed and the closed-loop stability is not guaranteed.

Factors related to the environment surrounding industrial systems, especially automobile control systems, and the required data-driven control in automobile systems were next introduced. Specifically, the following environmental factors related to automobile control systems were addressed:

- Parameters of the controller with a structure specified in advance, such as PID controllers, are tuned by trial and error, and their control performance depends on the tuner.
- The controlled objects are nonlinear systems.
- Controller performance is restricted by, for example, ROM/RAM capacity and CPU performance.
- The application of model-based control theory faces obstacles.

Given such factors, it was considered that the range of application to automobile systems could be expanded by constructing a data-driven control system that satisfies the following criteria:

- Parameters are tuned automatically for a controller whose structure is specified in advance.
- The control structure is easy to understand and simple and is suitable for mounting in mass production.
- Closed-loop stability is ensured.
- Measures against aging are implemented.
- The controller is designed for nonlinear systems.

To meet these requirements, it was aimed to construct new direct data-driven controls and examine their practical application to actual problems in automobile systems.

In Chapter 2, the direct tuning methods VRFT and FRIT were explained. VRFT and FRIT are model-referenced data-driven controls and are attractive for optimizing controller parameters directly from the input/output data of the controlled object acquired from a single experiment. The problem setting, in which the model reference control is considered, was explained as well as previous studies related to data-driven control. Each algorithm and the interpretation of the cost functions, and the use of prefilters were described. As previously noted, Chapter 2 described conventional VRFT and FRIT, which play an important role in this thesis.

In Chapter 3, a direct design method that ensures closed-loop stability and an automatic tuning method of the reference model parameters were proposed for the LTI system. A problem encountered in the conventional method is that a closed-loop system can become

unstable when a controller with obtained controller parameters is implemented. Moreover, it is necessary to tune the parameters of the reference model. It was first described why the stability is not ensured and a new method was proposed. To ensure stability, the pole-conserved output was predicted by estimating the transfer function whose input and output are the fictitious reference signal, which is a function of the control parameters, and the controlled object response in the time domain. By minimizing the cost function that includes this output, the optimal control parameters with guaranteed BIBO stability were obtained. An optimization algorithm for the reference model using the dead time was next proposed. Thus, the entire tuning process was automated. To verify the effect of the proposed method, a simulation was conducted on a system in which dead time was added to the benchmark problem of the process system. The proposed method obtained control parameters that ensured BIBO stability. In addition, a tuning method for the reference model enables the parameters to be automatically tuned for model matching. Therefore, the proposed method could be easily used by engineers because this tuning method does not require any design parameters except for a denoising process.

In Chapter 4, a direct tuning method for gain-scheduled PID control with sparsity as a nonlinear controller was proposed. As mentioned in Chapter 1, numerous industrial systems exhibit nonlinear characteristics. Gain-scheduled controls are known to be most effective for nonlinear systems, and PID control is used in more than 90% of such systems in industry. Therefore, a direct tuning method for gain-scheduled PID control using the least-squares method (GS-PID-LS) was proposed. A velocity-type PID controller suitable for gain-scheduled control was introduced for PID control, and a polynomial was adopted for the scheduling function. GS-PID-LS remains problematic in that overfitting occurs when the number of data points is insufficient, and demand exists for mass production controllers that reduce the calculation cost and ROM capacity as much as possible. To address these problems, a direct design method that considers sparsity by LASSO regression (GS-PID-LASSO) was proposed. Sparsity refers to a property in which the elements with little information become zeros. Because LASSO regression needs to be linear with respect to the control parameters, the proposed method is based on VRFT. The proposed method was examined by simulation for an LPV system and a Hammerstein model. The results confirmed that a controller with high sparseness can be obtained without knowing the characteristics of the controlled object for a large number of control

parameters of the gain scheduler. This approach eliminates the need for trial-and-error parameter tuning and enables gain-scheduled PID control with a low computational load.

In Chapter 5, for slip speed control of an automated transmission, a system which has coordinated control between the engine and clutch systems and the online automatic tuning method were constructed. Regarding coordinated control, in the conventional method, the control input is only the clutch torque, which leads to problems with torque fluctuations. In the proposed method, the clutch torque is the driver's operation value and the control input for realizing slip control is the engine torque. The control system consists of PID control law and disturbance observers. In addition, although nonlinear control was required in previous studies, the proposed control system can be described by a linear system, which facilitates controller design. For PID gain, online FRIT was introduced so that the parameters could be tuned in real time. The effect of the proposed method was confirmed using an actual vehicle test. The PID gain was optimized with a one-time shift, and the desired response was achieved. The proposed method reduces development man-hours and provides optimal parameters that do not depend on tuner skills. In addition, an automated transmission with a comfortable shift feeling can be realized, enhancing driver satisfaction.

In Chapter 6, a direct tuning method for gain-scheduled control parameters without using the controlled object model was constructed for the position control of a pneumatic clutch actuator. First, the pneumatic clutch actuator system was shown to exhibit strong nonlinearity resulting from an ON/OFF valve, air compression, and spring characteristics. A control law consisting of gain-scheduled control and valve dead-zone compensation were next derived. In the gain-scheduled control, the gain scheduler is represented by a polynomial and the number of tuning parameters is reduced compared with the number for the gain scheduler tuned using a conventional LUT. In addition, the direct tuning method for these parameters was derived and it was shown that the parameters can be obtained by optimization calculations such as the least-squares method. This algorithm is the same as that described in Chapter 4. However, the PD gain was adapted because the pneumatic clutch actuator system exhibits integral characteristics. An actual vehicle test was performed to confirm the effects of the control law and the direct tuning method. As a result, the controller parameters could be obtained directly from the input/output data

of the controlled object and good results were obtained. Control was achieved with a small computational load and without a tuning process required in industry for pneumatic clutch actuators with nonlinearity. In addition, the proposed method can be increased driver comfort during the automated transmission shift process and driver satisfaction.

Through the aforementioned results, the construction of direct design methods for the control systems required for automobile systems was realized. That is, theoretical extensions of conventional data-driven control and its contribution to industry were achieved. In the theoretical extensions of the data-driven control, new approaches were proposed and verified, such as ensuring closed-loop stability and considering sparsity in gain-scheduled controller. The contributions to industry will result in improved development efficiency and improved product performance for slip control of automated transmissions and position control of pneumatic clutch actuators.

7.2 **Future works**

Future works are summarized as follows.

(a) Experimental verification for MIMO system

Because most of the controlled objects are SISO systems, the systems in the present work were limited to SISO systems and the corresponding theory was developed and applied to actual industrial systems. However, the intake and exhaust of the engine and the vehicle motion systems are MIMO systems. The method proposed in Chapters 4–6 can be easily extended to MIMO systems, and verifying the effect of the proposed method using actual tests is important.

(b) Construction of a direct design method for the two-degree-of-freedom controller

In this work, the theory was developed for the feedback controller and applied to actual systems. However, two-degree-of-freedom control is expected to achieve a faster response. In addition, both stability and responsiveness can be achieved. In the future, constructing a direct design method for the two-degree-of-freedom controller, which is an extension of the proposed method, will be important.

(c) Construction of a direct design method with gain schedule controller for error axis

In the proposed method presented in Chapters 4 and 6, the scheduling parameters of a gain-scheduled controller are used as the states of the controlled object. In industry, there are control structures in which the scheduling parameter is an error, such as fuzzy control. In the future, it will be important to develop a direct design method for such control structures.

References

[1] S. Bennett, "A Brief History of Automatic Control," *IEEE Control Systems Magazine,* vol. 16, no. 3, pp. 17–25, 1996.

[2] K. Suyama and N. Sebe, "Essentials of Classical Control," *Journal of The Society of Instrument and Control Engineers,* vol. 42, no. 4, pp. 268–276, 2003 [in Japanese].

[3] E. Shimemura, Introduction to Automatic Control, Tokyo: CORONA Publishing, 1990 [in Japanese].

[4] T. Yoshikawa, Classical Control Theory, Tokyo: CORONA Publishing, 2014 [in Japanese].

[5] R. E. Kalman, "On the General Theory of Control Systems," *IFAC Proceedings Volumes,* vol. 1, no. 1, pp. 491–502, 1960.

[6] T. Yoshikawa and J. Imura, Modern Control Theory, Tokyo: CORONA Publishing, 2014 [in Japanese].

[7] K. Åström and T. Hägglund, "The future of PID control, Control Engineering Practice," *Control Engineering Practice,* vol. 9, no. 11, pp. 1163–1175, 2001.

[8] J. G. Ziegler and N. B. Nichols, "Optimum Settings for Automatic Controllers," *Transactions of the ASME,* vol. 64, pp. 759–768, 1942.

[9] J. G. Ziegler and N. B. Nichols, "Process lags in automatic control circuits," *Transaction of the ASME,* vol. 65, pp. 433–444, 1943.

[10] K. L. Chien, J. A. Hrones and J. B. Reswick, "On the Automatic Control of Generalized Passive Systems," *Transactions of the American Society of Mechanical Engineeing,* vol. 74, pp. 175–185, 1972.

[11] Z. S. Hou and Z. Wang, "From model-based control to data-driven control: Survey, classification and perspective," *Information Sciences,* vol. 235, pp. 3–35, 2013.

[12] J. C. Spall and J. A. Cristion, "Model-free control of general discrete-time system," in *Proceedings of 32nd IEEE Conference on Decision and Control*, San Antonio, USA, 1993.

[13] S. Ishizuka and I. Kajiwara, "Online adaptive PID control for MIMO systems using simultaneous perturbation stochastic approximation," *Journal of Advanced Mechanical Design, Systems, and Manufacturing,* vol. 9, no. 2, pp. 1–16, 2015.

[14] Z. S. Hou, The Parameter Identification, Adaptive Control and Model Free Learning Adaptive Control for Nonlinear Systems, PhD dissertation, Northeastern University, 1994.

[15] M. G. Safonov and T. C. Tsao, "The unfalsified control concept: a direct path from experiment to controller," in *Feedback Control, Nonlinear Systems and Complexity*, Springer, 1995, pp. 196–214.

[16] H. Hjalmarsson, S. Gunnarsson and M. Gevers, "A convergent iterative restricted complexity control design scheme," in *Proceedings of 1994 33rd IEEE Conference on Decision and Control*, Lake Buena Vista, FL, USA, 14–16 December 1994.

[17] H. Hjalmarsson, "Efficient Tuning of Linear Multivariable Controllers Using Iterative Feedback Tuning," *International Journal of Adaptive Control and Signal Processing,* vol. 13, no. 7, pp. 553–572, 1999.

[18] A. Karimi, L. Miskovic and D. Bonvin, "Convergence analysis of an iterative correlation-based controller tuning method," *IFAC Proceedings Volumes,* vol. 35, no. 1, pp. 413–418, 2002.

[19] L. Mišković, A. Karimi, D. Bonvin and M. Gevers, "Correlation-based tuning of decoupling multivariable controllers," *Automatica,* vol. 43, no. 9, pp. 1481–1494, 2007.

[20] G. O. Guardabassi and S. M. Savaresi, "Virtual reference direct design method: an off-line approach to data-based control system design," *IEEE Transactions, on Automatic Control,* vol. 45, no. 5, pp. 954–959, 2000.

[21] M. C. Campi, A. Lecchini and S. M. Savaresi, "Virtual Reference Feedback Tuning: A Direct Method for the Design of Feedback Controllers," *Automatica,* vol. 38, no. 8, pp. 1137–1146, 2002.

[22] S. Soma and O. Kaneko, "A new method of controller parameter tuning based on input-output data–Fictitious Reference Iterative Tuning (FRIT)," *IFAC Proceedings Volumes,* vol. 37, no. 12, pp. 789–794, 2004.

[23] O. Kaneko, "Data-Driven Controller Tuning: FRIT approach," *IFAC Proceedings,* vol. 46, no. 11, pp. 326–336, 2013.

[24] M. Uchiyama, "Formulation of high-speed motion pattern of a mechanical arm by trial," *Transactions of the Society of Instrument and Control Engineers,* vol. 14, no. 6, pp. 706–712, 1978 [in Japanese].

[25] S. Schaal and C. G. Atkeson, "Robot juggling: implementation of memory-based learning," *IEEE Control Systems Magazine,* vol. 14, no. 1, pp. 57–71, 1994.

[26] H. Chen, S. Bowels, B. Zhang and T. Fuhlbrigge, "Controller parameter optimization for complex industrial system with uncertainties," *Measurement and Control,* vol. 52, no. 7–8, pp. 888–895, 2019.

[27] M. Nakamoto, "An Application of the virtual reference feedback tuning method for multivariable process control," *Transactions of the Society of Instrument and Control Engineers,* vol. 41, no. 4, pp. 330–337, 2005 [in Japanese].

[28] S. Formentin, S. M. Savaresi and L. D. Re, "Non-iterative direct data-driven controller tuning for multivariable systems theory and application," *IET Control Theory and Applications,* vol. 6, no. 9, pp. 1250–1257, 2012.

[29] J. D. Rojas, R. Vilanova, "Data-driven based IMC control," *International Journal of Innovative Computing, Information and Control,* vol. 8, no. 3, pp. 1557–1574, 2012.

[30] S. Ishizuka, I. Kajiwara, J. Sato, Y. Hanamura and S. Hanawa, "Model-free adaptive control scheme for EGR/VNT control of a diesel engine using the simultaneous perturbation stochastic approximation," *Transactions of the Institute of Measurement and Control,* vol. 39, no. 1, pp. 114–128, 2017.

[31] I. Kajiwara, K. Furuya and S. Ishizuka, "Experimental verification of real-time tuning method of a model-based controller by perturbations to its poles," *Mechanical Systems and Signal Processing 2018,* vol. 107, pp. 396–408, 2018.

[32] S. Yahagi, I. Kajiwara and T. Shimozawa, "Slip control during inertia phase of clutch-to-clutch shift using model-free self-tuning proportional-integral-derivative control," *Proceedings of the Institution of Mechanical Engineers, Part D: Journal of Automobile Engineering,* vol. 234, no. 9, pp. 2279–2290, 2020. https://doi.org/10.1177/0954407020907257

[33] R. A. Fahmy, I. Badr and F. A. Rahman, "Adaptive PID Controller Using RLS for SISO Stable and Unstable Systems," *Advances in Power Electronics,* Article ID 507142, pp. 1–5, 2014.

[34] R. A. Fahmy, I. Badr and F. A. Rahman, "Alternative Approach to Use RLS Algorithm in Multivariable Online Adaptive PID Controllers for MIMO Systems," *IETE Journal of Research,* vol. 64, no. 1, pp. 27–35, 2018.

[35] Y. Wakasa, K. Tanaka and Y. Nishimura, "Online Controller Tuning via FRIT and Recursive Least-Squares," *IFAC Proceedings Volumes,* vol. 45, no. 3, pp. 76–80, 2012.

[36] Y. Wakasa, R. Azakami, K. Tanaka and S. Nakashima, "FRIT and RLS-based online controller tuning and its experimental validation," in *9th Asian Control Conference (ASCC)*, Istanbul, Turkey, 23–26 June 2013.

[37] O. Kaneko, T. Nakamura and T. Ikezaki, "A New Approach to Update of Feedfoward Controller in the Two-degree-of-freedom Control System – A Proposal of Estimated

Response Iterative Tuning (ERIT) –," *Transactions of the Society of Instrument and Control Engineers,* vol. 54, no. 12, pp. 857–864, 2018 [in Japanese].

[38] K. Yubai, H. Fujii and J. Hirai, "Ficitious Correlation-based Tuning integrating the Data-Based Stability Test at Each Parameter Update," *Electrical Power System and Computers,* vol. 3, pp. 511–518, 2011.

[39] K. Yubai, H. Fujii and J. Hirai, "Proposal of FCbT by Considering Closed-loop Stability at Each Parameter Update," *Electrical Engineering in Japan,* vol. 190, no. 1, pp. 607–615, 2015.

[40] V. Veselý and A. Ilka, "Gain-scheduled PID controller design," *Journal of Process Control,* vol. 23, no. 8, pp. 1141–1148, 2013.

[41] W. J. Rugh and J. S. Shamma, "Research on gain scheduling," *Automatica,* vol. 36, no. 10, pp. 1401–1425, 2000.

[42] M. Nagahara, Sparsity Methods for Systems and Control, Now Publishers, 2020.

[43] H. Langjord and T. Johansen, "Dual-Mode Switched Control of an Electropneumatic Clutch Actuator. Mechatronics," *IEEE/ASME Transactions on Mechatronics,* vol. 15, no. 1, pp. 969–981, 2010.

[44] M. G. Safonov and T. C. Tsao, "The unfalsified control concept and learning," *IEEE Transaction on Automatic Control,* vol. 42, no. 6, pp. 843–847, 1997.

[45] S. Yahagi and I. Kajiwara, "Direct tuning of the data-driven controller considering closed-loop stability based on a fictitious reference signal," *Measurement and Control,* vol. 54, no. 5–6, pp. 1026–1042, 2021. https://doi.org/10.1177/00202940211010834

[46] M. Kano and M. Ogawa, "The State of the Art in Chemical Process Control in Japan: Good Practice and Questionnaire Survey," *Journal of Process Control,* vol. 20, no. 9, pp. 969–982, 2010.

[47] M. Kano, K. Tasaka, M. Ogawa, A. Takinami, S. Takahashi and S. Yoshii, "Extended fictitious reference iterative tuning and its application to chemical processes," in *2011 international Symposium on Advanced Control of Industrial Processes*, Hangzhou, China, China, 23–26 May 2011.

[48] M. Nakamto, "AN APPLICATION OF THE VIRTUAL REFERENCE FEEDBACK TUNING METHOD TO A MULTIVARIABLE PROCESS CONTROL," *IFAC Proceedings Volumes,* vol. 38, no. 1, pp. 237–242, 2005.

[49] T. E. Passenbrunner, S. Formentin, S. M. Savaresi and L. Re, "Direct multivariable controller tuning for internal combustion engine test benches," *Control Engineering Practice,* vol. 29, pp. 115–122, 2014.

[50] R. Kajiwara, S. Masuda and Y. Matsui, "A Design Method for Optimal Pre-filter in FRIT Using Closed-loop Step Response Data," *Transactions of the Society of Instrument and Control Engineers,* vol. 54, no. 2, pp. 238–246, 2018 [in Japanese].

[51] S. Engell, T. Tometzki and T. Wonghong, "A New Approach to Adaptive Unfalsified Control," in *In Proc. European Control Conf.*, Kos, Greece, July 2007.

[52] T. Wonghong and S. Engell, "Application of a New Scheme for Adaptive Unfalsified Control to a CSTR," *IFAC Proceedings Volumes,* vol. 41, no. 2, pp. 13247–13252, 2008.

[53] E. G. Nabati and S. Engell, "Data-driven Adaptive Control: Making Unfalsified Control Work Better," *IFAC Proceedings Volumes,* vol. 44, no. 1, pp. 1285–1290, 2011.

[54] J. Imura, Stability Theory in Systems and Control, Tokyo: CORONA Publishing, 2000 [in Japanese].

[55] J. Kennedy and R. Eberhart, "Particle swarm optimization," in *Proc. of IEEE Int. Conf. on Neural Networks*, Perth, Australia, 27 Nov.–1 Dec. 1995.

[56] S. C. Ruangurai P, "Implementation of PSO Based Fictitious Reference Iterative Tuning to Embedded System," in *2019 7th International Conference on Control, Mechatronics and Automation (ICCMA)*, Delft, Netherlands, Nov. 2019.

[57] N. Hansen and A. Ostermeier, "Completely Derandomized Self-Adaptation in Evolution Strategies," *Evolutionary Computation,* vol. 9, no. 2, pp. 159–195, 2001.

[58] R. Storn and K. Price, "Differential Evolution – A Simple and Efficient Heuristic for global Optimization over Continuous Spaces," *Journal of Global Optimization,* vol. 11, no. 4, pp. 341–359, 1997.

[59] Y. Matsui, H. Ayano, S. Masuda and K. Nakano, "A Controller Tuning Method Based on Finite Impulse Response Estimation Using Closed-Loop Response Data," *IEEJ Transactions on Electronics, Information and Systems,* vol. 139, no. 8, pp. 858–865, 2019 [in Japanese].

[60] Y. Matsui and K. Nakano, "A Controller Tuning Using Information in Both Time and Frequency Domains of Closed-Loop Transient Data," *Journal of The Society of Instrument and Control Engineers,* vol. 52, no. 10, pp. 892–897, 2013 [in Japanese].

[61] S. Masuda and Y. Yasuda, "A PID gain tuning using fictitious reference iterative tuning approach with simultaneous tuning for the delay parameter of the reference model," in *SICE Annual Conference 2008*, Tokyo, Japan, 20–22 August 2008.

[62] S. Yahagi and I. Kajiwara, "Direct tuning of PID controller and reference model with input constraint," in *The 21st International Conference on Control, Automation and Systems (ICCAS 2021)*, Jeju, Korea, Octover 12–15, 2021.

[63] O. Kaneko, Y. Wadagaki and S. Yamamoto, "FRIT based PID parameter tuning for linear time delay systems -simultaneous attainment of models and controllers," *IFAC Proceedings Volumes,* vol. 45, no. 3, pp. 86–91, 2012.

[64] O. Kaneko, Y. Wadagaki, H. T. Nguyen and S. Yamamoto, "Fictitious reference iterative tuning for a system with a time-delay and/or unstable zeros in the internal model control architecture," in *2011 IEEE International Conference on Control Applications (CCA)*, Denver, CO, USA, 28–30 September 2011.

[65] S. Yahagi and I. Kajiwara, "Direct Tuning Method of Gain-Scheduled Controllers with the Sparse Polynomials Function," *Asian journal of Control,* pp. 1–16, 2021. https://doi.org/10.1002/asjc.2657 (Online published)

[66] Y. Liao, K. Koiwai and T. Yamamoto, "Design and implementation of a hierarchical-clustering CMAC PID Controller," *Asian Journal of Control,* vol. 21, pp. 1077–1078, 2019.

[67] F. Wu, A. Packard and G. Balas, "Systematic gain-scheduling control design: A missile autopilot example," *Asian Journal of Control,* vol. 4, no. 3, pp. 341–347, 2002.

[68] E. B. Ondes, I. Bayezit, I. Poergye and A. Hafsi, "Model-based 2-D look-up table calibration tool development," in *2017 11th Asian Control Conference (ASCC)*, Gold Coast, QLD, Australia, 2017.

[69] C. Guardiola, B. Pla, D. Blanco-Rodriguez and P. Cabrera, "A learning algorithm concept for updating look-up tables for automotive applications," *Mathematical and Computer Modelling,* vol. 57, no. 7–8, pp. 1979–1989, 2013.

[70] X. Bu, Y. Qiao, Z. Hou and J. Yang, "Model free adaptive control for a class of nonlinear systems using quantized information," *Asian Journal of Control,* vol. 20, no. 2, pp. 962–968, 2018.

[71] T. Yamamoto, K. Takao and Y. T, "Design of a Data-Driven PID Controller," *IEEE Transactions on Control Systems Technology,* vol. 17, no. 1, pp. 29–39, 2009.

[72] S. Wakitani, Y. Ohnishi and T. Yamamoto, "Design of FRIT-based nonlinear PID control systems," *Journal of The Society of Instrument and Control Engineers,* vol. 52, no. 10, pp. 885–891, 2013 [in Japanese].

[73] S. Wakitani, K. Nishida, M. Nakamoto and T. Yamamoto, "Design of a data-driven PID controller using operating data," *IFAC Proceedings Volumes,* vol. 46, no. 11, pp. 587–592, 2013.

[74] F. Tsukui and S. Masuda, "Data-driven control parameter tuning using feedback linearization," *IEEJ Transactions on Electronics, Information and Systems,* vol. 137, no. 7, pp. 891–897, 2017 [in Japanese].

[75] S. Formentin and S. M. Savaresi, "Virtual Reference Feedback Tuning for linear parameter-varying systems," *IFAC Proceedings Volumes,* vol. 44, no. 1, pp. 10219–10224, 2011.

[76] S. Formentin, G. Panzani and S. M. Savaresi, "VRFT for LPV systems: Theory and braking control application," *Robust Control and LPV Approaches,* pp. 289–309, 2013.

[77] S. Formentin, D. Piga, R. Toth and S. M. Savaresi, "Direct learning of LPV controllers from data," *Automatica,* vol. 65, pp. 98–110, 2016.

[78] S. Stenman, F. Gustafsson and L. Ljung, "Just in time models for dynamical systems," in *Proceedings of 35th IEEE Conference on Decision and Control*, Kobe, Japan, 13–13 Dec. 1996.

[79] K. J. Åström and T. Hägglund, PID controllers: Theory, Design and Tuning, 2nd edition, ISA, 1995.

[80] N. Suda, PID Control, Japan: Asakura Shoten, 1992 [in Japanese].

[81] M. Saeki and K. Ogawa, "Gain scheduled PID controller design by data-driven loop-shaping method," *IEEJ Transactions on Electronics, Information and Systems,* vol. 131, no. 4, pp. 758–763, 2011 [in Japanese].

[82] M. Bishop C, Pattern Recognition and Machine Learning (Information Science and Statistics), New York : Springer, 2006.

[83] M. Ogawa and M. Kano, "Development of a Two-stages E-FRIT Tuning Method for Generalized Two-degrees of Freedom PID Control System," *Transactions of the Society of Instrument and Control Engineers,* vol. 52, no. 11, pp. 631–638, 2016 [in Japanese].

[84] Z. Lang, "On identification of the controlled plants described by the Hammerstein model," *IEEE Transactions on Automatic Control,* vol. 39, no. 3, pp. 569–573, 1994.

[85] H. Tanaka and S. Hazue, "Identification of a Hammerstein Model equipped with a static nonlinear odd function, transactions of the institute of systems," *Control and Information Engineers,* vol. 20, no. 11, pp. 430–438, 2007 [in Japanese].

[86] K. Takao, T. Yamamoto and T. Hinamoto, "Design of a memory-based prefilter supplementing a robust PID control system," *Asian Journal of Control,* vol. 10, no. 3, pp. 301–313, 2008.

[87] H. Otsubo, "Robust Design Method for Automatic Calibration of Automatic Transmission Shift Control System," *Society of Automotive Engineers of Japan,* vol. 44, no. 3, pp. 815–821, 2013 [in Japanese].

[88] Y. Umemura and N. Sakamoto, "Optimal Servo Design for Lock-Up Slip Control for Torque Converter-Nonlinear Output Regulation Approach," *IEEE Transactions on Control Systems Technology,* vol. 23, no. 4, pp. 1587–1593, 2015.

[89] K. Adachi, Y. Ochi, S. Segawa and A. Higashimata, "Slip control for a lock-up clutch with a robust control method," in *SICE 2004 Annual Conference*, Sapporo, Japan, 4–6 Aug. 2004.

[90] Q. Lijun, Y. Nianjiong and W. Daojun, "Simulation of Clutch Slipping Control of Automatic Transmission," in *Second International Conference on Intelligent Human-Machine Systems and Cybernetics*, Nanjing, Jiangsu, China, 26–28 Aug. 2010.

[91] J. O. Hahn and K. I. Lee, "Nonlinear Robust Control of Torque Converter Clutch Slip System for Passenger Vehicles Using Advanced Torque Estimation Algorithms," *Vehicle System Dynamics,* vol. 37, no. 3, pp. 175–192, 2002.

[92] F. Meng, G. Tao, T. Zhang, Y. Hu and P. Geng, "Optimal shifting control strategy in inertia phase of an automatic transmission for automotive applications," *Mechanical Systems and Signal Processing,* vol. 60–61, pp. 742–752, 2005.

[93] K. D. Mishra and K. Srinivasan, "Robust control and estimation of clutch-to-clutch shifts," *Control Engineering Practice,* vol. 65, pp. 100–114, 2017.

[94] A. Haj-Fraj and F. Pfeiffer, "A model based approach for the optimisation of gearshifting in automatic transmissions," *International Journal of Vehicle Design,* vol. 28, no. 1–3, pp. 171–188, 2002.

[95] R. Hibino, M. Osawa, H. Yamada, K. Kono and M. Tanaka, "H∞ control design for torque-converter-clutch slip system," in *Proceedings of 35th IEEE Conference on Decision and Control*, Kobe, Japan, 13 Dec. 1996.

[96] B. Gao, H. Chen and K. Sanada, "Two-Degree-of-Freedom Controller Design for Clutch Slip Control of Automatic Transmission," *SAE International Journal of Passenger Cars - Mechanical Systems,* vol. 1, no. 1, pp. 430–438, 2009.

[97] B. Gao, H. Chen, Y. Hu and K. Sanada, "Nonlinear feedforward–feedback control of clutch-to-clutch shift technique," *Vehicle System Dynamics,* vol. 49, no. 12, pp. 1895–1911, 2011.

[98] K. Sanada, B. Gao, N. Kado and H. Takamatsu, "Design of a robust controller for shift control of an automatic transmission," *Proceeding Institution of Mechanical Engineers, PartD: Jounal of Automobile Engineering,* vol. 226, no. 12, pp. 1577–1584, 2012.

[99] F. Liu, L. Chen and D. Li, "Improved clutch slip control for automated transmissions. Proceeding Institution of Mechanical Engineers," *Proceedings of the Institution of Mechanical Engineers, Part C: Journal of Mechanical Engineering Science,* vol. 232, no. 18, pp. 3181–3199, 2017.

[100] H. Tsutsui, T. Hisano, S. A, M. Hijikata, M. Taguchi and K. Kojima, "Electro-Hydraulic Control System for AISIN AW New 6-Speed Automatic Transmission," *SAE Technical Paper, 2004-01-1638,* 2004.

[101] K. Ohnishi, "New development of servo technology in mechatronics," *IEEJ Journal of Industry Applications,* vol. 107, no. 1, pp. 83–86, 1987 [in Japanese].

[102] K. Ohnishi, "Robust motion control by disturbance observer," *Journal of Robotics and Mechatronics,* vol. 8, no. 3, pp. 218–225, 1996 [in Japanese].

[103] K. Ohnishi, M. Shibata and T. Murakami, "Motion control for advanced mechatronics," *IEEE/ASME Transaction Mechatronics,* vol. 1, no. 8, pp. 1389–1398, 2003.

[104] S. Haykin, Adaptive Filter Theory, Third Edition, Prentice Hall, 1996.

[105] K. J. Åström and R. M. Murray, Feedback Systems: An Introduction for Scientists and Engineers, Second Edition, Princeton University Press, 2009.

[106] C. A. Kluever, Dynamic Systems: Modeling, Simulation, and Control, Wiley, 2015.

[107] S. Yahagi and I. Kajiwara, "Direct tuning of gain-scheduled controller for electro-pneumatic clutch control," *Advanced in Mechanical Engineering,* vol. 13, no. 7, pp. 1–12, 2021. https://doi.org/10.1177/16878140211036017

[108] G. O. Kaasa, Nonlinear output-feedback control applied to electropneumatic clutch actuation in heavy-duty trucks. PhD dissertation, NTNU, 2006.

[109] J. Zhang, L. Chen and G. Xi, "System dynamic modelling and adaptive optimal control for automatic clutch engagement of vehicle," *Proceedings of the Institution of Mechanical Engineers, Part D: Journal of Automobile Engineering,* vol. 216, no. 12, pp. 983–991, 2002.

[110] G. Lucente, M. Montanari and C. Rossi, "Modelling of an automated manual transmission system," *Mechatronics,* vol. 17, no. 2–3, pp. 73–91, 2007.

[111] Y. Wakasa, "Data-driven control for systems with nonlinearities," *Journal of The Society of Instrument and Control Engineers,* vol. 52, no. 10, pp. 872–877, 2013 [in Japanese].

[112] B. Szimandl and H. Németh, "Robust servo control design for an electro-pneumatic clutch system using the H∞ method," in *2014 IEEE/ASME 10th International Conference on Mechatronic and Embedded Systems and Applications (MESA)*, Senigallia, Italy, 10–12 September 2014.

[113] B. Szimandl and H. Németh, "Sliding Mode Position Control of an Electro-Pneumatic Clutch System," *IFAC Proc Volumes,* vol. 46, no. 2, pp. 707–712, 2013.

[114] P. Qian, X. Ren, G. Tao and L. Zhang, "Simultaneous control of motion and maximized stiffness for an electro-pneumatic clutch actuator based on pressure observers," *Advances in Mechanical Engineering,* vol. 9, no. 6, pp. 1–9, 2017.

[115] A. Grancharova and T. A. Johansen, "Explicit Model Predictive Control of an electropneumatic clutch actuator using on/off valves and pulse-width modulation," in *2009 European Control Conference (ECC)*, Budapest, Hungary, 23–26 August 2009.

[116] A. Grancharova and T. A. Johansen, "Design and comparison of explicit model predictive controllers for an electropneumatic clutch actuator using on/off valves," *IEEE/ASME Transaction Mechatronics,* vol. 16, no. 4, pp. 665–673, 2011.

[117] D. Schindele, H. Aschemann and R. Prabel, "Nonlinear model-predictive control with hysteresis compensation of an electro-pneumatic clutch for truck applications," *Mathematical and Computer Modelling of Dynamical Systems,* vol. 20, no. 2, pp. 105–129, 2014.

[118] D. Schindele, R. Prabel and H. Aschemann, "Nonlinear model-predictive control of an electro-pneumatic clutch for truck applications," *IFAC Proceedings Volumes,* vol. 45, no. 2, pp. 526–531, 2012.

[119] G. O. Kaasa and M. Takahashi, "Adaptive Tracking Control of an Electro-Pneumatic Clutch Actuator," *Modeling, Identification and Control,* vol. 24, no. 4, pp. 217–229, 2003.

[120] T. Szabo, M. Buchholz and K. Dietmayer, "A feedback linearization based observer for an electro-pneumatic clutch actuated by on/off solenoid valves," in *2010 IEEE International Conference on Control Applications*, Yokohama, Japan, 8–10 September 2010.

[121] H. Li and L. Chen, "A Fuzzy Immune PSD Control Approach to Pneumatic Clutch of Heavy Trucks," in *Fourth International Conference on Fuzzy Systems and Knowledge Discovery (FSKD 2007)*, Haikou, China, 24–27 August 2007.

[122] H. Sande, T. A. Johansen, G. O. Kaasa, S. R. Snare and C. Bratli, "Switched backstepping control of an electropneumatic clutch actuator using on/off valves," in *2007 American Control Conference*, New York, USA, 9–13 July 2007.

[123] H. Langjord, G. O. Kaasa and T. A. Johansen, "Adaptive nonlinear observer for electropneumatic clutch actuator with position sensor," *IEEE Transactions on Control Systems Technology,* vol. 20, no. 4, pp. 1033–1040, 2012.

[124] P. Qian, G. Tao, H. Liu and X. Li, "Globally stable pressure-observer-based servo control of an electro-pneumatic clutch actuator," *Proceedings of the Institution of Mechanical Engineers, Part D: Journal of Automobile Engineering,* vol. 229, no. 11, pp. 1483–1493, 2015.

[125] X. J. Li, C. R. Zhang, H. B. Li and L. W. Xin, "Electronic Pneumatic Clutch Control of the Heavy Truck based on Neural Network PID," in *2006 IEEE International Conference on Vehicular Electronics and Safety*, Shanghai, China, 13–15 December 2006.

[126] ISO–Int. organization for standardization. ISO 6358 — Pneumatic Fluid Power — Components Using Compressible Fluids — Determination of Flow-Rate Characteristics, 1. edition, October 1989.

[127] T. Kagawa, J. Jang, W. Pan, T. Fujita and K. Sakaki, "Study on the dynamic characteristics of a pneumatic cylinder system," *Hydraul Pneumatics,* vol. 28, no. 4, pp. 444–450, 1997 [in Japanese].

[128] B. Szimandl, Observer based feedforward/feedback control of electro-pneumatic clutch systems. Ph.D. Thesis, Budapest University of Technology and Economics, 2015.

Publication Lists

[1] Naoki Hosoya, Shuichi Yahagi, Itsuro Kajiwara, "Non-Contact Vibration Tests with Detection-Free Input Based on Pulsed-Laser Ablation for Underwater Structures," TRANSACTIONS OF THE JAPAN SOCIETY OF MECHANICAL ENGINEERS Series C, vol. 78, no. 791, pp. 2426–2437, 2012. [in Japanese]

[2] Shuichi Yahagi, Yusuke Sato, Itsuro Kajiwara, Masahiko Konda. "Self-Sensing and Model-Free Active Vibration Control Based on DVFB (Demonstration of Control Method by Simulation)," TRANSACTIONS OF THE JAPAN SOCIETY OF MECHANICAL ENGINEERS Series C, vol. 78, no. 793, pp. 3104–3117, 2012. [in Japanese]

[3] Shuichi Yahagi, Itsuro Kajiwara, Tomoaki Shimozawa, "Slip control during inertia phase of clutch-to-clutch shift using model-free self-tuning proportional-integral-derivative control," Proceedings of the Institution of Mechanical Engineers, Part D: Journal of Automobile Engineering, vol. 234, no. 9, pp. 2279–2290, 2020

[4] Shuichi Yahagi, Itsuro Kajiwara, "Direct tuning of the data-driven controller considering closed-loop stability based on a fictitious reference signal," Measurement and Control, vol. 54, no. 5–6, pp. 1026–1042, 2021.

[5] Shuichi Yahagi, Itsuro Kajiwara, "Direct tuning of gain-scheduled controller for electro-pneumatic clutch control," Advanced in Mechanical Engineering, vol. 13, no. 7, pp. 1–12, 2021.

[6] Shuichi Yahagi, Itsuro Kajiwara, "Direct Tuning Method of Gain-Scheduled Controllers with the Sparse Polynomials Function," Asian journal of Control, pp. 1–16, 2021. (Online published)

Conference Papers

[1] Shota Yabui, Itsuro Kajiwara, Shuichi Yahagi, "Self-Sensing and Model-Free Active Vibration Control Based on Adaptive Feed-forward Cancellation," The Japan Society of Mechanical Engineers, IIP2013 The Proceedings of the Conference on Information, Intelligence and Precision Equipment, Toyo University (Tokyo), 2013. [in Japanese]

[2] Ryohei Okita, Shuichi Yahagi, Itsuro Kajiwara, Masahiko Kondo, Keiichiro, Matsumoto, "Self-Sensing and Model-Free Vibration Control Based on LQG Strategy," The Proceedings of the Symposium on the Motion and Vibration Control 2013, Kyushu Sangyo University (Fukuoka), 2013. [in Japanese]

[3] Shuichi Yahagi, Ryohei Okita, Itsuro Kajiwara, Masahiko Kondo, Keiichiro, Matsumoto, "Self-Sensing and Model-Free Active Vibration Control Based on DVFB (Demonstration of Control Method by Simulation)," The 55th Proceedings of the Japan Joint Automatic Control Conference, Kyoto University (Kyoto), 2012. [in Japanese]

[4] Shuichi Yahagi, Yusuke Sato, Itsuro Kajiwara, Masahiko Kondo, "Sensorless Model-Free Vibration Control without Model of Controlled Object," The Proceedings of Mechanical Engineering Congress Japan 2012, Kanazawa University (Kanazawa), 2012. [in Japanese]

[5] Shuichi Yahagi, Naoki Hosoya, Itsuro Kajiwara, "Non-contact Vibration Testing of Underwater Structures by Using Laser Ablation," The Proceedings of the Dynamics & Design Conference 2011, Kochi University of Technology (Kochi), 2011. [in Japanese]

[6] Shuichi Yahagi, Itsuro Kajiwara, "Direct tuning of PID controller and reference model with input constraint," The 21st International Conference on Control, Automation and Systems (ICCAS 2021), Ramada Plaza Hotel, Jeju, Korea, Oct. 12–15, 2021.

Awards

[1] Student Encouragement Award of the Japan Society for Precision Engineering Hokkaido Branch, 2012.

Patents

Sixteen patents have been registered and more than forty patents have been filed.